

# JNMMM

Journal of Nuclear Materials Management

Foreword: Safe Interim Storage of Plutonium Containing Materials Natraj Iyer, Steve Bellamy, Allen Gunter, and Gary Roberson	4
Supporting Safe Storage of Plutonium-bearing Materials Through Science, Engineering, and Surveillance Kerry A. Dunn, Gregory T. Chandler, Curtis W. Gardner, McIntyre R. Louthan, Jr., Elizabeth R. Hackney, James W. McClard, Laura A. Worl, and Gary Roberson	5
Container Materials, Fabrication, and Robustness Kerry A. Dunn, McIntyre R. Louthan, Jr., George B. Rawls, Robert L. Sindelar, Philip E. Zapp, and James W. McClard	17
Closure Weld Development for 3013 Outer Containers William L. Daugherty, Stanley R. Howard, Kurt D. Peterson, Mitchell W. Stokes, Gary R. Cannell, and Scott A. Breshears	25
Residual Stresses in 3013 Containers John I. Mickalonis and Kerry A. Dunn	31
Long-term Aging and Surveillance of 9975 Package Components Elizabeth N. Hoffman, T. Eric Skidmore, William L. Daugherty, and Kerry A. Dunn	39
Thermal Analysis of 3013/9975 Configuration Narendra K. Gupta	47
Thermal Conductivity of High-purity and Impure Plutonium Oxide Materials D. Kirk Veirs and F. Coyne Prenger	55
Article-Particle-Induced Prompt Gamma-Ray Analysis of Plutonium-Bearing Materials Packaged in 3013 Containers Joshua E. Narlesky, Lynn A. Foster, Elizabeth J. Kelly, and Roy E. Murray IV	61
Salt Phases in Calcined Materials and Their Hydration Properties Stephen A. Joyce, Joshua E. Narlesky, D. Kirk Veirs, Eduardo Garcia, Obie W. Gillispie, J. Matt Jackson, Brian L. Scott, and Laura A. Worl	69
Sampling Approach to Validate the Safe Storage of Plutonium-bearing Materials Elizabeth J. Kelly, Larry G. Peppers, Laura A. Worl, and James W. McClard	79

Non-Profit Organization  
U.S. POSTAGE  
PAID  
Permit No. 2066  
Eau Claire, WI



# Imagine Yourself **Solving** Some of the Most Challenging **Problems** in Managing Nuclear Materials...

That's exactly what researchers at Argonne National Laboratory are doing. They have developed a unique radiofrequency identification (RFID) tracking technology that also monitors the environmental and physical conditions of containers of nuclear materials in storage and transportation.



"This new RFID technology for the management of nuclear materials has many applications in nuclear industries, and as the technology is further developed, the need for talent to advance its growth is essential."

*Dr. James Shuler, Manager DOE Packaging Certification Program, Office of Packaging and Transportation.*

<http://rampac.energy.gov/RFID/RFID.htm>



To learn more about science and engineering opportunities at Argonne, please visit [www.anl.gov](http://www.anl.gov).

Argonne is an equal opportunity employer and values diversity in the workforce.

**Technical Editor**  
Dennis Mangan

**Assistant Technical Editor**  
Stephen Dupree

**Managing Editor**  
Patricia Sullivan

**Associate Editors**

Gotthard Stein and Bernd Richter,  
International Safeguards

Cameron Coates, Materials Control and Accountability  
Leslie Fishbone, Nonproliferation and Arms Control

Glenn Abramczyk, Packaging and Transportation  
Felicia Duran, Physical Protection  
Scott Vance, Waste Management

**INMM Technical Program Committee Chair**  
Charles E. Pietri

**INMM Executive Committee**

Stephen Ortiz, President  
Scott Vance, Vice President

Chris Pickett, Secretary  
Robert U. Curl, Treasurer

Nancy Jo Nicholas, Immediate Past President

**Members At Large**

Corey Hinderstein

Larry Satkowiak

Grace Thompson

J. Michael Whitaker

**Chapters**

Rusty Babcock, California

Teresa McKinney, Central

James Lemley, Northeast

Cary Crawford, Pacific Northwest

Jeff Jay, Southeast

Keith Tolk, Southwest

Yoshinori Meguro, Japan

Hun-Gyu Lee, Korea

Gennady Pshakin, Obninsk Regional

Alexander Izmaylov, Russian Federation

Marco Marzo, Vienna

Brian Blue, United Kingdom

Yuri Churikov, Urals Regional

Vladimir Kirischuk, Ukraine

Adrienne Lafleur, Texas A&M Student

Kristan Wheaton, Mercyhurst College Student

David Vermillion, University of Tennessee Student

James Cole, University of Missouri Student

Eric C. Miller, University of Michigan Student

Bruce Pierson, Idaho State University Student

**Headquarters Staff**

Leah McCrackin, Executive Director

Jodi Metzgar, Administrator

Deb Pederson, Administrator

Lyn Maddox, Manager, Annual Meeting

Kim Santos, Administrator, Annual Meeting

**Design**

Shirley Soda

**Layout**

Brian McGowan

**Advertising Director**

Jill Hronek

INMM, 111 Deer Lake Road, Suite 100

Deerfield, IL 60015 U.S.A.

Phone: +1-847-480-9573; Fax: +1-847-480-9282

E-mail: jhronek@inmm.org

JNMM (ISSN 0893-6188) is published four times a year by the Institute of Nuclear Materials Management Inc., a not-for-profit membership organization with the purpose of advancing and promoting efficient management of nuclear materials.

**SUBSCRIPTION RATES:** Annual (United States, Canada, and Mexico) \$200.00; annual (other countries) \$270 (shipped via air mail printed matter); single copy regular issues (United States and other countries) \$55; single copy of the proceedings of the Annual Meeting (United States and other countries) \$175. Mail subscription requests to JNMM, 111 Deer Lake Road, Suite 100, Deerfield, IL 60015 U.S.A. Make checks payable to INMM.

**DISTRIBUTION** and delivery inquiries should be directed to JNMM, 111 Deer Lake Road, Suite 100, Deerfield, IL 60015 U.S.A., or contact Jodi Metzgar at +1-847-480-9573; fax, +1-847-480-9282; or E-mail, inmm@inmm.org. Allow eight weeks for a change of address to be implemented.



Opinions expressed in this publication by the authors are their own and do not necessarily reflect the opinions of the editors, Institute of Nuclear Materials Management, or the organizations with which the authors are affiliated, nor should publication of author viewpoints or identification of materials or products be construed as endorsement by this publication or by the Institute.

© 2010 Institute of Nuclear Materials Management


## Topical Papers

<b>Foreword: Safe Interim Storage of Plutonium Containing Materials</b>	4
Natraj Iyer, Steve Bellamy, Allen Gunter, and Gary Roberson	
<b>Supporting Safe Storage of Plutonium-bearing Materials Through Science, Engineering, and Surveillance</b>	5
Kerry A. Dunn, Gregory T. Chandler, Curtis W. Gardner, McIntyre R. Louthan, Jr., Elizabeth R. Hackney, James W. McClard, Laura A. Worl, and Gary Roberson	
<b>Container Materials, Fabrication, and Robustness</b>	17
Kerry A. Dunn, McIntyre R. Louthan, Jr., George B. Rawls, Robert L. Sindelar, Philip E. Zapp, and James W. McClard	
<b>Closure Weld Development for 3013 Outer Containers</b>	25
William L. Daugherty, Stanley R. Howard, Kurt D. Peterson, Mitchell W. Stokes, Gary R. Cannell, and Scott A. Breshears	
<b>Residual Stresses in 3013 Containers</b>	31
John I. Mickalonis and Kerry A. Dunn	
<b>Long-term Aging and Surveillance of 9975 Package Components</b>	39
Elizabeth N. Hoffman, T. Eric Skidmore, William L. Daugherty, and Kerry A. Dunn	
<b>Thermal Analysis of 3013/9975 Configuration</b>	47
Narendra K. Gupta	
<b>Thermal Conductivity of High-purity and Impure Plutonium Oxide Materials</b>	55
D. Kirk Veirs and F. Coyne Prenger	
<b>Article-Particle-Induced Prompt Gamma-Ray Analysis of Plutonium-Bearing Materials Packaged in 3013 Containers</b>	61
Joshua E. Narlesky, Lynn A. Foster, Elizabeth J. Kelly, and Roy E. Murray IV	
<b>Salt Phases in Calcined Materials and Their Hydration Properties</b>	69
Stephen A. Joyce, Joshua E. Narlesky, D. Kirk Veirs, Eduardo Garcia, Obie W. Gillispie, J. Matt Jackson, Brian L. Scott, and Laura A. Worl	
<b>Sampling Approach to Validate the Safe Storage of Plutonium-bearing Materials</b>	79
Elizabeth J. Kelly, Larry G. Peppers, Laura A. Worl, and James W. McClard	

## Institute News

 <b>President's Message</b>	2
 <b>Editor's Note</b>	3

## Departments

 <b>Author Submission Guidelines</b>	86
<b>Membership Application</b>	87
<b>Calendar</b>	88

## Thanking and Honoring Volunteers

By Steve Ortiz  
INMM President



The first issue of the *Journal* for the New Year is a good opportunity to recognize and thank all of you for the hard work and the time you put into the Institute. The Institute of Nuclear Materials Management is very successful as a volunteer organization. Every nuclear materials management professional who serves in a leadership or supporting role of the INMM is a volunteer. *Volunteers are individuals or groups who give their time, talent and abilities to a cause they believe in, without pay.* We are successful because either you personally and/or the company you work for receives value from your participation in the Institute of Nuclear Materials Management. As volunteers we give our personal time and sometimes spend our own money to support the mission and activities of INMM. This is part of the reason why volunteer organizations are inherently strong organizations—the members truly believe in the mission.

Following is a quote on volunteers that I especially like:

“Snowflakes melt alone—but together they can be traffic stoppers! Teamwork allows common people to attain uncommon results. Some people want it to happen, some wish it to happen, others make it happen. Volunteers aren't paid, not because they are worthless, but because they are priceless.”  
*Anonymous*

With the importance of volunteers in mind, I encourage you to think about the volunteers and others who give so much to our organization and/or our profession. Think about what they contribute and how they contribute and ask yourself, “Who among my colleagues and friends in our profession would I nominate for

an award if I could?” Of course, through INMM's award program you can nominate them. Take a few minutes to read the INMM Web site's award page and then nominate your friend or colleague who has contributed so much and made such a difference. You'll find all the information you need at [www.inmm.org/awards/](http://www.inmm.org/awards/).

Again, I want to personally thank all of you for the time and effort you put into the institute to maintain it as the premiere organization in nuclear materials management. I look forward to working with you for another year in being a service to nuclear materials management professionals. We serve our community. That is the reward.

*INMM President Steve Ortiz can be reached at [sortiz@sandia.gov](mailto:sortiz@sandia.gov).*



## Supporting Safe Storage of Plutonium-Bearing Materials Through Science, Engineering, and Surveillance

By Dennis Mangan  
INMM Technical Editor

Toward the end of April 2009, the *JNMM* was approached by Dr. Mac Louthan, a senior consulting scientist emeritus at the Savannah River National Laboratory (SRNL), about the possibility of having an issue dedicated to articles describing the tremendous amount of work that has been accomplished addressing the safe storage of plutonium. He noted that this endeavor, although to be spear-headed by SRNL, would be a multi-laboratory effort. He opined that our audience as well as others in the United States and around the world might find this work interesting, and he suggested perhaps ten technical articles might adequately cover the topic. We responded favorably, and informed him that such issues devoted to a particular topic normally come through a chair of one of our Institute's Technical Divisions. Louthan contacted Steve Bellamy, chair of our Packaging and Transportation Technical Division, who was also very supportive, as was Dr. Samit Bhattacharyya, director of SRNL.

Patricia Sullivan, *JNMM's* managing editor, and I met with Kerry Dunn,

an advisory engineer at SRNL, and Glenn Abramczyk, also from SRNL and our associate editor representing the Packaging and Transportation Technical Division. We were surprised when we learned that they had commitments for twenty articles. In the course of the conversation, we discussed the possibility of splitting the twenty articles into two consecutive issues. As it turned out, the decision was made to have two consecutive issues cover the twenty articles. This issue is the first and the Spring 2010 issue will be the second. We also discussed the possibility of getting these articles peer reviewed. For those of you not familiar with our peer-review process, when we receive an article for publication, we assign it to an associate editor of the appropriate Technical Division (or more than one if appropriate) who then arranges for a peer review. When a special *JNMM* issue is requested by a chair of a Technical Division, and the decision is made that a peer review is desired, then naturally that division (and its associate editor) is responsible for accomplishing

the peer reviews. That was done for all the articles in this issue as well as the upcoming Spring issue.

I trust you will enjoy reading these articles dedicated to the safe storage of plutonium. I personally found the articles to be interesting, and quite varied. They provide good reading for a wide audience ranging from chemists to engineers to mathematicians. The theme might be described as "supporting safe storage of plutonium-bearing materials through science, engineering, and surveillance."

Dunn served as an excellent point of contact and accomplished her mission quite effectively and efficiently, and we express our appreciation to her and all the authors for a job well done.

Should you have any questions or comments, please do not hesitate to contact me.

*JNMM Technical Editor Dennis L. Mangan can be reached at [dennismangan@comcast.net](mailto:dennismangan@comcast.net).*





Special Issue

# Safe Interim Storage of Plutonium-Containing Materials

Natraj Iyer and Steve Bellamy

Savannah River National Laboratory, Aiken, South Carolina USA

Allen Gunter

U.S. Department of Energy, Washington, DC USA

Gary Roberson

U.S. Department of Energy, Aiken, South Carolina USA

The safe storage and disposition of plutonium containing materials and other radioactive elements is a legacy responsibility of nations that have nuclear reactors, access to nuclear materials, and/or facilities for nuclear materials separation. This responsibility is virtually global because of the widespread use of nuclear power. With the emergence of nuclear technology, large quantities of plutonium-containing materials have been produced around the world in developed countries, both as an outgrowth of national weapons programs and the proliferation of nuclear power. Therefore the handling, storage, and disposal of plutonium materials inventories is of worldwide concern and must be carefully managed until the inventory is either used as a nuclear fuel or placed in a safeguarded nuclear materials repository. The articles contained in the winter and spring 2010 issues of the *Journal of Nuclear Materials Management* summarize the engineering, science, and surveillance activities that support the U.S. Department of Energy's (DOE) efforts to assure that the excess plutonium materials within the DOE Complex are stored in a safe and environmentally friendly manner. While the papers focus on plutonium materials, the approach and technical methodology presented is widely applicable to the storage of other nuclear materials. We hope that the information contained in these articles will contribute to assuring the safe and responsible management of the existing and emergent nuclear inventories throughout the world.

Plutonium is one of the most intriguing elements in the periodic table. Plutonium isotopes have been used in various forms including for space power, e.g., for U.S. NASA's Cassini mission and Mars mission, as source materials for calibration of analytical instruments, as fuel elements in nuclear power, and in weapons technology. The extensive technology and the comprehensive understanding of plutonium materials behavior facilitate the development of the science and technology necessary to ensure a robust technical basis for the safe storage and handling of these materials. The DOE is storing excess plutonium materials at the Savannah River Site near Aiken, South Carolina, USA. The materials being stored basically exist in two forms: plutonium metal and plutonium oxide. The inventory is stored in a safeguarded facility (K-Area Materials Storage or the KAMS facility) located within the 340-square-mile area that is the Savannah River Site. The storage inventory is packaged and handled according to DOE-STD-3013, a standard that was developed by a team of plutonium materials and packaging experts assembled from the various sites within the DOE Complex.

Effective long-term storage of plutonium-containing materials requires that the stored materials do not interact with the container and that age related degradation of the containment system does not occur. This could be readily accomplished if the plutonium existed as either a pure metal or a pure oxide. However the presence of halides in the DOE's excess plutonium materials inventory challenges the development and validation of the storage basis. The DOE-STD-3013 states that the storage containers be fabricated from "ductile, corrosion resistant materials such as 300 series stainless steel." Types 304L and 316L stainless steels have been used by the packaging sites for the containment system. The DOE-STD-3013 requires stabilization of the plutonium materials prior to packaging and limits the moisture content to 0.5 wt percent moisture to mitigate the potential for chloride corrosion-induced degradation of the 300 series stainless steel containers. Additionally, the standard requires that a surveillance program be established to monitor the condition of the storage inventory and enable validation of the robustness of the storage technical basis. Because of the potential for corrosion-induced degradation, many of the articles in these issues focus on corrosion and stress-corrosion cracking processes and the associated surveillance activities. The processes of corrosion and alpha-irradiation-induced radiolysis also provide the potential for pressure development within a container and many of the manuscripts focus on the modeling and measurement of container pressures.

The peer-reviewed manuscripts published in the winter and spring 2010 issues of this *Journal* illustrate the investment in technology required to assure long-term safe storage of the plutonium materials. The manuscripts provide only a snapshot of the ongoing effort. Other manuscripts describe completed efforts that qualified packaging materials and processes, investigated material compositions or provided statistical relevance to the investigations.

We are pleased to have played a role in the development and execution of a program to assure responsible storage of the excess plutonium materials existing within the DOE Complex. We are also pleased that the international Institute of Nuclear Materials Management chose to publish the engineering, science, and surveillance activities associated with the plutonium storage and surveillance program in these two special issues of the *Journal*.

# Supporting Safe Storage of Plutonium-Bearing Materials Through Science, Engineering, and Surveillance

*Kerry A. Dunn, Gregory T. Chandler, Curtis W. Gardner, McIntyre R. Louthan Jr.  
Savannah River National Laboratory, Aiken, South Carolina USA*

*James W. McClard and Elizabeth R. Hackney  
Savannah River Nuclear Solutions, Aiken, South Carolina USA*

*Laura A. Worl  
Los Alamos National Laboratory, Los Alamos, New Mexico USA*

*Gary D. Roberson  
U.S. Department of Energy, Aiken, South Carolina USA*

---

## Abstract

Reductions in the size of the U.S. nuclear weapons arsenal resulted in the need to store large quantities of plutonium-bearing metals and oxides for prolonged periods of time. To assure that the excess plutonium from the U.S. Department of Energy (DOE) sites was stored in a safe and environmentally friendly manner the plutonium-bearing materials are stabilized and packaged according to well-developed criteria published as a DOE standard. The packaged materials are stored in secure facilities and regular surveillance activities are conducted to assure continuing package integrity. The stabilization, packaging, storage, and surveillance requirements were developed through extensive science and engineering activities including those related to plutonium-environment interactions and container pressurization, corrosion and stress-corrosion cracking, plutonium-container material interactions, loss of sealing capability, and changes in heat transfer characteristics. This paper summarizes some of those activities and outlines ongoing science and engineering programs that assure continued safe and secure storage of the plutonium-bearing metals and oxides.

## Introduction

The end of the Cold War caused dramatic reductions in the size of the U.S. nuclear arsenal and has resulted in large quantities of excess special nuclear materials. This excess includes plutonium-bearing metals and oxides that require safe and secure containment for prolonged periods of time. Plutonium is a transuranium, actinide metal that is of practical importance because various isotopes, principally  ${}_{94}\text{Pu}^{239}$ , have attractive properties for energy production and nuclear weapons. Although trace quantities of plutonium occur naturally in uranium ore deposits, the vast majority of plutonium on earth today has been produced in nuclear reactors. Operating nuclear power reactors are currently producing approximately

20,000 kg of plutonium per year, worldwide, as a byproduct of reactor operations. This power reactor produced plutonium is either reprocessed to produce mixed plutonium and uranium oxide fuel or remains contained in spent fuel elements. The spent fuel is stored in a variety of ways including storage pools, dry storage canisters, and geologic repositories. The plutonium produced in power reactors is typically either fuel grade (~80-93 percent  $\text{Pu}^{239}$ ) or reactor grade (generally <80 percent  $\text{Pu}^{239}$ ).

On the other hand, the excess plutonium in the U.S. nuclear arsenal was produced in nuclear materials production reactors primarily located at the Hanford and Savannah River Sites, and was extracted from fuel elements designed specifically to produce plutonium for nuclear weapon applications. This plutonium is considered weapons grade because it contains generally >93 percent  $\text{Pu}^{239}$ . The breakup of the Soviet Union and the associated reduction in nuclear weapons in the U.S. stockpiles created an excess of plutonium at various U.S. Department of Energy (DOE) sites including, Hanford, Los Alamos, Rocky Flats, Savannah River, Lawrence Livermore and Idaho. To assure that the excess plutonium from the DOE sites is stored in a safe, environmentally friendly manner the plutonium-bearing metals and oxides are stabilized and packaged according to criteria provided in DOE-STD-3013.<sup>1</sup>

The DOE Standard applies to plutonium-bearing metals and oxides that contain at least 30 wt percent actinides and is designed to assure that storage containers maintain integrity for at least fifty years. Significant research and development was required to provide the technical basis for the Standard. This research has generated the data and analyses required to predict that the plutonium-bearing materials will be safe and stable for long-term storage at DOE facilities and that the containers will maintain integrity and require only minimal surveillance under anticipated handling, shipping, and storage conditions. The stored containers will ultimately be accepted by the DOE's Materials Disposition Program for disposition<sup>2</sup> or converted to a mixed



plutonium-uranium oxide for use as a fuel in nuclear reactors.

Assuring against failure is a difficult concept especially when the storage conditions may change with time. Providing such assurance for the plutonium storage containers involves proving that age-related degradation processes cannot occur if certain conditions are established prior to storage and if certain conditions are maintained throughout the storage period. This paper summarizes a continuing multi-year multi-laboratory program conducted to assure that the excess plutonium in the DOE inventory is safely handled and maintained under conditions conducive to future deposition or conversion. Basically, the program described is a failure-prevention program that involves the application of science, engineering, and surveillance to assure the continuing integrity of stored containers containing plutonium-bearing materials.

### The 3013 Standard

The DOE Standard for stabilization, packaging, and storage of plutonium-bearing materials is a living document that may be revised based on emergent information including beneficial comments and pertinent data sent to the Technical Standards Project Office.<sup>1</sup> Since its inception, the Standard has been revised several times. The 2004 version of the Standard notes that a significant portion of the DOE plutonium oxide inventory contains chlorides and recommends that storage containers be fabricated from ductile, corrosion-resistant materials such as the 300 series stainless steels. These two notations almost immediately imply that a potential exists for stress-corrosion cracking in the container material and attention must be given to assuring that, even if such cracking occurs, the container system will not be compromised. This assurance is addressed by concluding that “the Standard does not impose a limit on chloride contamination because the extent of corrosion is limited by the available moisture, rather than the available chloride. The moisture content limitation in this Standard (0.5 wt percent) is considered sufficient to avoid significant corrosion.” The Standard also imposes criteria for the stabilization of the plutonium-bearing materials, design of the containers for the materials and places limits on the container contents. The criteria for plutonium metal and plutonium oxide differ significantly because of the differences between these two types of material.

### Plutonium Metal

Plutonium metal may exist in six different allotropic forms, depending on temperature as shown in Table 1.

The low temperature allotropes,  $\alpha$ ,  $\beta$ , and  $\gamma$ , have low symmetry and consequently low ductility. In fact the  $\alpha$ -phase is so brittle that  $\alpha$ -phase alloys are fabricated primarily by casting and machining. However, the face-centered cubic allotrope,  $\delta$ , which, in pure plutonium is only stable at temperatures above 310°C, is quite ductile and amiable to wrought processing technologies. The  $\delta$ -phase can be stabilized to room temperature by alloying

Table 1. Allotropic forms of Pu metal as a function of temperature

Crystal Structure, Density, and Range of Stability for Plutonium Allotropes			
Phase	Crystal Structure	Density, g/cm <sup>3</sup>	Range of Stability, °C
Alpha, $\alpha$	Simple Monoclinic	19.86	Below 112
Beta, $\beta$	Body-Centered Monoclinic	17.70	112-185
Gamma, $\gamma$	Face-Centered Orthorhombic	17.14	185-310
Delta, $\delta$	Face-Centered Cubic	15.92	310-452
Delta Prime, $\delta'$	Body-Centered Tetragonal	16.00	452-480
Epsilon, $\epsilon$	Body Centered Cubic	16.51	480-640
Liquid		16.65	Above 640

with small amounts (1 to 2 at. percent) aluminum or gallium.

The heat generated by radioactive decay of the various plutonium isotopes may raise the temperature of the plutonium in the storage container. The equilibrium temperature will depend on the mass and isotopic content of the stored plutonium as well as the heat transfer characteristics of the storage system. However, because of the heat generation by radioactive decay of the plutonium and associated fissile materials, the potential for phase instability must be considered and because plutonium is a reactive metal, corrosion and oxidation may occur, depending on the exposure atmosphere. Additionally, a storage temperature of only 184°C places the plutonium metal at one-half its absolute melting temperature and virtually assures vacancy migration and diffusion within the stored metal. Diffusion across metal-to-metal interfaces could support solid state interactions between the stored plutonium and the container material and these interactions must also be considered.

### Plutonium Oxide

Plutonium oxide, PuO<sub>2</sub>, has excellent chemical stability, a high melting temperature (<2450°C), and undergoes no phase transformations. Pellets of this face-centered cubic oxide made with the isotope <sup>94</sup>Pu<sup>238</sup> have provided the heat sources for electrical production in virtually all of NASA's deep space missions. These heat sources operate at about 1350°C and, because of the oxide stability, do not react with the container material, an iridium alloy. However, the oxide will adsorb moisture from the surrounding environment if the relative humidity is not very low. The added moisture, especially with salt impurities, is known to generate hydrogen gas within the environment. Therefore, the 3013 packaging requirements require that the amount of moisture in the oxide not exceed 0.5 wt percent at the time of packaging. This moisture specification is considered critical for the prevention of corrosion



of the container materials because many of the oxide mixtures at the various DOE sites are impure and contain chlorides. The chlorides are also hygroscopic and the combination of chlorides and moisture is a well-known corrosion-causing environment.

The DOE sites packaging plutonium oxide materials are required by DOE-STD-3013 to ensure that the behavior of the materials they package are represented by one or more samples in the Materials Identification and Surveillance (MIS) Program. More than 60 items that are believed to reasonably represent the behavior of the currently identified 3013 material in storage for 50 years are within this MIS Program. The MIS represented inventory includes material from the packaging sites and is intended to represent the principal processes that DOE used to produce oxides that are now stored in the 3013 containers. The selected items are considered part of the MIS inventory and the justification for representation was documented by each site and subsequently verified via sample characterization. The representative materials in the MIS inventory are characterized for chemical and physical attributes, and then some items are selected to be placed in instrumented containers as part of a shelf-life inventory. The purpose of the shelf-life inventory is to provide an early warning of storage behavior that could result in container failures in storage facilities. In addition to the materials that are provided by the sites, materials that have characteristics that push the limits of the standard are included in the shelf-life studies to gain an understanding of the sensitivity of the DOE-STD-3013 limits to actual phenomena associated with storage container failure<sup>3</sup>.

There are explicit requirements for stabilizing the oxides prior to packaging. These requirements include heating the oxide material in an oxidizing environment at a temperature of at least 950°C for not less than two hours with a resulting moisture content of <0.5 wt percent. Properly stabilized oxides should not interact with either the container or the surrounding environment. The DOE-STD-3013 requires that the headspace of each container be inerted to remove all but 5 percent O<sub>2</sub> to limit the

**Figure 1.** The 3013 container used by Savannah River Site (SRS) for oxides. The outer container is consistent for all packaging sites in the DOE Complex.



amount of reactive gases present. However, any adsorbed moisture could experience transfer from the stabilized oxides to the container wall or storage environment and undergo corrosion reactions with the container material or radiation induced decomposition to hydrogen and water.

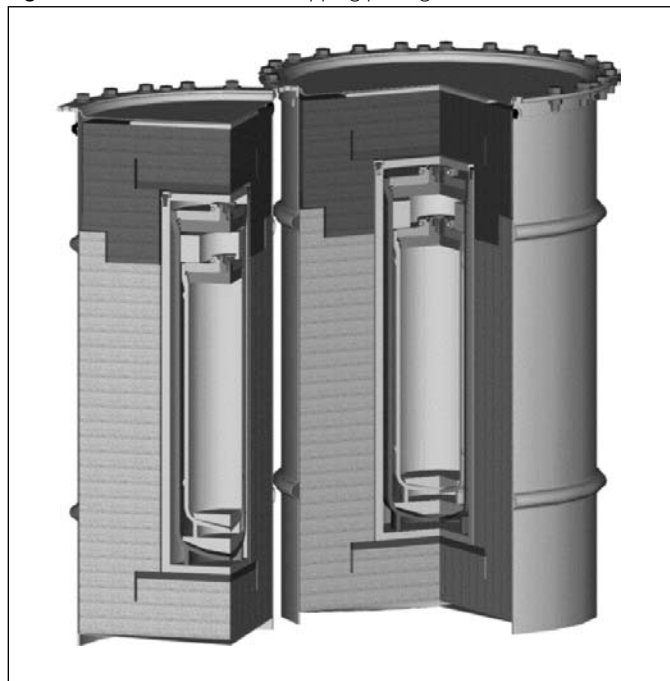
### The Containers

The 3013 container includes properly prepared plutonium-bearing materials stored in a nested set of welded austenitic stainless steel containers (Figure 1). Type 316L and 304L stainless steel containers have been used in the packaging process, although the standard does not explicitly require the use of these alloys. The multi-barrier storage container system is essentially designed to be maintenance free over a storage period that may stretch to fifty years. The 3013 standard requires a minimum of two nested containers with weld closure but most packaging sites have also provided a third container, or convenience container, as the innermost container of the assembly. The minimum design pressure for the outer container is 699 psi, which is about seven times the maximum pressure that could develop based on known credible mechanisms in properly packaged systems.

The outer pressure vessel in the container system is designed and fabricated to meet ASME code requirements but is not stamped as being compliant with the ASME pressure vessel code. The fact that the final seal weld cannot be pressure tested precludes an ASME code stamp. However, because the final weld cannot be pressure tested, the weld qualification process was quite extensive.

The design, fabrication, packaging, and sealing processes for the 3013 container systems have been developed to assure the long-term safe storage of the plutonium-bearing materials.

**Figure 2.** Schematic of 9975 shipping package





To accomplish the storage mission the containers of plutonium-bearing materials must be handled and transferred from location to location and the transfer may include cross country shipment. Shipments involve loading the plutonium bearing 3013 containers into U.S. Department of Transportation Type B packages certified for interstate shipping of radioactive materials and transfer of the containers between DOE sites. Additionally, many of the plutonium-bearing 3013 containers are stored in shipping packages at the Savannah River Site. Therefore a series of drop tests was conducted to assure that the 3013 containers could withstand an accidental drop of 9 meters (the maximum anticipated storage height) and remain leak tight (maximum leak rate less than  $1 \times 10^{-7}$  cm<sup>3</sup>/sec). Additionally, the inner containers were dropped from a height of 1.33 meters to assure that an accidental drop during packaging would not cause a leak in the 3013 inner container. These drop tests were part of the qualification program

Figure 3. Lower assembly fiberboard from 9975 shipping package



Figure 4. O-ring seal from 9975 shipping package primary containment vessel (PCV)



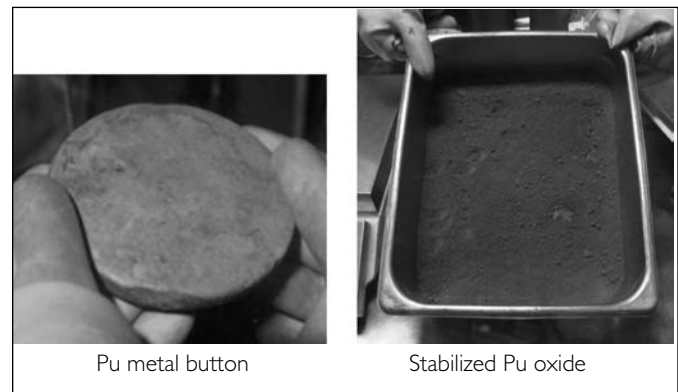
to support the handling necessary for placement of plutonium-bearing 3013 containers inside shipping packages. A schematic of a 9975 shipping container is shown in Figure 2.

The engineering design and testing necessary to qualify a container for shipping radioactive materials is extensive and well-developed.<sup>4,5</sup> However, the use of a 9975 shipping package for the long-term storage of plutonium-bearing 3013 containers required a basic knowledge of the long-term behavior of the shipping 9975 package materials. Among the variety of materials used to manufacture the 9975 are fiberboard for insulation (Figure 3) and Viton O-rings to seal the plutonium containers inside stainless steel containment vessels (Figure 4). The effects of long-term exposure to low-level radiation at anticipated storage temperatures on these two materials were determined to assure that the heat transfer characteristics of fiberboard and the sealing capabilities of the O-rings will not be compromised during the storage period at SRS.

### The Contents

The nuclear characteristics that make plutonium useful in weapons and reactors limit the amount of plutonium that can be safely stored in any container or group of containers. Nuclear physics calculations made to assure that, even under the worst possible accident scenario (flooding; for example), a nuclear criticality event cannot occur, demonstrate that a 4.53 kg sphere of <sup>239</sup>Pu is not a critical mass even when fully water reflected. The  $k_{\text{eff}}$  of such a sphere is 0.95 and a  $k_{\text{eff}}$  of 1.0 is required for nuclear criticality. Therefore, the absence of a criticality event is assured by limiting the fissile material content in any container to 4.4 kg. The margin of safety under these conditions is high because there is not enough plutonium to support a criticality, the plutonium is not a sphere (the geometry that best supports a criticality) and the reflectivity of the container is nowhere near that of water. Photographs of plutonium metal samples and stabilized plutonium oxide are shown in Figure 5.

Figure 5. Examples of plutonium metal button and stabilized plutonium oxides



Properly packaged plutonium metal is considered relatively easy to store. To minimize the potential for ignition, the 3013 standard requires that the specific surface area of the metal be less than 200 mm<sup>2</sup>/g and that the metal be free of non-adherent



surface oxides and organic materials. Turnings from machining processes, wires and foils are specifically excluded and tramp materials are removed, if practical. The oxide materials are stabilized, as previously described, and the moisture content of the stabilized materials is determined by testing.

The radioactive decay of plutonium (and any other fissile material) generates heat that is removed by heat transfer through the storage system. The heat transfer processes are modeled and the models verified by experiment. The maximum amount of heat generated in any plutonium container is limited to 19 watts by the DOE-STD-3013. Although this value is less than the wattage of a typical room light, the equilibrium maximum temperature inside a 19-watt package may exceed 200°C. The maximum metal-container interface temperature is calculated to be 189°C (above one-half the absolute melting temperature of plutonium). Analytical evaluation of the impact of long-term storage at this temperature on potential interactions between the stored plutonium and the storage container show that diffusion-induced material exchange across the plutonium-container interface is very unlikely because of the low elemental diffusivities and the protective qualities of the surface films formed on both the plutonium and the container surfaces.

Thermal gradients inside the container may cause moisture, especially water vapor, relocation to the colder portions of the container. Such relocation may impact the potential for corrosion of the container. For example, moisture condensation coupled with the presence of chlorides can lead to stress corrosion cracking of austenitic stainless steels. An experimental program to evaluate the potential for corrosion and stress corrosion cracking in properly packaged 3013 containers has been ongoing for well over a decade.

Stress-corrosion cracking is an electrochemical process and, as such, requires the presence of an electrolyte such as moisture on the container material. The tendency for moisture adsorption will depend on the relative humidity of the environment inside the container and the relative humidity will depend on the moisture content of the container, the amount and type of salts present in the container and the temperature or temperature gradients within the container. Analytical and experimental studies to establish the role of relative humidity in influencing the potential for stress corrosion cracking are also ongoing.

### The Environment

The fill gas atmosphere over the plutonium-bearing material in the 3013 containers, including a convenience container, if used, is not specified but must not react adversely with the container or the plutonium-bearing materials. Additionally, the environment must allow for leak testing of the sealed containers. Helium gas is generally used to meet these requirements. The gas pressure inside the container may change during storage as a result of helium generation by the radioactive decay of the stored fissile materials, because of gases generated by evaporation and/or hydrolysis of

contained moisture, and because of gas generation by moisture induced corrosion. The gas pressure inside the container at any given time will be determined by the temperature of the system, the free volume in the container and the total gas present at the time of interest. Extensive studies to determine the pressure in a container as a function of packaging and storage variables (volume of plutonium-bearing material stored, moisture content, gas fill pressure, alpha decay rates, storage time, etc.) have shown that the maximum conceivable pressure (~100 psig) is significantly less than design pressure (699 psig) of the container.

### Surveillance

The design, materials selection, container fabrication, and material requirements for the packaging and storage of plutonium-bearing materials were carefully established to minimize the probability that the integrity of any container will be compromised during the storage period. The overall goal of the storage program is that none of the thousands of containers processed will contain significant defects and that no defects adverse to storage will develop. However, engineering experience and conventional wisdom suggest that destructive and non-destructive surveillance programs are necessary to support a safe, efficient, and environmentally friendly storage program. For example, the three conditions necessary for stress-corrosion cracking, 1) a susceptible material, 2) applied or residual tensile stresses, and 3) an electrolyte containing chloride may exist in properly packaged containers. The goal of the surveillance program is to use destructive and non-destructive inspections of a small fraction of the storage inventory to provide a statistically justifiable conclusion that the integrity of the overall inventory of stored plutonium materials is not compromised during prolonged storage. To accomplish this goal, regular, routine surveillance of selected samples from the storage inventory must continue over the lifetime of the storage program. The container selection and evaluation processes are based on statistical methods to assure that known differences in container contents and storage temperatures are evaluated.

### Examples of Science and Engineering Support

The science and engineering activities supporting the storage of plutonium-bearing materials in 3013 container systems are continuing and include work that has been conducted over the past several decades. This R&D has been conducted, reviewed and/or evaluated by well-established technical experts at numerous DOE sites, including members of the Materials Identification and Surveillance (MIS) Working Group. The MIS working group is an organization made up of highly qualified engineers and scientists who were selected because their expertise was relevant to the safe handling and storage of plutonium-bearing materials. A significant portion of the work that supports the standard has been published in the peer-reviewed literature. For example, the references in the DOE-STD-3013 include papers authored by



more than sixty-five different researchers from within the DOE complex and numerous other individuals from university and international laboratories. This paper describes a small fraction of the science and engineering activities that support the basis for the safe storage of plutonium-bearing materials. The activities are divided into six basic categories:

- 1) ties between the containers and the 3013 standard requirements,
- 2) temperature related issues,
- 3) material characterization,
- 4) statistical approaches to 3013 container surveillance,
- 5) corrosion and corrosion prevention,
- 6) gas generation and pressure buildup, and
- 7) validating safe storage.

The following sections provide selected examples of work from each category to demonstrate the types and variety of work associated with developing a safe storage strategy for plutonium-bearing materials. This overview provides a flavor for the R&D required to support the safe storage of plutonium-bearing materials. The compendium of papers in the winter and spring 2010 special issues of *JNMM* also, highlights a significant portion of the program.

#### Weld Qualification:

##### A Tie Between Containers and the 3013 Standard

The outer 3013 containers are fabricated from Type 316L stainless steel and conform to the ASME Section IX Pressure Vessel Code except that the filled container cannot be hydrostatically tested and the closure weld is not made by the container fabricator. The DOE standard does not specify the welding process but states that container safety should be equal or superior to the intent of the code. Different weld processes are used for container closure. These processes create an autogenous closure by either laser or gas tungsten arc welding. The laser welding process was developed in England and transferred to the United States by analysis and duplication of the weld system and qualification processes. However, both Hanford and Savannah River close the outer container by autogenous gas tungsten arc welding (GTAW), using an automated welder designed, qualified, and assembled by the Savannah River Technology Center (SRTC) (now the Savannah River National Laboratory, SRNL).

The weld joint, illustrated in Figure 6, seals the outer container top to the 0.118 inch thick container side wall. The lip on the container top is 0.157 inches thick and the full penetration weld fusion zone must be confined between the top and the side wall. The rigor required to qualify the welding process is demonstrated by the volume of data presented during a qualification review for the welder that SRTC assembled and shipped to Hanford. A summary of the data is provided in the next several paragraphs.

The acceptance criteria for the qualification welds were that the welds must be: 1) leak tight (leak rate <  $2 \times 10^{-7}$  cc/sec He), full

Figure 6. GTA weld joint for 3013 outer container



Table 2. Target welding parameters for GTA seal welding of 3013 containers

Target Welding Parameters	
Weld Tip Material	Tungsten with 2% Th,
Weld Tip Geometry	60° angle, 0.030 inch flat, 6-8 Ra finish
Gas	97% Ar – 3% H <sub>2</sub> shield gas
Tack Welds	Seven small, equi-spaced tack welds
Amperage	185 Amps primary welding current @ 0.45 s with 40 Amps background @ 0.02 s
Arc Gap	0.072"
Travel Speed	0.62 RPM
Additional	Modified weld start, chill block used to control temperature

Figure 7. 3013 outer container after burst testing



penetration, sound (meet ASME VIII radiographic acceptance), meet strength criteria (burst strength, for example), and meet the ASME VIII weld bead geometry shown in Figure 7. Tests were conducted to evaluate controllable parameters affecting arc density, including the tungsten alloy used for the tip, tip geometry, weld shield gas and pulsed currents. Additionally, weld travel speeds, tacking prior to seal welding and the use of chill blocks were also evaluated. These evaluations led to the target welding parameters shown in Table 2.

After the target welding parameters were developed, one hundred production certified containers were welded and evaluated. The welds were made with an ASME Section IX qualified welding procedure specification (WPS) by an ASME qualified welding operator. All welds passed the leak test requirements. Seventy-five of the welds were made at the nominal target parameters and twenty-five were made under upset conditions for process evaluation. Metallographic evaluations of selected containers were made at the weld start/stop position and at 90°, 180°, and 270° from the start/stop position. Five consecutive welds made under nominal welding conditions were evaluated to assure that the ASME weld geometry requirements were met and then a statistical parameter study was made to evaluate three primary variables. The welding current was varied from 160 to 200 amps, the travel speed varied from 0.58 to 0.66 RPM, and the arc gap varied from 0.062 to 0.082 inch. The variables were controlled so that heat input extremes were evaluated. All these welds met leak and weld bead geometry acceptance criteria.

Selected welded containers were burst tested and none failed in the closure welds (Figure 7). The burst pressures (essentially 4,600 psig) met the ASME Section VIII requirement of exceeding 3,920 psig. The weld metallography (Figure 8) and radiography revealed sound, essentially pore-free welds that met the ASME Section VIII requirements.

### Fiberboard and O-ring Behavior: A Temperature Related Topic

Fiberboard and Viton O-rings are two essential non-metallic materials in the 9975 shipping containers. The Viton O-rings provide the seals that separate the external environment from the 9975 containment volume. This separation is required to assure that, regardless of the behavior of the 3013 container, plutonium-bearing materials cannot contaminate the environment outside the 9975 containment vessels. The fiberboard provides the impact resistance, insulation, and criticality spacing necessary for the 9975 shipping container to meet DOT and other regulatory requirements. Additionally, the thermal behavior of the 3013 containers inside the 9975 will depend on the time dependent behavior of the fiberboard. The radiation levels and temperatures inside the 9975 shipping container could, with time, affect the behavior of both the O-rings and the fiberboard and thereby impact the behavior of the storage system.

The effect of irradiation, time, and temperature on the sealing capacity of the Viton O-rings was evaluated by exposing O-

rings to gamma irradiation while the material was compressed in the apparatus shown in Figure 9. The time, temperature, and irradiation dose were controlled so that the individual and combined effects of these exposure variables on the sealing capacity of the O-ring could be determined. Sealing capacity was determined by measuring the compression stress relaxation (CSR) in the O-rings after the various exposures and as the CSR increased the sealing capacity decreased. Examples of O-ring sections having various compression sets are shown in Figure 10. Data obtained in labo-

Figure 8. Cross-section of typical GTA weld on 3013 outer container

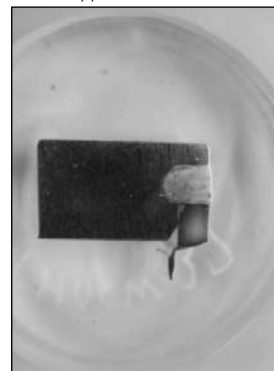


Figure 9. Apparatus used to compress O-rings for testing the effects of time, temperature and irradiation on the sealing capacity

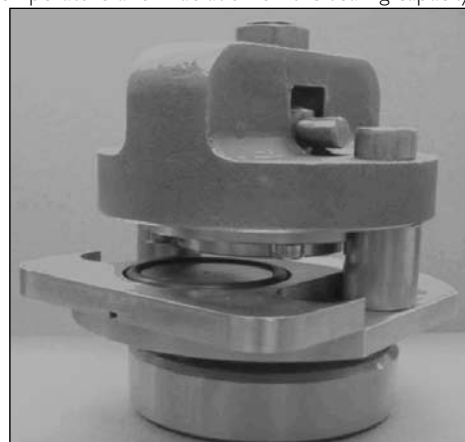
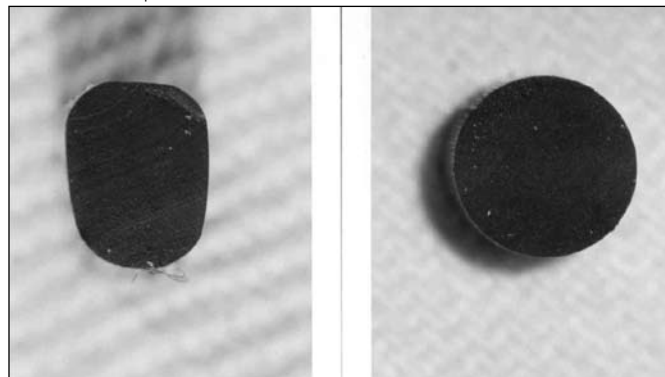


Figure 10. Compression set in O-rings exposed to gamma irradiation at various temperatures





ratory testing suggest that the O-rings at nominal service conditions should remain functional throughout an extended storage period greater than twelve years. Ongoing laboratory and surveillance tests will provide predictive capabilities of O-ring lifetime for storage periods greater than twelve years.

The effects of irradiation, time, and temperature on the density and heat transfer characteristics of fiberboard were also measured. These studies demonstrate that the behavior of fiberboard has not been compromised by the storage conditions.

### Plutonium/Stainless Steel Interactions: A Material Topic

The thermal analysis of the plutonium/container interface in a 3013 container filled with plutonium shows that the interface temperature can exceed 200°C if the plutonium is producing 19 watts and the 3013 container system is in a 9975 shipping container. At this temperature vacancies in the plutonium should be mobile and the potential exists for solid-state reactions between the plutonium and iron, chromium, and nickel in the stainless steel container. The phase diagrams for Fe-Pu and Ni-Pu show plutonium-rich eutectics that melt at 413°C and 465°C respectively. The Fe-Pu phase diagram is reproduced in Figure 11. The addition of about 1 percent gallium (gallium may be an alloy element in some plutonium metal pieces) to the iron eutectic can lower the melting temperature to about 400°C. This temperature represents the lowest temperature liquid that could develop by solid state reactions between the plutonium and the container wall. Thus the lowest temperature where liquid metal could form in the container system

is over 150°C above the bounding interface temperature during the transport and storage of plutonium. This temperature difference is certainly sufficient to assure the absence of interfacial liquids, even if the plutonium metal makes intimate contact with the stainless steel. However, intimate contact is highly unlikely because of the surface films that will be present on both the plutonium and the stainless steel.

Stainless steel is corrosion resistant because of the chromium rich film that naturally forms and protects the underlying metal from further reaction with the surrounding environment. Plutonium metal surfaces are also covered with a naturally occurring protective film. The surface film, on either or both materials, will prevent or at least limit metal-to-metal contact between the stored plutonium and the container. In the absence of such contact, diffusion of iron, chromium, or nickel from the container into the plutonium is highly unlikely even though vacancy movement may occur in the plutonium. The films will also mitigate any tendency for plutonium to diffuse into the container material. Additionally, even if intimate contact was established between the plutonium and container material, diffusion into the container is not anticipated because the temperatures are too low for significant vacancy migration in the austenitic stainless steel. For example, sensitization of austenitic stainless steel does not generally occur at temperatures below 300°C because of the inability of chromium to diffuse from the austenitic grains into the grain boundaries. This analysis suggests that there will be no solid state reactions between the plutonium and the storage container, a conclusion consistent

Figure 11. The plutonium-iron phase diagram

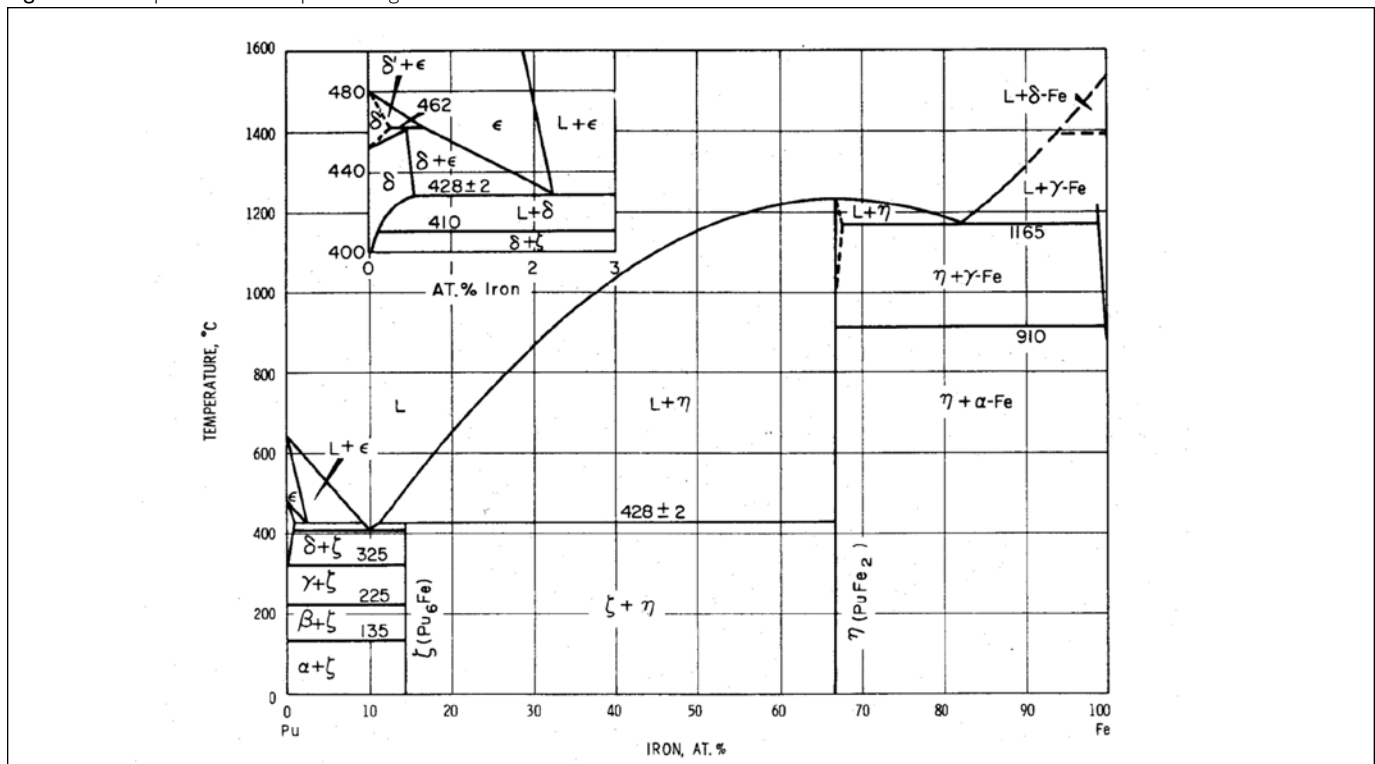




**Figure 12.** Stress-corrosion cracks in 3013 container sections exposed to boiling  $MgCl_2$  Solutions



with observations made for plutonium metals stored in steel containers for decades.

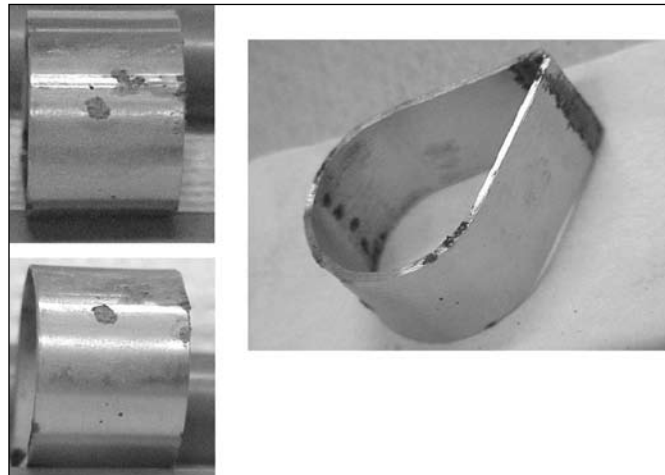
## Corrosion and Corrosion Prevention Topics

### Stress-Corrosion Cracking

The potential for stress-corrosion cracking exists whenever a susceptible material is simultaneously exposed to tensile stresses and an environment that promotes stress corrosion in the exposed material. Chloride environments have the potential to promote stress corrosion cracking in austenitic stainless steels. The plutonium oxide residues within the DOE complex frequently contain chlorides and forming processes used to fabricate the 3013 containers produce high residual stresses in the as-fabricated containers. The presence of high residual stresses was demonstrated by exposing container sections to  $MgCl_2 - H_2O$  solutions boiling at approximately  $150^\circ C$ . These tests caused extensive cracking in the containers (Figure 12). The crack patterns revealed the regions of high residual tensile stresses and outlined the regions in the container expected to be most susceptible to stress corrosion cracking. Knowledge of these locations provided the technical basis to focus the stress corrosion cracking surveillance activities in the susceptible regions.

The amount of water in any storage container is severely limited ( $<0.5$  wt percent) and stress-corrosion cracking of the container walls was not anticipated. However, to demonstrate the lack of stress-corrosion cracking under simulated storage conditions a series of tests were conducted. One group of Type 304 stainless steel tear drop (U-bend) samples cracked within 166 days during exposure to plutonium oxide mixtures containing  $CaCl_2$  salts at room temperature (Figure 13). The moisture content of this test group, 0.6 wt percent, was slightly larger than permitted by the 3013 Standard but the results demonstrate that the potential for cracking in properly packaged 3013 containers may exist. Companion samples of Type 316 stainless steel did not crack after similar exposures. Type 316 stainless steel is known to be more resistant to stress-corrosion cracking than Type 304 but the increase in resistance is often simply a delay in the time to crack initiation and/or a decrease in crack propagation rates rather than immunity vs. susceptibility. Since the exposure times for these tests were less than a year, the absence of cracking in the Type 316 stainless steel samples may not be relevant to a fifty year storage life. The observations of stress-corrosion cracking under unanticipated but

**Figure 13.** Stress-corrosion cracks in type 304L U-bend samples exposed to plutonium oxide-salt mixtures



storage relevant conditions caused the initiation of a test program designed to elucidate the results of this group of tests. Those tests are in progress and will be evaluated as results become available.

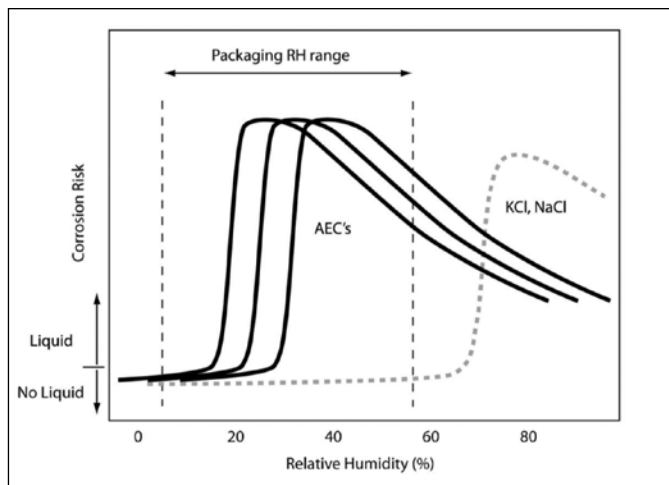
### Relative Humidity

Stress-corrosion cracking is generally thought to be an electrochemical process and as such, an electrolyte is required for cracking to occur. The electrolyte may simply be a monolayer or two of moisture on the surface of the stainless steel but regardless of the amount required, an electrolyte is necessary. Under equilibrium conditions, the distribution of moisture among the various components inside the 3013 container will depend on the relative humidity that is present inside the container. The relative humidity will depend on the amount of moisture contained in the container, the amount of corrosion and irradiation induced hydrolysis that has occurred, the temperature distribution in the container and the amount and types of chloride salts present. The occurrence of stress-corrosion cracking in seemingly dry environments has been known for decades and well-known since the discovery of hot salt stress-corrosion cracking in titanium alloys. However, the knowledge that chloride-induced stress-corrosion cracking occurs in austenitic stainless steels in fairly dry environments is relatively new.

Recent studies have shown that  $MgCl_2$  and  $CaCl_2$  deposits on austenitic stainless steels will cause stress-corrosion cracking at temperatures below  $50^\circ C$  when the relative humidity is barely above the deliquescence relative humidity for the salt. Under these conditions, the tendency for cracking increases as the temperature increases and decreases as the relative humidity decreases. This effect is illustrated in Figure 14. The observations in this published study are consistent with the observation of stress-corrosion cracking in the Type 304 stainless steel U-bend samples exposed to plutonium oxide/chloride salt environments, as observed in the 3013 corrosion program. Because of the importance of relative humidity to stress-corrosion cracking suscep-



**Figure 14.** Conceptual plot of corrosion risk as a function of relative humidity within a container: Curves are shown for alkali chlorides (NaCl, KCl) [dotted line] and for a representative collection of alkaline earth chlorides (labeled AEC's) [solid lines]. Risk is shown as increasing rapidly beginning at the threshold for liquid formation (deliquescence). The range of relative humidity to which material was exposed during packaging is shown for comparison.



tibility, and because the relative humidity inside a 3013 container may be estimated by considering the amount of moisture present in the container along with the container contents and temperature distributions, a program has been initiated to assess the role of relative humidity and packaging conditions in determining the potential susceptibility of a container of plutonium-bearing material to stress-corrosion cracking.

#### Pressure Development: A Gas Generation and Pressure Buildup Topic

The environment inside sealed 3013 containers storing plutonium-bearing materials will change with time because of the alpha radiation and interactions between adsorbed moisture and the stored materials. For example, alpha irradiation may cause radiolysis of adsorbed water to produce hydrogen and oxygen and may also cause radiolytic recombination of hydrogen and oxygen to water. Adsorbed moisture can evaporate, react with plutonium to form plutonium oxide and hydrogen, or with stoichiometric plutonium oxide to form super-stoichiometric plutonium oxide and hydrogen. Gasses such as HCl may be generated in containers having impure, salt containing plutonium oxides and helium is generated by the plutonium decay processes. The DOE-STD-3013 requires that the headspace of each container be inerted to remove all but 5 percent O<sub>2</sub> to limit the amount of reactive gases present. Therefore, there are basically three sources for gas pressure inside the container:

- 1) the container fill gas,
- 2) the gas mixture created by vaporization, radiolysis, desorption, and chemical reactions, and
- 3) helium produced by alpha decay.

The pressures generated by these gasses will depend on the temperature and free volume of the sealed container as well as the number of moles of each gas present in the container. The amount of container fill gas should not change during storage and the alpha decay helium will increase in a predictable fashion. However, the gas mixture created by radiolysis, desorption, and chemical reaction is not readily predictable from first principals but can be modeled based on the results of laboratory testing and analytical assessments.

The free volume inside the sealed inner 3013 container will depend on the volume of the inner container, the volume of the convenience container, and the volume of plutonium-bearing materials loaded into the container. Each of these volumes can be calculated, or accurately estimated, based on container dimensions and the characteristics of the plutonium-bearing materials. For example the volume occupied by a convenience container may be calculated by dividing the container weight by the density of the container material (generally a 300 series austenitic stainless steel) and the volume of the plutonium-bearing material can be calculated in the same fashion except that the particle density may not be accurately known for the impure oxide powders. However, the particle density can be satisfactorily estimated through weight measurements, knowledge of the particle packing factors and an established empirical relationship between bulk density and pycnometer density.

A wide variety of measurements have shown that, typically, the pressure in sealed plutonium-bearing material containers increases slightly with storage time. Originally, over-pressurization of properly packaged containers was considered to be a viable failure mechanism, however, laboratory testing and surveillance data have determined that to be very unlikely. For example, the measured pressure increase with stored containers undergoing surveillance has been less than 20 psi and the pressure increases in laboratory tests at bounding conditions are generally less than 100 psi.

#### Surveillance: A Statistical Approach to Validating Safe Storage

The goal of the surveillance program is to detect any incipient failures in the storage inventory before such failures affect the safety or integrity of the inventory. Safety/integrity issues include container degradation, pressure buildup, and changes in the plutonium-bearing materials or in the storage systems. The packaging and storage requirements were established to minimize, if not eliminate, the potential for safety to be compromised. Therefore, if the packaging requirements program is totally successful, the surveillance program will not identify any issues and may appear inconsequential. However, unforeseen issues often emerge in unique or novel systems and surveillance is necessary to detect and mitigate any unanticipated emergent problem.

The amount or number of surveillances required to assure continuing safe performance in any program depends on sev-



eral factors including: experience, understanding of the factors affecting performance, and the risk involved with unsatisfactory performance. The total risk to the storage program is also the combination of risk factors, including: risk to the general public, risk to workers, economic risks, and perception risks. When dealing with nuclear materials, especially plutonium, economic, and perception risks often overwhelm any physical risks to plant personnel or the general public. Consequently, the success of the surveillance program for the 3013/9975 plutonium storage systems is dependent upon enabling one of two very different statements. The program must be able to conclude that either:

- 1) "We have recently examined the inventory and found nothing," or
- 2) "We detected a potential issue and acted to mitigate the effects of that issue."

The statement, "We examined the inventory several years ago and found nothing," cannot satisfy the perception risk and can create economic risks simply by causing extensive interactions with intervenor groups and regulatory agencies.

The 3013 container surveillance program is based on a statistical approach designed to validate safe storage through both destructive and non-destructive examination of containers from the storage inventory.

The non-destructive evaluations include weight measurements, radiography to determine the condition of the container inventory and the position of container lids and other pressure indicating devices, and visual examinations. Because the corrosion program has identified the most likely sites for corrosion-induced degradation in the 3013 containers, the radiographic studies can focus on these likely sites. The destructive examinations determine the condition of the container walls, the condition of the plutonium-bearing materials, and the pressure and content of gasses inside the storage containers.

## Discussion

The examples of science and engineering activities summarized above demonstrate, to a limited extent, the huge effort that is involved in assuring against failure during prolonged storage of plutonium-bearing materials. Failure prevention in such storage systems is paramount because of the environmental hazard of plutonium. The failure-prevention process involves virtually all aspects of the handling, packaging, and storage processes. For example, the storage containers and packaging processes are designed to meet the intent of the ASME Pressure Vessel Codes and numerous tests are conducted to ensure that containers conform to the appropriate acceptance criteria. Conformance to acceptance criteria is required for the materials selected and used, for the container fabrication processes and, as illustrated in the welding process section of this paper, in weld closures. Visual inspections, metallography, and radiography are used on selected containers to assure that quality welds continue to be made. All

containers are leak tested after welding. Although no significant degradation of the 3013 containers is anticipated, the continuing surveillance program is designed to detect any unanticipated degradation processes in their incipient stages. The use of multi-layer robust containment also assures that even if an unanticipated event compromises the inner containment vessel, plutonium-bearing materials will not be released to the environment.

Potential age-related degradation processes were considered and packaging processes controlled to mitigate, or at least minimize, the potential for degradation. Some potential degradation processes such as solid state interactions between the stored materials and the storage containers could be discounted through analysis and comparison with related experiences. Other processes, such as stress-corrosion cracking could not be totally discounted and laboratory studies were established to help determine which portions of the stored inventory are most vulnerable. The observation of stress corrosion cracking in U-bend samples exposed to chloride containing plutonium oxide mixtures containing only 0.6 wt percent moisture was unexpected at room temperature and within such a short period of time. Because of this observation, extensive new testing and analyses programs were instituted. The literature related to the corrosion and stress corrosion cracking processes is constantly being reviewed and analyzed and laboratory tests are initiated to assess the role of irradiation in accelerating the processes. The results of the corrosion studies are being published in the peer-reviewed literature, as is other work in the failure prevention program.

The surveillance activities demonstrate that seven years of storage has not compromised the integrity of the containers examined. The program also demonstrates that pressure buildup inside the storage containers is not significant and there is no indication that the container pressure will reach the 100 psig maximum conservatively estimated by pre-exposure testing and analysis. The overall results of the surveillance program confirm the quality of the failure prevention program and provide assurance that container degradation is not occurring. However, the unanticipated observation of stress-corrosion cracking in laboratory samples demonstrated the need for continuing surveillance and laboratory testing.

It is significant that this currently very successful failure-prevention program has involved the cooperative efforts of hundreds of investigators from at least ten laboratories within the DOE complex. Discussion, team work, and expert assessment have been the cornerstones of the program. Hopefully, this paper and the compendium of related papers included in this issue and the spring 2010 issue of the *Journal of Nuclear Materials Management* will serve as an example of success through cooperation and demonstrate that failures in nuclear materials storage systems can be prevented through the application of engineering and science to design, fabrication, and operation problems.



## Conclusions

The engineering and science determinations of the behavior of plutonium and plutonium oxide containers provide a technical basis to establish criteria for the packaging and storage of excess plutonium-bearing materials currently in the U.S. DOE inventory. Although this paper outlines only a small fraction of the supporting work, the data and analysis presented demonstrate the long-term safety of materials packaged and stored according to the DOE 3013 Standard. This safety is assured by the prevention of container failures through: 1) the design, fabrication, and robust conservative nature of the 3013 container, 2) the strict plutonium packaging requirements, 3) ongoing laboratory activities that assess the behavior of container materials under simulated and actual storage conditions, and 4) the surveillance and monitoring of the 3013 storage containers.

The optimism expressed in this paper is certainly reflected by the willingness to declare the program to store plutonium-bearing materials a success before the program is completed. However, it is our judgment that the worth of saying, "I told you" based on the results of a strong engineering and science program far exceeds that of an "I told you" after a failure has occurred. We hope that this paper and the associated papers also published in the *Journal of Nuclear Materials Management* will encourage other investigators to describe of how they used engineering and science in failure prevention processes to assure safe and environmentally friendly management of nuclear materials.

*Kerry A. Dunn is an advisory engineer at the Savannah River National Laboratory. She has an M.S. in materials science and engineering and a B.S. in metallurgy from Pennsylvania State University.*

*Gregory T. Chandler is a manager at the Savannah River National Laboratory. He has an M.S. in materials science and engineering from the University of Florida and a B.S. in chemical engineering from Clemson University.*

*Curtis W. Gardner is a manager at the Savannah River National Laboratory. He has a B.S. in electrical engineering from Virginia Polytechnic Institute & State University.*

*Elizabeth R. Hackney is a lead technical engineer at Savannah River Nuclear Solutions. She has a B.S. in mechanical engineering from Vanderbilt University.*

*Gary D. Roberson is a nuclear material manager for the U.S. Department of Energy. He has a B.S. and M.S. in geology from Baylor University.*

*McIntyre R. Louthan, Jr. is a retired consulting scientist at Savannah River National Laboratory. He has a Ph.D. in materials science and engineering from University of Notre Dame.*

*James W. McClard is a fellow technical advisor at Savannah River Nuclear Solutions. He has a B.S. in chemical engineering from Clemson University.*

*Laura A. Worl is a technical staff member in the nuclear technology division at Los Alamos National Laboratory. She has a Ph.D. in chemistry from the University of North Carolina*

## References

1. DOE. 2004. DOE Standard: Stabilization, Packaging, and Storage of Plutonium-Bearing Materials. *DOE-STD-3013-2004*. Washington, D.C.: U.S. Department of Energy.
2. DOE. 1998. Acceptance Criteria for Plutonium Bearing Materials to be Dispositioned by Immobilization, *DOE/MD-0013*, Washington, E.C.: U.S. Department of Energy.
3. Narlesky, J.E., Peppers, L.G., Friday, G.P. 2009. Complex-Wide Representation of Material Packaged in 3013 Containers, *Los Alamos National Laboratory*, LA-14396.
4. WSRC. 2003. Safety Analysis Report for Packaging, Model 9975, *Westinghouse Savannah River Company*, WSRC-SA-2002-00008, Rev. 0.
5. SRNL. 2008. Safety Analysis Report for Packaging – Model 9975, B(M)F-96, *Savannah River National Laboratory*, S-SARP-G-00003, Rev. 0.



# Container Materials, Fabrication, and Robustness

Kerry A. Dunn, McIntyre R. Louthan, Jr., George B. Rawls, Robert L. Sindelar, Philip E. Zapp  
Savannah River National Laboratory, Aiken, South Carolina USA

James W. McClard  
Savannah River Nuclear Solutions, Aiken, South Carolina USA

## Abstract

The multi-barrier 3013 container used to package plutonium-bearing materials is robust and thereby highly resistant to identified degradation modes that might cause failure. The only viable degradation mechanisms identified by a panel of technical experts were pressurization within and corrosion of the containers. Evaluations of the container materials and the fabrication processes and resulting residual stresses suggest that the multi-layered containers will mitigate the potential for degradation of the outer container and prevent the release of the container contents to the environment. Additionally, the ongoing surveillance programs and laboratory studies should detect any incipient degradation of containers in the 3013 storage inventory before an outer container is compromised.

## Introduction

The Materials Identification and Surveillance (MIS) Working Group (WG) is a selected group of technical experts from each of the participating sites within the U.S. Department of Energy (DOE) Complex. These experts are responsible for coordinating and resolving issues associated with the stabilization, packaging, and storage programs for excess nuclear materials in the DOE Complex. The MIS Working Group determined that the only potentially viable degradation mechanisms for the container materials are pressurization due to gas generation and/or corrosion associated with impurities (specifically chlorides and fluorides) and moisture in the plutonium-oxides.<sup>1</sup> The MIS WG was instrumental in identifying critical features of a containment package system to mitigate these potential degradation mechanisms. The packaging features for plutonium-bearing materials are specified in the DOE-STD-3013.<sup>2</sup> These critical features include specifications that:

- The 3013 package shall consist of at least two individually welded, nested containers to isolate the stored materials from the environment.
- The use of an additional container, sometimes referred to as a convenience container, is optional. However, to date, all DOE Complex packaging sites have used convenience containers as the innermost vessel to contain the plutonium-bearing materials.
- The minimum design pressure of the outer container shall

be 4,927 kPa (699 psig). This design pressure is based on the maximum viable pressure that could be reached within the 3013 system and will thus preclude any pressure induced release of the container contents to the surrounding environment.

- All containers must be fabricated of ductile, corrosion-resistant materials, such as 300 series stainless steel.

In addition to the features required of each package, the outer 3013 container was standardized to facilitate compliance with shipping and storage at the different facilities in the DOE Complex. The standardization included dimensions, material type (316L SS), and fabrication method. A typical 3013 container set is shown in Figure 1 which shows an outer container, an inner container, and a convenience container. The convenience container is not a requirement of the DOE-STD-3013, however, it has been used in all cases where plutonium-bearing oxides have been packaged.

The requirements and standardizations provide a robust package designed to contain plutonium-bearing materials for a proposed fifty-year system lifetime. However, to validate the assumptions related to the safety of these containers multi-pronged technical evaluations that include laboratory testing and surveillance activities are conducted.

**Figure 1.** The 3013 container used by Savannah River Site (SRS) for oxides. The outer container is consistent for all packaging sites in the DOE Complex.





## Background

The technical conclusion that the only viable degradation mechanisms for the 3013 containers are pressurization due to gas generation and/or corrosion associated with impurities (specifically chlorides and fluorides) in the plutonium-oxides<sup>1</sup> was based on significant research and development. The 4927 kPa (699 psig) design pressure of the outer container is based on the maximum gas pressure that could develop in a system that contained 0.5 wt percent moisture, was generating 19 watts of heat, and had a gas temperature of 211°C. These conditions provide an upper bound to the conditions that could exist in a properly packaged 3013 container system. Thus, the 4,927 kPa (699 psig) design pressure exceeds the pressure that would develop in a container if all the moisture were converted to gas and the gas temperature was at the maximum conceivable level. Additionally, a number of experiments have been done to measure pressurization<sup>3</sup> as a function of gas composition, time, and temperature. The resultant data convincingly demonstrate that the maximum pressure measured is only a small fraction of the design pressure. Therefore, the pressure boundaries of the 3013 package, as defined in the 3013 standard, are sufficiently robust to contain any pressure that could conceivably develop within the outer container.

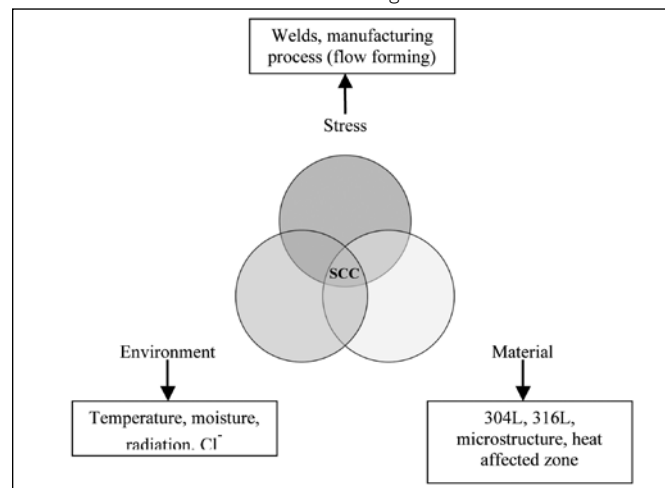
Potential forms of corrosion, the second viable degradation mechanism for the 3013 package, have also been evaluated<sup>4</sup> and include pitting, crevice corrosion, and stress-corrosion cracking (SCC). Corrosion is possible because of the impurities in the plutonium-bearing materials, mainly chlorides and fluorides, and the presence of moisture (an electrolyte) in the container. The DOE-STD-3013 moisture limit of <0.5 wt percent for the material is fairly conservative; however, the presence of chlorides and fluorides along with the very small quantity of moisture is of concern. Literature studies along with laboratory testing and surveillance activities have shown that it is unlikely for crevice corrosion or pitting to penetrate even one barrier let alone the multi-barrier 3013 package.<sup>5</sup>

However, in small-scale laboratory experiments designed to bound the aggressive exposure conditions possible in actual 3013 containers packaged across the DOE Complex, stress-corrosion cracks developed in two Type 304L stainless steel test specimens.<sup>6,7</sup> The significance of these tests is that the cracking occurred at room temperature after only 166 days of exposure. The cracks developed at the plutonium-oxide stainless steel interface and only occurred in test samples exposed in actual plutonium-oxide. Similar samples exposed to surrogate non-radioactive oxides did not crack. Such cracking illustrates the importance of environment-specific testing. The cracking of these laboratory samples was not anticipated and the results suggest that the potential effects of stress corrosion of the convenience can and the inner container must be evaluated to assure that the multi-barrier design provides a robust package that maintains its integrity, even if the inner container should experience stress-corrosion cracking.

## Stress-corrosion Cracking

Stress-corrosion cracking (SCC) is caused by the simultaneous presence of a susceptible alloy, sustained tensile stresses, and a particular environment<sup>8</sup> as shown in a Venn diagram in Figure 2. Remove any one of these parameters and SCC will not occur. A discussion of the 3013 package relative to stress, material and environment is developed below.

Figure 2. Venn diagram showing relationship of stress, environment and material on stress-corrosion cracking.



### Stress

In the 3013 containers, the primary stresses are the residual stresses induced by the forming operations used to fabricate the containers and the residual weld stresses developed by the weld closure operations. Experience has shown that gas pressures that develop in the containers are well below the design pressure and therefore the pressure induced tensile stress imparted to the container is insignificant relative to the residual stresses. The residual fabrication stresses from the forming operation are not well defined but should approach the yield strength of the container material as will the residual weld stresses. Taken together, these residual stresses will provide sufficient stress in any 3013 container to support stress-corrosion cracking should the other two conditions for cracking be achieved.

### Material

Austenitic stainless steels, such as the 300 series stainless steels used for the 3013 containers, are often chosen for applications that require a corrosion-resistant material that is fabricable and weldable. Although generally a good option, the 300 series steels are susceptible to chloride-induced stress-corrosion cracking and sensitization. Sensitization is a metallurgical change that can occur when austenitic stainless steels are heated under conditions that promote the grain boundary precipitation of chromium rich carbides. This precipitation reduces the resistance of the steel





to corrosion and can lead to intergranular corrosion and stress-corrosion cracking in specific environments. Type 316L SS was chosen as the material of construction for the outer container and either 304L or 316L SS was chosen as the material of construction for the inner and convenience containers. The “L” indicates a low carbon content and was selected to minimize the tendency for sensitization, however, it is possible for sensitization to occur in the L grade steels. The heat-affected zones in welded 300 series austenitic stainless steels are often sensitized and, even without sensitization, are often susceptible to SCC. Additionally, annealed microstructures and the microstructures associated with wrought processes such as flow forming are also susceptible to SCC. Therefore, several regions in the 3013 containers are susceptible to chloride-induced SCC. These regions include the closure welds in both the inner and outer containers and the heavily deformed regions of the inner and outer containers as well as the convenience containers. There is also a container fabrication weld in the outer container.

The evaluations of the 3013 container stresses and materials demonstrate that both of these factors place the containers under conditions where SCC is possible if the environment will support the cracking process. Such evaluations provide one of the reasons that the moisture content of the packages is controlled to such a low level and illustrate the significance of the cracking observations in the small scale test specimens.

## Environment

Environmental parameters in the 3013 package include temperature, moisture, radiation, and plutonium-oxide/salt composition. The small scale test results suggest that SCC is possible in a 3013 container. However, to date, SCC has not been observed in any packaged container. Stress-corrosion cracking has only been observed in a laboratory test that exposed highly stressed, welded coupons to plutonium-oxide/salt mixtures at bounding moisture contents. In this focused laboratory setting, only one composition of plutonium-oxide/salt at bounding moisture levels resulted in stress-corrosion cracking. The cracking occurred near the weld interface which was in contact with the plutonium-oxide/salt material. No evidence of SCC was seen in similar laboratory samples exposed in the headspace gas region.

The design of the tear drop laboratory test coupons used in the small scale tests includes a highly stressed region with a weld interface and a potentially sensitized microstructure in the heat affected zone (HAZ) of the weld. There are two significant factors associated with the small scale test results: 1) cracking did not occur in the non-welded regions of the stressed test samples, even though those regions were in contact with the plutonium-oxide/salt mixtures and the stresses in those regions were high enough to support stress corrosion, and 2) no cracking was observed in samples that were not in contact with the plutonium-oxide/salt mixtures. The microstructures in the laboratory coupons corre-

late to microstructures in the nested 3013 containers. However, no welds in the 3013 container configuration are in direct contact with the plutonium-oxide/salt mixture because they are only located in the headspace gas region.

The occurrence of SCC in the small scale test specimens exposed to the plutonium-oxide/salt mixtures at the bounding environmental conditions (except for temperature) was not anticipated. This observation suggests that the environment in the 3013 containers may support SCC under certain circumstances.

The evaluation of the three factors shown in the Venn diagram demonstrates that under conditions that closely correspond to conditions anticipated in some 3013 container systems, stress-corrosion cracking may occur in areas where the plutonium-oxide/salt mixtures contact the container surface. Cracking in the headspace gas regions and other regions where contact is not achieved has not been demonstrated but cannot be entirely discounted at this time. However, because of the nested arrangement of the container system, cracking of the outer container will require the presence of an appropriate environment to crack the convenience container, movement of the environment through the cracks in the convenience container into the inner container and the development of new cracks in the inner container, which propagate through the inner container wall. After the inner container cracks, the environment must reform inside the outer container and another set of new cracks must initiate and propagate. Experimental observations, outlined in the following sections of this report, suggest that this will not occur.

## Cracking Observations

Stress-corrosion cracking in the two 304L stainless steel tear drop coupons only initiated in regions where the samples contacted a plutonium-oxide/2 percent chloride salt mixture (with 0.2 percent calcium chloride) loaded with approximately 0.6 percent water.<sup>6,7</sup> The cracking occurred mainly along the interface between a transverse autogenous weld at the center of curvature of the coupon and the parent metal. The depth of the weld was about half the parent metal thickness. Metallography showed that the highly branched cracks propagated along the parent metal/weld interface, across the weld itself, and finally through the weld into the underlying parent metal. The cracks within the parent metal were transgranular and consistent in appearance with aqueous chloride-induced stress-corrosion cracking of 304L stainless steel.

The teardrop coupons were chosen as a screening test for stress-corrosion cracking because of their compact size, the elimination of a need for hardware or fixturing to maintain a stressed condition, and the ability to simulate the metallurgical conditions and stresses in the containers. The stresses in the sample are a combination of tensile stress developed by clamping and welding the specimen ends to form a teardrop and other residual stresses developed during sample fabrication. A transverse autog-



enous weld was placed on the metal strip before the strip was bent into the teardrop shape. This weld was used to simulate the microstructure of the closure weld in the 3013. Testing of similar teardrop samples in boiling  $MgCl_2$  solutions demonstrated that numerous regions contained stresses sufficient to support stress corrosion. These regions included the autogenous weld, the machined edges of the coupons, the weld made to produce the teardrop shape and the stresses in the U-bend region of the sample. As previously stated, the only area to crack in the plutonium-oxide/salt tests was associated with the autogenous weld where the weld interface contacted the plutonium-oxide/salt mixture. The lack of cracking in the other, very SCC-susceptible areas of the teardrop samples demonstrates the critical role that plutonium-oxide/salt mixture contact plays in the cracking process and suggests that the only regions of the 3013 container system that may be susceptible to SCC in the packaging environments are the regions where such contact exists. This observation demonstrates that the potential regions for SCC may be limited, even though the residual stresses in the 3013 containers are sufficient to support cracking in numerous regions.

The stress in the teardrop coupon is above the yield stress of the non-bent steel,<sup>9</sup> and should be approximately equal to the residual stresses in the 3013 containers because of the severe deformation that accompanies the container fabrication processes. The applied stress from the pressure loading of the containers is at levels much below the yield stress of the material. The pressure boundary on the outer container was built to ASME Code<sup>5</sup> allowable stresses, which are limited to two-thirds of the material yield strength. After the first five years of the Integrated Surveillance Program,<sup>1</sup> forty-three destructive examinations have been performed. The ages of the containers examined ranged from three to six years and all pressures observed have been below 20 psig. This data shows that the pressure levels in the 3013 containers are well below the design pressure further assuring that the applied stress is significantly below the yield strength.

Therefore the main driving force for the stress-corrosion cracking in the 3013 package is the residual stress from fabrication just as the main driving force for cracking of the teardrop samples was residual stresses created by fabricating the tear drop. Sources of residual stress in the containers include the welding operations and the forming operations used to fabricate the containers. The inner containers also include through-wall closure welds that attach the top to the containers. The outer container has two welds. The bottom head is attached to the outer container with a single groove full penetration circumferential butt weld and the lid of the outer container is attached with a full penetration circumferential corner joint weld that seals the container during packaging. The residual stresses created by the container fabrication and welding processes establish numerous regions where the residual stresses are sufficient to support SCC and to determine the "most SCC susceptible" locations in the 3013 containers, a series of tests were conducted in boiling  $MgCl_2$  solutions.

In 2002,<sup>10</sup> a stress-corrosion cracking test was performed for the outer container and more recently in 2009 for the inner and convenience containers.<sup>11</sup> The testing was performed to ASTM G thirty-six using boiling  $MgCl_2$  solutions. Several of the tests were terminated after forty-eight hours. Severe cracking was observed in the container walls, however no leakage of the  $MgCl_2$  was observed through the container. The metallurgical evaluations following the tests confirmed that through-wall cracks were present in the containers. Although these branching, primarily transgranular cracks penetrated the container walls, the crack system was so torturous and the crack openings so small that the  $MgCl_2$  solution did not leak through the crack system. The residual stresses in the container components were the driving force for cracking and the occurrence of cracking illustrates that residual tensile stresses were in excess of 10 ksi.<sup>8</sup> The top closure weld in the outer container has been evaluated using finite element techniques and shown to have residual stress levels as high as yield.<sup>12</sup> This evaluation is consistent with upper bound welding residual stresses at yield levels being used in the pressure vessel and piping industry for the evaluation of crack like flaws. Additionally, when weld heat input is high, the stress distribution can be at yield levels through the wall.<sup>13,14</sup> These observations demonstrate that although the residual stresses in the 3013 containers are high, these fixed displacement stresses do not cause significant crack openings and therefore do not create an easy path for the migration of the plutonium-oxide/salt mixtures.

The residual stress levels resulting from the forming of the convenience and inner container have not been fully evaluated. A literature review, however, indicates the residual stress level resulting from deep draw forming processes can be significant in both the axial and circumferential directions.<sup>15,16</sup> Additional evaluations would be required to quantify the forming residual level in the convenience and inner containers. Analysis of the metallurgical data that is currently available from the destructive examination being performed as part of the 3013 Surveillance Program will provide qualitative evidence of the presence of forming residual stress. A review of the fabrication procedures could provide a qualitative assessment of forming residual stress in the convenience and inner container. However, regardless of the outcome of these evaluations, the  $MgCl_2$  tests have demonstrated that residual stress driven cracks in the containers will provide relatively tight, tortuous paths, even if they should penetrate the container wall.

Quantifying the residual stress magnitude in the 3013 package remains a priority because such quantification would allow direct comparisons with stress corrosion testing as performed in the tear drop test<sup>9</sup> and better define the potential for crack openings as the residual stress fields redistribute during the cracking process. The stress analysis of the teardrop coupon showed that the Von Mises stress at the location of the crack was approximately 70,000 psi. This stress is slightly above the yield stress of the parent metal, which was assumed in this analysis to be 66,000 psi, before the metal is deformed into the tear drop shape.



The stress analysis showed further that the maximum Von Mises stress in the coupon was not found at the center of curvature, but rather was found to be about 93,000 psi at the *shoulders* of the coupon, due to the cold working operation as the metal is bent into the teardrop shape. The observation that the cracks in the teardrop samples exposed to plutonium-oxide/salt environments developed near the weld, rather than in the highest stress regions suggests that the welding process increased the material susceptibility to cracking. Increases in SCC susceptibility have been observed in SCC situations where weld-induced alterations in the microstructure of the material are present.

The experimental observations of cracking in the teardrop samples and the 3013 container sections provide a technical basis to conclude that if stress-corrosion cracking does occur in the 3013 container system, the cracking will:

- 1) Occur in regions where the container material is in contact with the plutonium-oxide/salt mixtures, and
- 2) Produce a torturous crack path with minimal crack openings, even if the container wall is breached.

These conclusions, as will be further discussed in the next section, demonstrate that the nested, multi-barrier 3013 container design virtually precludes the initiation of SCC in the outer container.

### Multi-Barrier Container Arrangement, Welds, and Stress-corrosion Cracking

A detailed summary of each of the DOE Complex packaging site's 3013 container configuration and its corresponding weld regions are provided in Table 1. A subset of Hanford and SRS containers is expected to represent those containers with the highest potential for SCC due to relative humidity conditions at loading. The 3013 container configuration is a robust package because of the multiple barriers that contain plutonium-oxide against release to the environment. Although the mechanism by which the observed SCC occurred is not fully understood, current data from the experimental program supports the conclusion that SCC of the containers requires that the plutonium-oxide material to be in contact with a high stress region of the 304L and 316L stainless steel materials.<sup>6,7</sup> This conclusion is further supported by the fact that SCC has not been observed in the headspace gas region with any of the numerous 3013 corrosion tests conducted at SRNL or LANL.<sup>17</sup>

When considering the potential for plutonium-oxide material to transfer from one container to the surrounding container, each site's storage configuration and container design, including welds, need to be considered. There are no welds in several of the convenience containers used for packaging the plutonium-bearing material. These convenience containers provide a barrier to material contact with the 3013 inner container. The Hanford

**Table 1.** 3013 container assemblies used at RFETS, SRS, and Hanford. The containers are nested in the following order: CC - convenience container; IC - inner container; OC - outer container. A short description of each container is given along with the welds.

RFETS and LLNL Configuration		
	Container Description	Weld Description
CC	BNFL convenience container body 316 SS sheet with container threads that are 316 SS bar. The threads are silver plated threads to mitigate galling. Threaded lid is fabricated from Type 416 SS bar to permit remote handling via magnetic mechanism.	Smooth (on external surface) and continuous full penetration weld on the container body ~6.5" from bottom of container. No closure weld.
IC	BNFL inner container ASTM A240 316 SS. IC lid also ASTM A240 316 SS.	Hollow plug press fit into inner container to allow for laser closure weld. No container fabrication welds.
SRS configuration		
	Container description	Weld Description
CC	SRS convenience container 304L SS with threads. Threaded 304L SS lid with slots in screw threads to facilitate venting.	Fabrication method for container was flow-forming method. Threads of the container were machined once the container was formed. There are no welds in either the container or lid.
IC	Bagless transfer inner container 304L SS with low sulfur content fabrication using precision flow-forming, IC lid also 304L SS	No fabrication welds in the container. GTAW closure welded only
Hanford configuration		
	Container description	Weld Description
CC	Hanford convenience container. Very similar to the SRS convenience container. Lid material is 304/304L and contains vent filter.	Lid has vent filter welded in place via a seam fusion weld. Seam weld on exterior of lid and does not penetrate through wall. No welds in container.
IC	Bagless transfer inner container 304L SS with low sulfur content. Container body fabrication using precision flowforming. IC lid also 304L SS.	No fabrication welds in the container. GTAW closure welded only.
Outer container description		
OC	BNFL outer container body 316L SS seamless pipe, base is 316L SS plate and lid 316L SS plate.	Smooth and continuous full penetration autogenous weld ~0.5" from bottom of container to connect container body to base cap. Lid press fit into body and laser (RFETS & LLNL) or GTAW (SRS & Hanford) closure welded.

convenience container lid contains a filter for venting. The filter is attached to the container using a seam fusion weld. The SRS convenience container lids contain notches for venting purposes. The seam weld on the Hanford convenience container filter is initiated on the external side of the convenience container lid, is



not through wall, and therefore, it is not in direct contact with plutonium-oxide powder. In the SRS convenience containers the notch may allow for some small amount of plutonium-oxide material to transfer into the inner container. It is expected that this material will settle at the bottom the inner container away from the closure weld region that is considered to have the most SCC susceptible microstructure in the container. Basically, however, the transfer of significant quantities of plutonium-oxide into the inner container of either the Hanford or SRS packages requires a breach of the convenience container.

The residual stresses in the convenience containers<sup>11</sup> are sufficient to support SCC in boiling  $MgCl_2$  solutions, however a susceptibility to cracking in relevant plutonium-oxide/salt/moisture environments has not been demonstrated. The only plutonium-oxide induced cracking that has been observed has occurred in near weld regions, even when these regions contained lower stresses than were present in non-cracked regions of the same samples. This observation suggests that the stress level is less significant than the metallurgical condition of the material that results from a welding operation. Therefore, the 3013 packaging process results in the plutonium-bearing materials being in direct contact with low susceptibility regions of the convenience containers and stress-corrosion cracking of the convenience containers is not expected. However, in order to conservatively assess the robustness of the 3013 package, a through-wall crack due to stress-corrosion cracking of a 3013 convenience container is postulated. Intuitively, a through-wall crack may provide a path for potential material transport through the container. However, because of the tight, torturous path created by the stress corrosion crack, the transport of oxide and salt particulates through a SCC in a 3013 container is not considered credible.

Stress-corrosion cracks have occurred in stainless steel piping in aqueous systems and in laboratory experiments. As a result, models have been developed to evaluate water leakage through such cracks in leak-before-break demonstrations.<sup>18</sup> Although not directly applicable to the analysis of particulate transport, the mechanistic description of water flow through a stress-corrosion crack with an area controlled by crack length, pressure loading, and material compliance, with flow rates directly related to stress-corrosion-crack tortuosity and the fluid velocity regime, is relevant to an assessment of particulate transport.

A through-wall crack in a material is opened (crack opening displacement) under membrane and bending stresses. The amount of opening is depending on the crack length and stress level.<sup>18</sup> That is, a crack that has grown under a residual stress field cannot be opened unless a sustained pressure loading is present or the residual stress is not significantly relieved by crack propagation. Furthermore, the channel traversing the section of steel is not smooth—the morphology of stress corrosion cracks in stainless steel show crack paths to be comprised of numerous turns and branches along the crack channel as observed in the SRNL results.<sup>18</sup> Particles of plutonium-oxide at sizes even well below the

typical stainless steel container material grain sizes of 25-50  $\mu m$  could not be expected to pass through the crack channel. In addition, a driving force would be needed to move a particle through the crack channel. Only entrainment in a fluid flow (e.g., water or high velocity gas) could provide a driving force on the particle.

This case is not credible in any of the containers in the 3013 system, first because high gas pressures have not been observed and second because any gas pressure loading on a crack would be expected to be quickly relieved without any significant transport of material from one nested container into the next. Additionally, because of the Hanford filter and the SRS notches, neither of those convenience containers is capable of pressurization, which means that entrainment of particulates through stress corrosion cracks in those containers is not credible. Therefore, bulk transport of oxide and salt particulate material through a stress corrosion crack without wide openings due to high membrane stresses and sustained flow is not feasible. As discussed earlier, the applied stress due to pressure is much below the yield stress of the material and even if high pressures did develop those pressures would dissipate as soon as the container wall was breached. Additionally, a sustained pressure would be needed to keep the crack open. This conclusion is supported, in part, by the observations in the  $MgCl_2$  test of the outer container that showed that a high-viscosity solution ( $MgCl_2$ ) did not leak through a container.<sup>6</sup>

Additionally, because of the ductile nature of 304L and 316L stainless steels, the container will not fall apart or crumble, even if a crack is present in the 3013 containers. This is a common and well known metallurgical phenomenon. The integrity of the convenience container, because it is austenitic stainless steel, is adequate to maintain the containment of the plutonium-oxide material, except for contamination levels and the inner container provided yet another barrier to reaching the outer container. Therefore, it is not likely that the quantities of plutonium-oxide/salt mixtures necessary to initiate SCC will reach the inside of an outer 3013 container packaged at any of the packaging or storage sites. To reach the outer container the plutonium-oxide must transfer from the convenience container into the inner container in sufficient quantities to create a through-wall SCC then transfer enough material to the outer container to create another SCC. A single crack initiation-material transfer process is, for reasons described in this report, unlikely, and the possibility that the initiation/transfer event will occur multiple times in a 3013 container system is not considered credible.

## Conclusion

Evaluations of the container materials, fabrication, and residual stresses in the 3013 package suggest that the multi-barriers and robust nature of the system will mitigate the potential for degradation of the outer container even though stress-corrosion cracking was observed in small scale laboratory coupons. The technical basis for this conclusion is focused on the following:



- The robust, multi-barrier nature of the 3013 container system, monitored through the surveillance program, should preclude a breach of the outer container.
- Transport of oxide and salt particulates through a stress corrosion crack in a 3013 container is not credible.
- Regardless of whether a crack is present in any of the 3013 containers, the ductile nature of 304L and 316L stainless steels prevents the container from falling apart or crumbling.
- Welds, which are known to contribute high residual stresses and potentially stress-corrosion cracking susceptible microstructures, are not present in the convenience container.
- Plutonium-oxide material is not in contact with welded region of inner container, the area most susceptible to stress-corrosion cracking.

This technical basis is also supported by other observations, including the facts that:

- The cracks were observed in Type 304L stainless steel, which is more susceptible to stress-corrosion cracking than the Type 316L stainless steel used to fabricate the outer 3013 containers.
- Cracking was observed in the oxide/coupon contact region for only one composition of oxide salt. In previous corrosion studies, many other samples have been exposed to salt bearing, plutonium-oxide materials and no evidence of stress-corrosion cracking was found.

However, an evaluation of the SCC behavior and the potential for SCC within the 3013 package headspace is continuing because of the importance of the conclusion that, under 3013 relevant conditions, contact with salt material in an aqueous solution is necessary for cracking to occur.

*Kerry A. Dunn is an advisory engineer at the Savannah River National Laboratory. She has an M.S. in materials science and engineering and a B.S. in metallurgy from Pennsylvania State University.*

*Philip E. Zapp is a fellow engineer at Savannah River National Laboratory. He holds a Ph.D. in metallurgical engineering from University of Illinois at Urbana-Champaign, and a B.A. in physics from Cornell University.*

*Robert L. Sindelar is an advisory engineer at Savannah River National Laboratory. He holds a Ph.D. in nuclear engineering from the University of Wisconsin.*

*McIntyre R. Louthan, Jr., is a retired consulting scientist at Savannah River National Laboratory. He has a Ph.D. in materials science and engineering from University of Notre Dame.*

*James W. McClard is a fellow technical advisor at Savannah River Nuclear Solutions. He has a B.S. in chemical engineering from Clemson University.*

## References

1. LANL. 2001. Integrated Surveillance Program in Support of Long-term Storage of Plutonium-Bearing Materials. *Los Alamos National Laboratory*, LA-UR-00-3246, Rev. 1.
2. DOE. 2004. DOE Standard: Stabilization, Packaging, and Storage of Plutonium-Bearing Materials. *DOE-STD-3013-2004*. Washington, D.C.: U.S. Department of Energy.
3. Veirs, D. K. 2004. Gas Generation and Corrosion in Salt-containing Impure Plutonium Oxide Materials: Initial Results for ARF-102-85-223, *Los Alamos National Laboratory*, LA-14148.
4. Kolman, D. G. 1999. An Assessment of the Corrosion, Stress-corrosion cracking, and Embrittlement Susceptibility of 3013 Storage Containers, *Los Alamos National Laboratory*, LA-UR-98-5762.
5. Lillard, R. S., D.G. Kolman, M. A. Hill, M. B. Prime, D. K. Veirs, L. A. Worl, and P. E. Zapp. 2009. Assessment of Corrosion-Based Failure in Stainless Steel Containers Used for the Long-Term Storage of Plutonium-Based Salts, *Corrosion*, Vol. 65, No. 3.
6. Duffey, J. M., and P. E. Zapp. 2008. Status Report for SRNL 3013 Corrosion Tests, *Savannah River National Laboratory*, WSRC-STI-2008-0046.
7. Zapp, P. E., J. M. Duffey, K. A. Dunn, R. R. Livingston, and D. Z. Nelson, 2009. Localized Corrosion of Austenitic Stainless Steel Exposed to Mixtures of Plutonium-Oxide and Chloride Salts, *NACE International Corrosion Conference 2009*, Paper No. 09409.
8. ASM International. 1987. *Materials Handbook, Volume 13, Corrosion*, ASM International.
9. Lam, P-S. 2008. Initial Stress in Tear Drop Corrosion Specimens, *Savannah River National Laboratory*, SRNL-MST-2008-00032.
10. Dunn, K. A. 2004. Residual Stress Testing of Outer 3013 Containers, *ASME Conference Proceedings*, 155(2004).
11. Mickalonis, J. I. 2009. Assessment of Residual Stresses in SRS and Hanford 3013 Inner and Convenience Cans, *Savannah River National Laboratory*, SRNL-STI-2009-00121, Rev. 0.
12. T-ESR-G-00004 Evaluation of Weld Porosity of the 3013 Container Closure Weld April 23, 2002
13. ASME Boiler & Pressure Vessel Code, Section VIII, Division 1, Rules for the Construction of Pressure Vessels, 2007. ASME.
14. ASME FFS1 Fitness-For-Service, Second Edition, 2007. ASME.
15. Gnaeupal-Herold, T., T.Foecke, H. J. Prask, and R. J. Fields, 2005. An Investigation of Springback Stresses in AISI 1010 Deep Drawn Cups, *Material Science and Engineering A Structural Materials Properties Microstructure and Processing*, Volume 399.



16. Berrahmoune, M.R., S. Berveiller, K. Inal, and E. Patoor. 2006. Delayed Cracking in 301LN Austenitic Steel after Deep Drawing, *Material Science and Engineering A Structural Materials Properties Microstructure and Processing*, Volume 438.
17. Zapp, P. E. and R. R. Livingston. 2005. Corrosion Tests of 304L and 316L Stainless Steels for the 3013 Container, *Savannah River National Laboratory*, WSRC-TR-2005-00191, Rev. 0.
18. WSRC. 1990. Reactor Materials Program – Single Phase Leak Rates Through Intergranular Stress Corrosion Cracks, *Westinghouse Savannah River Company*, WSRC-RP-90-93.
19. Zahoor, A. 1989. Ductile Fracture Handbook: Volume 1 Circumferential Through-wall Cracks, *Electric Power Research Institute, Inc.*, Palo Alto, CA, NP-6301-D, N14-1.



# Closure Weld Development for 3013 Outer Containers

William L. Daugherty, Stanley R. Howard, Kurt D. Peterson, and Mitchell W. Stokes  
Savannah River National Laboratory, Aiken, South Carolina USA

Gary R. Cannell  
Fluor Enterprises, Inc., Greenville, South Carolina USA

Scott A. Breshears  
Los Alamos National Laboratory, Los Alamos, New Mexico USA

## Abstract

Excess plutonium materials in the U.S. Department of Energy (DOE) Complex are packaged and stored in accordance with DOE-STD-3013. This standard specifies requirements for the stabilization of such materials and subsequent packaging in dual nested seal-welded containers. Austenitic stainless steels have been selected for container fabrication. The inner 3013 container provides contamination control while the outer 3013 container is the primary containment vessel and is the focus of this paper. Each packaging site chose a process for seal welding the outer 3013 containers in accordance with its needs and expertise. The two processes chosen for weld closure were laser beam welding (LBW) and gas tungsten arc welding (GTAW). Following development efforts, each system was qualified in accordance with DOE-STD-3013 prior to production use.

The 3013 outer container closure weld joint was designed to accommodate the characteristics of a laser weld. This aspect of the joint design necessitated some innovative process and equipment considerations in the application of the GTAW process. Details of the weld requirements and the development processes are presented and several potential enhancements for the GTAW system are described.

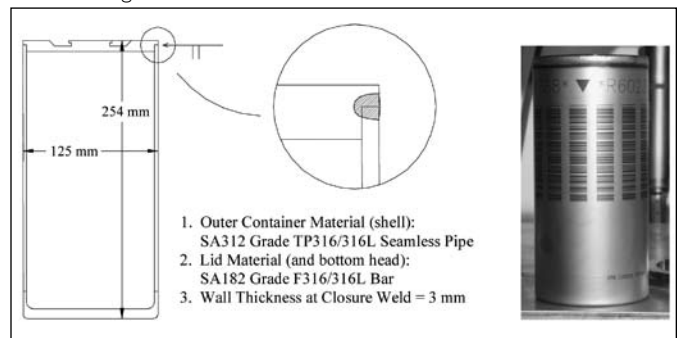
## Introduction and Background

DOE-STD-3013<sup>1</sup> governs the stabilization and packaging of plutonium-bearing materials within the U.S. Department of Energy (DOE) Complex. This standard specifies that the material be stored in two nested containers that are fabricated from a ductile, corrosion resistant metal or alloy and seal welded. Austenitic stainless steels (Types 304L and 316L) were selected for container fabrication. Furthermore, material shipped to the Savannah River Site for storage must meet requirements<sup>2</sup> in addition to those specified in the 3013 standard. The integrity of containment is assured through the container design, material specification and fabrication requirements, closure weld integrity, and post-closure testing. This paper focuses on the closure weld integrity for the outer

container, and the weld systems that have been developed to provide an acceptable closure weld.

The corner joint of the 3013 outer container is formed by pressing an interference-fit (nominally 0.04 mm interference) lid into the container, creating a square-groove, weld preparation (Figure 1). The closure weld is made autogenously (without addition of filler).

Figure 1. Sketch of 3013 outer container (left) and photo container after welding



## Description of Closure Weld Systems

Five sites within the DOE complex have packaged plutonium-bearing materials in accordance with DOE-STD-3013. Rocky Flats Environmental Technology Site (RFETS) and Lawrence Livermore National Laboratory (LLNL) used a laser beam welding (LBW) system, while Hanford Site (Hanford), Savannah River Site (SRS), and Los Alamos National Laboratory (LANL) used a gas tungsten arc welding (GTAW) system.

The LBW system was developed by British Nuclear Fuels Limited (BNFL), which also established the design details for the outer container. As the first site to begin packaging excess plutonium material, RFETS used the BNFL system, which was originally envisioned for use throughout the DOE complex. However, because of site-to-site differences in expertise and economic considerations, alternate weld closure solutions were developed and deployed. The weld closure systems that emerged include:

1) Rocky Flats Environmental Technology Site: The RFETS



system was a fully automated, glovebox enclosed system that integrated plutonium stabilization operations with packaging the material in both the 3013 inner and outer containers. The LBW system used a 2 kW Nd:YAG laser for both the inner and outer container closure welds. A packaging control system controlled the closure weld process, and a data management system provided some data collection capability.<sup>3,4</sup>

- 2) Lawrence Livermore National Laboratory: LLNL chose to use the same laser technology, but incorporated several modifications. The LLNL system used much less automation, and changed some of the weld parameters (slower speed, increased power) to improve the weld bead shape.<sup>4,5</sup>
- 3) Hanford Site: Hanford decided to pursue the development of a GTAW system, and contracted with Savannah River National Laboratory (SRNL) for this effort. It was believed that a *hands-on*, less complex system would provide a more robust process (i.e., more forgiving of minor process variations), which would better support Hanford's plutonium packaging cost and schedule requirements.

The Hanford system consisted of standard off-the-shelf orbital GTAW equipment modified to accommodate the outer container design, including the addition of a copper alloy chill block, modifications to the clamping system, the use of a thoriated (2 percent ThO<sub>2</sub>) tungsten electrode and other mechanical features. In addition, a data acquisition system (DAS) was developed.<sup>6,7</sup> The DAS acquired information to assure that proper process control was maintained throughout the welding process. The actual weld sequence was programmed to proceed automatically, but all other mechanical operations were performed manually.

- 4) Savannah River Site: SRS used the GTAW technology that was developed for Hanford, with several improvements based on the experience at Hanford. The system retained the same degree of manual operation and the DAS was upgraded to capture more weld process information. During initial testing, a number of weld failures (blowouts) were experienced due to the pressure developed in the container interior. Insertion of the container lid increases the internal pressure to above atmospheric and this pressure can increase further as the weld operation heats the container. Occasionally the internal pressure reached the point that a weld blowout occurred and elimination of such blowouts presented an operational challenge to the welding process. This challenge was addressed by backfilling the container with less than 760 torr (1 atm) pressure, so that inserting the interference-fit lid would create an internal pressure just above, but not significantly greater than 760 torr (1 atm).
- 5) Los Alamos National Laboratory: LANL developed its own closure weld system based on GTAW technology. The LANL system used a fixture to rotate the outer container during welding. The weld head and fixture were located inside a welding enclosure (similar to a small glovebox) with

a helium atmosphere. This ensured that the container was filled with 100 percent helium. The interference fit between the body and the lid was overcome by heating the top of the body to about 120°C (250°F) with a band heater; thermal expansion then allowed the lid to be seated manually through a gloveport.

Each of these DOE sites pursued the development and/or acquisition of a closure weld system that was consistent with their expertise, needs and available resources. Each system offered advantages, and performed the assigned mission.

Following their respective development, each of the closure weld technologies (LBW, GTAW) underwent testing to demonstrate the closure system met the requirements of References 1 and 2. This included 9.1 m (30 ft) drop tests (dropping a container onto a flat surface), 3 m (10 ft) crush tests (dropping a container onto a second container), hydrostatic proof and burst testing, metallographic and radiographic examination, and stacking (stack of multiple containers) tests. Leak tightness had to be demonstrated following the drop, crush, proof, and stacking tests.

At each site, the outer container welder (OCW) underwent an initial qualification run, as required by the governing standard,<sup>2</sup> before it was placed into production. This run consisted of completing twenty-five successive successful welds, and performing subsequent analysis to demonstrate the integrity of all twenty-five welds. This analysis included:

- Visual examination of closure weld
- Leak test of the sealed container
- X-ray examination of the entire length of closure weld
- Metallographic examination of four (or more) cross-sections through the closure weld

## Post-Weld Quality Checks

Once approved for production use, every container that is successfully seal welded receives several inspections to ensure its integrity. These inspections include the following:

- The data acquisition system report is reviewed to verify that the weld parameters were within established ranges.
- The weld receives a visual inspection for surface flaws or discontinuities.
- The container, which was filled with helium prior to welding, is placed under a belljar for a helium leak test. Separate criteria are used to identify gross leakage and fine leakage. The leak rate must be < 2.0 E-7 std cc He/sec, per ANSI 14.5.
- In order to fit within a shipping package, the container must meet strict dimensional requirements. The height and diameter are verified to meet these requirements. (A small relaxation of the diameter requirement was approved for RFETS.)



Beyond these minimum requirements, LANL also recorded a video of each production weld, both during the weld and after the weld was completed. SRS performed digital radiography on every closure weld, to screen for unacceptable porosity or other internal defects.

As a minimum, every twenty-fifth production weld is made on a container with surrogate content. After all other inspections are completed, the lid (with the closure weld) is separated from the outer container. The closure weld is x-rayed and sectioned for required metallographic examination.<sup>2</sup> The x-ray examination is conducted and evaluated in accordance with ASME Section VIII, Division 1, UW-51 (7.3). The metallographic examination interrogates the weld cross-section at four (or more) locations, and must show full penetration, be free of cracks and lack of fusion (at 10X magnification), and have a weld bead geometry in compliance with ASME Section VIII, UW-13.2 (d). RFETS received relief from the weld bead geometry requirement,<sup>4</sup> which evolved from arc welding processes and is difficult to meet with a highly focused laser weld. This is one reason that LLNL changed the welding parameters from those used at RFETS.

### Process Challenges Inherent to Each System

There are inherent differences between the LBW and GTAW systems that presented both opportunities and challenges in meeting the requirements of the 3013 closure. Some of these include:

- The LBW system is more complex than a GTAW system. In the RFETS system, several integrated functions were housed together. Activities such as content stabilization, container loading, inner can welding/cutting were interconnected, with a chain of automation that hampered reliability and increased operational difficulties. As a result, this system was unreliable and difficult to operate.<sup>3</sup>
- The relative simplicity of the GTAW system led to lower capital and maintenance costs. It also reduced down-time and supported a more aggressive packaging schedule.
- The LBW system was capable of faster welding speed and demanded less heat input, so the welded canisters required less cool-down time before post-weld operations. However, integration with other controlling steps such as nuclear accountability negated much of the production rate advantage.
- GTAW is a mature technology, with a long history of use in similar applications. Some of the sites had a greater institutional familiarity with this technology, and were therefore more comfortable in its use.
- The LBW produces a weld bead with a narrower/deeper aspect ratio than GTAW. This created a challenge for the LBW systems in meeting the ASME Section VIII, UW-13.2(d) requirement. The same weld bead dimension requirement created a challenge for the GTAW systems to achieve full joint penetration without melting into the top edge of the lid.

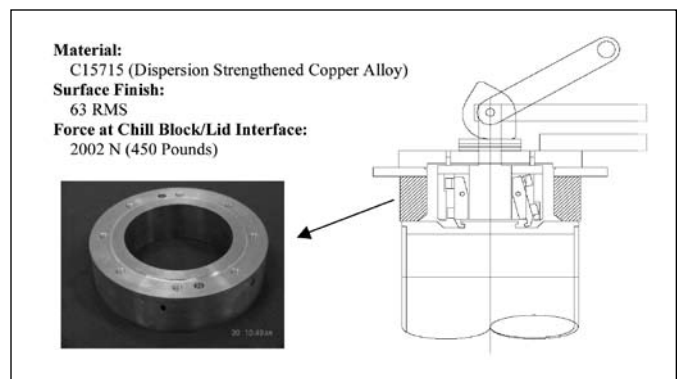
Aside from the above issues that are specific to the 3013 outer container closure, each weld system had several challenges based on its particular characteristics. For the LBW systems, the challenges included energy dispersion from plume disturbance, beam to surface coupling, control of pool depth, personnel protection controls, gas entrapment (porosity) issues, and underbead inconsistencies. For the GTAW systems, the challenges included achieving the correct depth to width profile, gas coverage, gas entrapment (porosity) at overlap areas, and depth of penetration.

The challenges presented to both technologies by the ASME Section VIII, UW-13.2(d) requirement were met in different ways. RFETS was granted regulatory relief from the requirement. LLNL successfully met the requirement for weld bead aspect ratio by implementing a reduced weld speed and increasing the heat input. The challenges this requirement presented to GTAW systems were different. The aspect ratio for the weld bead is relatively easy for a GTAW system to meet, but the closure joint design provided inadequate space for the relatively wide GTAW weld bead. This was addressed primarily through the use of a chill block, as discussed in the next section.

### Development Efforts for GTAW Systems

The 3013 outer container closure, designed for LBW, incorporates a corner joint placed very close to the top edge of the container (Figure 1). This placement was selected because the LBW weld profiles are characterized by a relatively small weld width to depth aspect ratio that allows the weld to be readily made without melting the lid edge. However, GTAW welding tends to produce welds having a larger aspect ratio. Because of the closure joint placement, the requirement to not consume (melt) the lid edge necessitated additional development activities to produce an acceptable GTAW weld. It should be noted that redesign of the 3013 Outer Container closure joint, to accommodate the typical GTAW weld profile, was not an available option. The following describes some specific modifications and other activities performed during development of acceptable weld processes using the GTAW systems.

Figure 2. Chill block sketch and details





The Hanford and SRS systems used an off-the-shelf orbital weld head, modified to incorporate a dispersion-strengthened copper alloy chill block (Figure 2). The chill block, which coupled to the top of the container, removed excess heat at the lid corner, restricting bead width and thus preventing melting of the lid edge. In addition, the chill block helped register and align the closure joint to the electrode. The container was welded while in an upright position, such that the weld was made on a vertical surface moving in a horizontal plane (2G position).

A series of test welds designed to identify welding parameters that would produce the needed bead shape (small aspect ratio) was performed. The test welds were designed to evaluate electrode materials, shielding gases, and other parameters affecting bead shape. Based on the results of these tests, a 2 percent thoriated tungsten electrode material and 2.6 – 2.9 percent hydrogen (argon remainder) shielding gas were selected for this pulsed arc weld. A parametric study was then conducted to optimize the weld parameters (current, arc gap, travel speed). The weld schedule synchronized the pulsed weld current with the stepped advance of the electrode. This allowed a high current while controlling the weld pool freeze rate to improve the width to depth aspect ratio.

The LANL system used an automated GTA welder mounted on a three-bar fixture that was used to rotate the container. The container was on its side so that the weld was made on a horizontal surface (1G position). A copper chill block wrapped around the container body and another cooled the lid. The lid/container cooling induced by these copper chill blocks prevented consumption of the lid edge during the welding operation.

The LANL system provided programmable control of the electrode position. The weld process was completed within a helium-filled weld enclosure to ensure helium content in the container after weld completion. Development tests with this system led to the selection of a 1.5 percent lanthanated tungsten electrode material and helium shielding gas. Weld data collection included arc current and voltage, rotation (travel) speed, and electrode position.

The effects of sulfur on bead penetration and shape in fusion-welded austenitic stainless steels are well documented.<sup>8</sup> To limit the potential for variation in bead shape and penetration, testing was performed to identify acceptable levels of sulfur. From this work, sulfur limits more restrictive than those specified in the general material specification were established. The limits are: 50 – 250 ppm sulfur in the shell and 100 – 250 ppm sulfur in the lid.

The evaluation of early Hanford production welds showed that weld penetration was relatively low near the weld start, and increased as the weld advanced along the joint. To increase the tendency toward deeper weld penetration, a preheat phase was added at the weld start location, and the weld speed was reduced for the first several inches of travel. The LANL system maintained a single weld speed, but improved the initial depth of penetration with a two second preheat at the weld start.

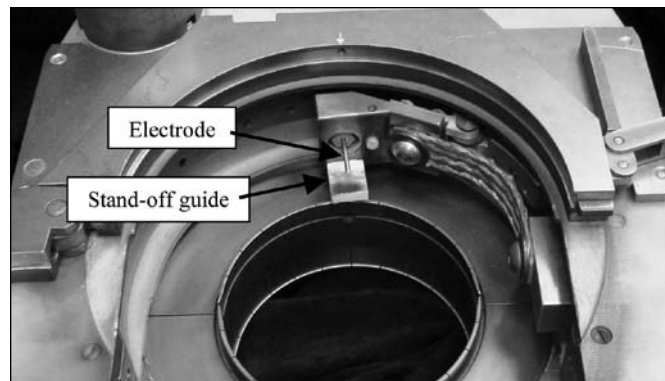
Because there is an interference fit between the lid and the container body, pressure buildup in the container can occur as the lid is pressed into position and increase further during welding, as the internal gases heat up. On occasion, this internal pressure would affect the molten weld puddle, creating a weld void defect. This was addressed in the SRS system by backfilling the container to a pressure slightly less than atmospheric prior to pressing the lid. The LANL system approached this issue differently, by adding a small vent path to the lid. The vent was positioned to be welded closed at the end of the weld sequence. Both of these methods effectively eliminated weld defect issues associated with internal pressurization.

### Improvements for Next Generation GTAW System

With the planned construction of a new facility at SRS that will handle and package plutonium materials, the SRS GTAW system has been reviewed, and potential improvements identified. Development efforts have begun on several such improvements, including:

- Arc length controller—Occasional loss-of-arc upsets to the GTAW process were observed during the outer container welding campaigns. These upsets were typically arc initiation failure, arc loss, or stub-out (contact between the electrode and weld pool). A portion of these upsets were attributed to variations in the gap between the outer container surface and the electrode. An “arc length controller” (Figure 3) was developed to provide a more consistent arc gap by providing a constant standoff from the weld joint surface. The arc length controller includes a spring-loaded compliance mechanism with a standoff guide that allows the electrode to follow the outer container contour and maintain a consistent arc gap throughout its orbit, regardless of variations in can-to-weld-head alignment.

Figure 3. Arc length controller installed in the SRS GTAW weld head





Limited testing of the arc length controller mechanism indicates that it reduces failures relating to arc initiation, arc loss and stub-outs. Maintaining a consistent arc gap may also be expected to result in a more uniform weld profile, though this attribute has not been evaluated yet. The validity of the arc length controller design has been demonstrated, but additional work is needed to make it more robust for a production environment.

- Vented lid—Most of the outer containers that were welded during development of the arc length controller utilized the LANL vented lid design. No defects from internal pressure occurred during this period. Although the number of containers welded during these tests was insufficient for meaningful comparison with the occurrence of such defects in production, plans are to adopt the vented lid for future campaigns to eliminate the need to closely control the helium pressure prior to pressing the lid into place.
- Increased current—Limited testing was performed to investigate the impact of increased weld current on the outer container weld profile, especially with respect to penetration. As expected, the containers welded at higher current levels exhibited greater average penetration and greater penetration at the minima locations.

However, higher current also generated a wider weld bead, the edge of which increasingly approached the top edge of the lid as current was increased. Since the outer container weld is performed in the 2G position at SRS, increased weld current can increase the sag of the weld bead. Excessive sagging of the weld bead can cause the finished outer container to exceed the maximum allowable diameter. Additional testing is needed to optimize the weld current. The greater margin of penetration produced by higher current must be balanced with a) the diminished clearance between the weld bead and the top edge of the lid, and b) the increased sagging of the weld bead potentially exceeding the maximum allowed diameter.

- Rewelding—Limited testing was performed to determine if rewelding an outer container could be used to reduce weld porosity, thus potentially salvaging a noncompliant outer container. Five outer containers that had initially failed the porosity criteria (as determined by radiography) were rewelded using a reduced weld current (170 vs 180 amps). Subsequent radiographic analysis showed that although not all rewelded outer containers passed the porosity criteria, porosity was significantly reduced. Additional testing is needed to evaluate the feasibility of rewelding to reduce porosity and salvage outer containers that are initially rejected.

## Conclusions

Five DOE sites have developed systems to successfully complete the closure weld on 3013 outer containers. The details of imple-

mentation at each site varied, but all sites used either a LBW or GTAW system. Each site has been successful in performing its mission with its selected system. Additional improvements and feedback from the experience of the other sites are being considered in a next-generation GTAW system at the Savannah River Site.

*William L. Daugherty is a fellow engineer at Savannah River National Laboratory. He holds a Ph.D. in nuclear engineering from North Carolina State University.*

*Stanley R. Howard is a principal engineer at Savannah River National Laboratory. He holds a B.S. engineering technology and an M.S. industrial technology from Texas A&M University.*

*Kurt D. Peterson is a principal engineer at Savannah River National Laboratory. He has a B.S. in mechanical engineering from the University of Minnesota.*

*Mitchell W. Stokes is a senior fellow engineer at Savannah River National Laboratory. He has an M.S. in mechanical engineering from Mississippi State University.*

*Gary R. Cannell is Technical Director of the Fluor Government Group. He has a B.S. in welding engineering technology from Utah State University.*

*Scott A. Breshears is technical staff member at Los Alamos National Laboratory. He has a bachelor of mechanical engineering from Georgia Institute of Technology.*

## References

1. DOE. 2004. DOE Standard: Stabilization, Packaging, and Storage of Plutonium-Bearing Materials. *DOE-STD-3013-2004*. Washington, D.C.: U.S. Department of Energy.
2. Gupta, S. K., J. W. McClard, D. H. Poss II, A. P. Rangus, and B. R. Seward. 2000. Savannah River Site Stabilization and Packaging Requirements for Plutonium Bearing Materials for Storage, *G-ESR-G-00035*, Westinghouse Savannah River Company.
3. 2006. Rocky Flats Closure Legacy Special Nuclear Material Removal Project, USDOE Rocky Flats Project Office, <http://rockyflats.apps.em.doe.gov/>.
4. Louthan, Jr., M. R., Sessions, C. E., West, S. L., and J. W. Wong. 2001. Comparison Study of Laser and Gas Tungsten Arc Welder Systems for Closure Welding Inner and Outer DOE Standard 3013 Canisters, *WSRC-TR-2001-00071*, Westinghouse Savannah River Company.
5. Riley, D., and K. Dodson. 2001. Modifications to LLNL Plutonium Packaging System (PuPS) to Achieve ASME VIII UW-13.2(d) Requirements for the DOE Standard 3013-00



- Outer Can Welder, UCRL-ID-142335, Rev. 1, Lawrence Livermore National Laboratory.
6. Cannell, G., W. Daugherty, L. Gaston, L. S. Howard, P. Korinko, D. Maxwell, G. McKinney, C. Sessions, and S. West. 2003. GTA Welding Research and Development for Plutonium Containment, *Proceedings of the 6th International Trends in Welding Research Conference*, 15-19 April 2002, ASM International.
  7. Cannell, G. R., W. L. Daugherty, and M. W. Stokes. 2002. Welds Safeguard Plutonium-Bearing Containers, *Welding Journal*, 81, No. 7, 42-46.
  8. Korinko, P. S., and S. H. Malene. 2001. Considerations for the Weldability of Types 304L and 316L Stainless Steels” *Practical Failure Analysis*, 1, Issue 4, 61-68.



# Residual Stresses in 3013 Containers

John I. Mickalonis and Kerry A. Dunn  
Savannah River National Laboratory, Aiken, South Carolina USA

## Abstract

The U.S. Department of Energy (DOE) Complex is packaging plutonium-bearing materials for storage and eventual disposition or disposal. The materials are handled according to the DOE-STD-3013, which outlines general requirements for stabilization, packaging, and long-term storage. The storage vessels for the plutonium-bearing materials are termed 3013 containers. Stress-corrosion cracking has been identified as a potential container degradation mode and this work determined that the residual stresses in the containers are sufficient to support such cracking. Sections of the 3013 outer, inner, and convenience containers, in both the as-fabricated condition and the closure welded condition, were evaluated per ASTM standard G-36. The standard requires exposure to a boiling magnesium chloride solution, which is an aggressive testing solution. Tests in a less aggressive 40 percent calcium chloride solution were also conducted. These tests were used to reveal the relative stress-corrosion cracking susceptibility of the as fabricated 3013 containers. Significant cracking was observed in all containers in areas near welds and transitions in the container diameter. Stress corrosion cracks developed in both the lid and the body of gas tungsten arc welded and laser closure welded containers. The development of stress corrosion cracks in the as-fabricated and in the closure welded container samples demonstrates that the residual stresses in the 3013 containers are sufficient to support stress-corrosion cracking if the environmental conditions inside the containers do not preclude the cracking process.

## Introduction

The U.S. Department of Energy (DOE) Complex is packaging plutonium-bearing materials for storage according to the DOE-STD-3013,<sup>1</sup> which outlines, in part, the specification for the 3013 storage containers. The internal environment for some 3013 containers is such that chloride stress-corrosion cracking (SCC) is a potential degradation mode of the stainless steel containers during storage.<sup>2</sup> The three factors necessary for SCC are a susceptible material, a corrosive environment, and a tensile stress. The stress can result from either an applied load or a residual stress resulting from fabrication or welding processes. For the 3013 containers, both fabrication and welding residual stresses may be present. The outer container has both a fabrication weld that joins the bottom to the sidewall and a closure weld. The convenience and inner

containers tested were made by a flow form process, which cold works the stainless steel during fabrication. The inner containers also are sealed at the container top with a closure weld to the sealing plug. The residual stresses that are produced by fabrication and welding processes may exceed the nominal yield strength of the stainless steel and are particularly problematic in the weld heat affect zone (HAZ) where microstructure also contributes to the potential for SCC.<sup>3</sup>

Testing was performed under several conditions to determine if the residual stresses were sufficient for the initiation and propagation of SCC. Testing in boiling magnesium chloride is an accepted ASTM standard practice for assessing the effects of material properties (composition, surface finish, microstructure, heat treatment, etc.) and stress conditions on susceptibility to chloride SCC.<sup>4</sup> The boiling magnesium chloride solution is a severe environment that may be much more aggressive than the actual exposure environment as that encountered in 3013 containers during storage.<sup>4,5</sup>

Less aggressive SCC testing has been developed so that the test results correlate better with actual industrial service. Two such environments are a boiling acidified sodium chloride solution (ASTM G123<sup>6</sup>) and a 40 percent calcium chloride solution at 100°C. The 40 percent calcium chloride solution was used in this study because cracking had occurred during corrosion tests under simulated storage conditions with salts containing calcium chloride.<sup>7,8</sup> For these simulated storage tests, the test coupons were teardrop-shaped coupons fabricated of Type 304L stainless steel. Similar teardrop-shaped coupons and an inner-container welded-top section were tested in the 40 percent calcium chloride solutions to provide comparative results for assessing the effect of residual stresses in a less aggressive environment that is more relevant to 3013 containers.

## Experimental Test Setup

The SCC testing was performed with different solutions, exposure conditions, and samples to assess the effect of residual stresses on the SCC susceptibility of 3013 containers. The various test conditions are discussed herein.

## Test Samples

Test samples consisted of both standard commercial teardrop coupons and specimens cut from 3013 containers. The teardrop



coupons were made of 304L stainless steel (304L). Two sizes were used with dimensions of 0.16 cm (0.0625 in) thick × 1.91 cm (0.75 in) wide × 10.16 cm (4.0 in) length and 0.16 cm (0.0625 in) thick × 1.27 cm (0.5 in) wide × 6.35 cm (2.5 in) length. The different sizes were used to develop comparison data with previous testing performed in simulated 3013 environments containing plutonium and the test results with actual 3013 containers.

A 3013 container system consists of up to three containers, outer, inner, and usually a convenience container, which are shown in Figure 1. The outer container is made of 316L stainless steel (316L), while the inner and convenience containers are made of 304L. The 316L outer container is fabricated from a formed bottom, a sidewall, and a top lid. The sidewall and bottom sections are butt joined together by GTA welding. The two types of closure welds approved for use on the outer container were tested, namely a laser beam weld and a gas tungsten arc (GTA) weld. The inner and convenience container bodies are fabricated by a flow form process. Flow forming is a cold metal forming process where a preform is extruded over a rotating mandrel to produce a rotationally symmetrical hollow component. At the Savannah River Site and Hanford Site, the inner container lid is also GTA welded, while a convenience container, if used, does not have a welded top. For these tests, the containers were sectioned by electrodischarge machining (EDM) at the center height so that the residual stress states would remain as undisturbed as possible. Each container half was used as both a test specimen and a solution container.

Figure 1. 3013 containers (outer, inner, convenience) used by Savannah River Site for oxides



The inner containers had been used previously for other types of testing and had several small holes in the bottom and side walls. To prevent the test solution from leaking through the container sections, these holes were filled with weld filler metal and then ground flat. The holes on the bottom were not completely

filled so a small 0.64 cm (0.25 in) diameter hole partially through the bottom was present on the solution side.

Table 1 gives the test matrix for the container sections and teardrop coupons. Post-test analyses were primarily visual evaluations documented by photography. Limited metallographic examinations and dye penetrant testing were performed also.

Table 1. Test matrix

Test Sample	Boiling MgCl <sub>2</sub> at 155 °C	40 percent CaCl <sub>2</sub> at 100 °C
Outer container – welded top	×	
Outer container – bottom	×	
Inner container – bottom	×	
Inner container – welded top	×	×
Hanford convenience	×	
SRS convenience	×	
304L teardrops	×	×

### Test Solutions

Test samples were exposed to either a boiling magnesium chloride solution per ASTM G36 or a 40 percent calcium chloride solution at 100°C following the guidance of ASTM G123. ASTM G36 is an accelerated, aggressive test and involves exposing test samples to a boiling magnesium chloride solution for a user-defined test period. The calcium chloride test at 100°C was performed to determine crack initiation and propagation rates in an environment that was more similar to the small scale corrosion test environment where SCC was observed.<sup>6</sup>

### Test Setup

The magnesium chloride tests used the container section as the sample as well as the vessel to contain the chloride solutions. The test section was placed in a larger containment vessel to collect any solution that may leak through the container specimen if cracking occurred during testing. The nested assembly was then placed on a hot plate. The test solution (45 percent magnesium chloride) components, 600 g of MgCl<sub>2</sub> · 6H<sub>2</sub>O and 15 mL of water, were placed into the container specimen. A glass lid was made to fit snugly into the opening of the container specimen with ports for a thermometer and a water-cooled condenser, which had a liquid trap on top. A solution of 25 percent magnesium chloride was placed in the liquid trap per the ASTM standard. Once the boiling temperature of the test solution was established at 155.0 ± 1°C, any necessary temperature adjustments were made during the test by either adding additional magnesium chloride or water. The teardrop coupons were suspended in boiling (155°C) magnesium chloride solutions contained in glass vessels. Tests generally were conducted until the samples cracked.



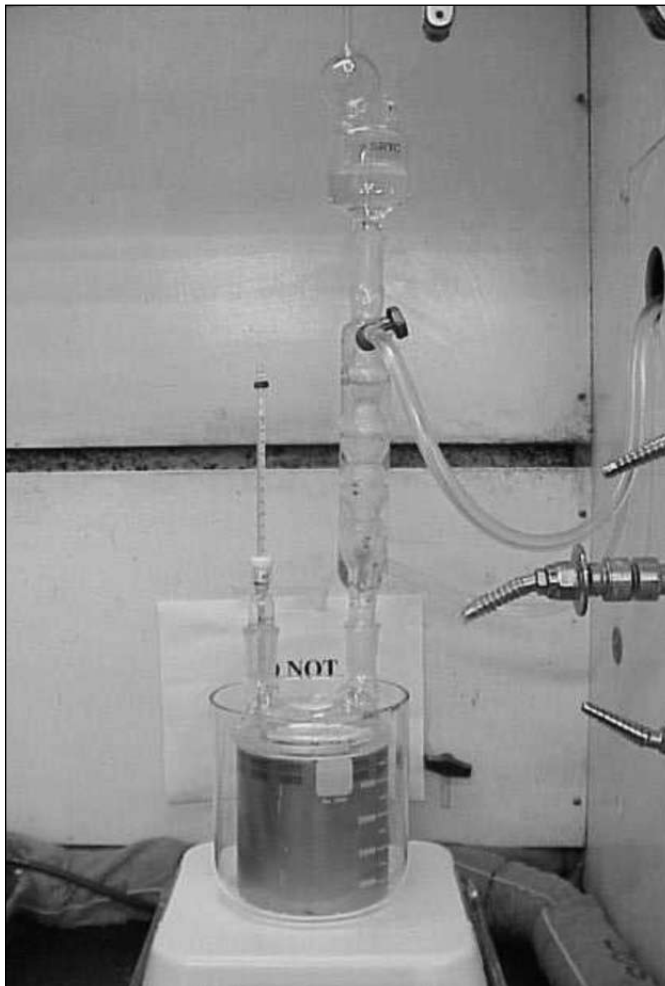


At the conclusion of a test, the container specimens were filled with water to determine if leaking occurred from both known and unknown cracks. If leaking did not occur the container specimens were tested with dye penetrant to determine if cracking had occurred.

The potential for corrosion in the interior vapor space of 3013 containers was tested on one inner container with a welded top that was suspended over a boiling magnesium chloride solution for five days. The solution and container top section were enclosed in a glass vessel. The remainder of the set up was similar to the procedure described above.

The calcium chloride test solutions were prepared using standard reagent chemical and distilled water that was added to either the container specimen or standard laboratory glassware for the teardrop coupons. The container specimen set up was similar to that used for the magnesium chloride testing shown in Figure 2. The test solution was heated to 100°C and maintained until the container specimen or teardrop coupons cracked.

Figure 2. Test setup for boiling magnesium chloride testing



## Results

Cracking occurred in all container specimens exposed to either the boiling magnesium chloride or the 40 percent calcium chloride solutions. These results demonstrate that residual stress levels were sufficient to cause SCC in numerous locations in the 3013 containers. The test results for the 3013 container specimens tested in boiling magnesium chloride solutions are summarized in Table 2. Multiple tests were performed on inner container bottom sections because of the variable results and the complications from the previous testing holes, which were located in the bottom and sidewall. Two inner container top sections were tested for reproducibility.

Table 2. Boiling magnesium chloride test results for 3013 container specimens

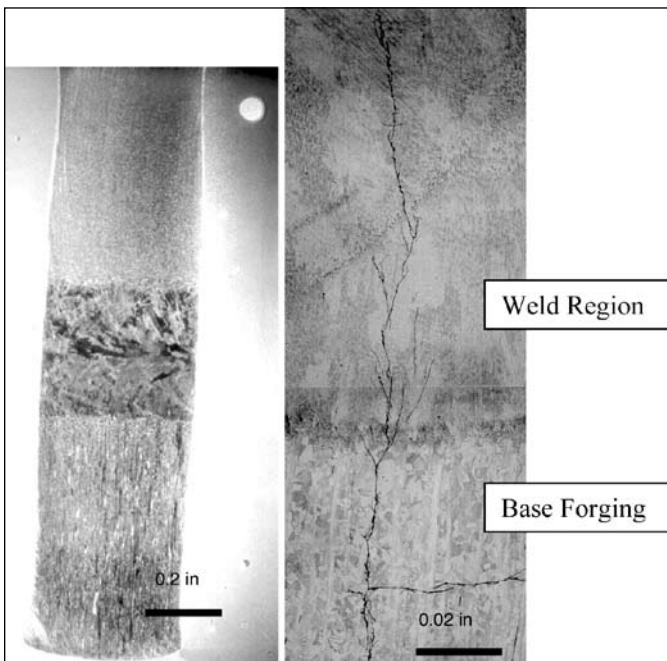
Container Section	Hours in Test	Crack Locations
Outer Container – bottom with fabrication weld	48	Axial cracks in sidewall Radial cracks in bottom
GTAW closure weld outer container	48	Axial cracks in sidewall Radial cracks in bottom Parallel crack near weld
LBC Weld outer container	48	Axial cracks in sidewall Radial cracks in bottom Pitting on interior container bottom
Inner container #1 – bottom No sidewall hole	5	EDM cut rim Bottom drilled hole Circumferential
Inner container #4 – bottom	24	Sidewall hole Bottom drilled hole Circumferential
Inner container #2 – bottom	48	Sidewall hole Bottom drilled hole Circumferential and axial in sidewall
Inner container #3 – bottom No sidewall hole	48	EDM cut rim Bottom drilled hole
Inner container #3 – top	2	Perpendicular to weld
Inner container #1 – top	3.5	Parallel and perpendicular to weld
Inner container #2 – top – vapor	120	Small cracks in crevice perpendicular to weld
SRS convenience container	5.5	Axial in sidewall and radial in bottom
Hanford convenience container	48	Circumferential and axial in sidewall
304L teardrops	1.3	Through-wall near weld



**Figure 3.** Bottom of as-fabricated 3013 outer container after boiling magnesium chloride test: a) Exterior through-wall cracks; b) Interior cracks, arrows indicate cracks



**Figure 4.** Metallographic cross section of through-wall crack at the container to base fabrication weld in 3013 outer container after boiling magnesium chloride test: a) Overall macrograph showing base of container through fabrication weld and container body; b) Stress-corrosion crack from sample shown in (a). Note the crack branching and the position of the crack, beginning in the weld region and propagating into the base of the container



#### Outer Container — Fabrication Weld

Through-wall cracks were observed in the bottom half of the as-fabricated container specimen after forty-eight hours of testing in boiling magnesium chloride solutions (Figure 3). Other cracks were observed on the interior of the container specimen that did not appear to propagate through the wall. Five through-wall cracks which ranged in length from 0.38-2.06 cm (0.15-0.81 in) were visible. All of the cracks observed were generally perpendicular to the base-to-container fabrication weld. Metallographic examination of one crack showed that the cracking initiated in the HAZ and grew into the weld and base of the container specimen (Figure 4). The cracks were typical of stress corrosion cracks with regions

of branching along their length and some areas of cracking 90° from the main crack. The location and orientation of the cracks are consistent with the residual stresses expected as a result of the base-to-container weld and indicate that the residual stress state is significant in the weld region of the as-fabricated container.

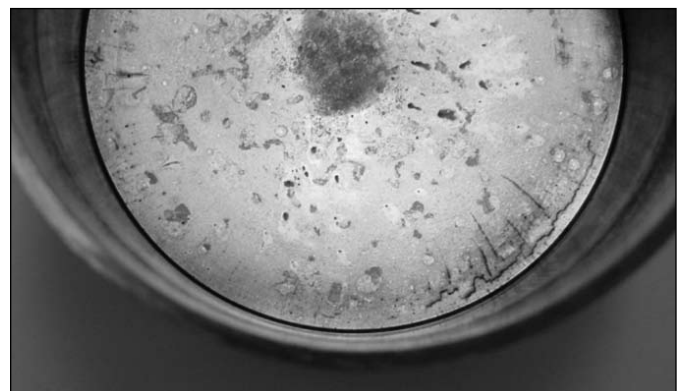
#### Outer Container — GTAW Closure Weld

Through-wall stress corrosion cracks perpendicular to the GTAW closure weld and along the length of the container specimen body were observed after forty-eight hours of testing in boiling magnesium chloride solutions. See Figure 5 (a). Through thickness radial cracks were also observed on the lid. See Figure 5 (b). All of these cracks are consistent with the residual stresses expected as a result of the GTAW closure weld. A crack, which grew perpendicular to the weld while in the weld metal turned to be parallel to the closure weld in the heat affected zone was also observed using dye penetrant testing. The external cracks in the lid and through the weld along the length of the container specimen (Figure 5) were not imaged using dye penetrant testing. This observation indicates that the external crack was insufficiently open to allow the dye penetrant to move into the crack even though the cracks penetrated through the container wall.

**Figure 5.** Top half of GTAW closure welded 3013 outer container section with through-wall cracks after boiling magnesium chloride test: a) Exterior of container with cracks perpendicular to GTAW weld and running into container body (b) Exterior of lid showing appearance of cracks perpendicular to GTAW weld in lid



**Figure 6.** Laser beam closure welded 3013 outer container after boiling magnesium chloride test with interior pitting on lid as well as crack indications



### Outer Container — Laser Beam Welds

Through-wall cracks perpendicular to the weld and along the length of the container specimen body were observed in a sample containing a laser closure weld. These cracks were observed after the sample was exposed to boiling magnesium chloride solution for forty-eight hours. Radial cracks on the lid were also observed, (Figure 6). All of these cracks are consistent with the residual stresses expected as a result of the laser closure weld. Pits were also observed inside the container specimen (Figure 6). The pits may be chloride induced pits that are exacerbated by the high residual stresses developed during the closure weld. Dye penetrant testing of the exterior of the container specimen showed that the cracks in both the lid and the body were through-wall cracks and ran continuously from the lid into the body.

### Inner Container — Bottom

The cracking in inner container bottom specimens occurred at several locations and not all container specimens cracked at each location. The container specimens all had a hole drilled in the bottom, which was sealed with weld metal as discussed previously. The container specimens cracked and generally leaked at this location. Two container specimens had a hole in the sidewall, which was formed during a container puncture test and cracking also occurred at these holes. Cracks from both these holes followed an irregular circuitous path.

Post-test water leak checks showed leaks only from the bottom and the sidewall drilled hole. Dye penetrant testing on the container interiors however showed a circumferential crack near regions of the container where the diameter changed (Figure 7). Small portions of these cracks were through-wall. One inner container bottom section did not develop any cracks other than those associated with the drilled holes. This variability in cracking for the inner container bottom may be associated with differences in container fabrication as well as testing variability.

**Figure 7.** Dye penetrant testing of 3013 inner container bottom section; dark lines indicate crack locations and dark spots are the drilled hole locations



### Inner Container — Welded Top

The welded tops on the inner container specimens cracked after two and three-and-a-half hours exposure in the boiling magnesium chloride. Testing was stopped because large amounts of the test solution leaked from the cracks. The cracks were along the weld, perpendicular to the weld along the container specimen axis, and radial from the plug perimeter (Figure 8). The crack along the weld occurred in the container specimen that was exposed for the longer time and covered approximately 60 percent of the perimeter. The cracks in the sidewall were greater in number than those in the plug. Additionally, the cracks were longer (0.5-0.9 cm [0.2-0.35 inch] length) and a greater number of the cracks had propagated through-wall. The radial and perpendicular cracks were straight and unlike the cracks typically generated at the drilled holes.

**Figure 8.** 3013 inner-container welded-top section after exposure to boiling magnesium chloride showing container interior with sidewall and plug cracks

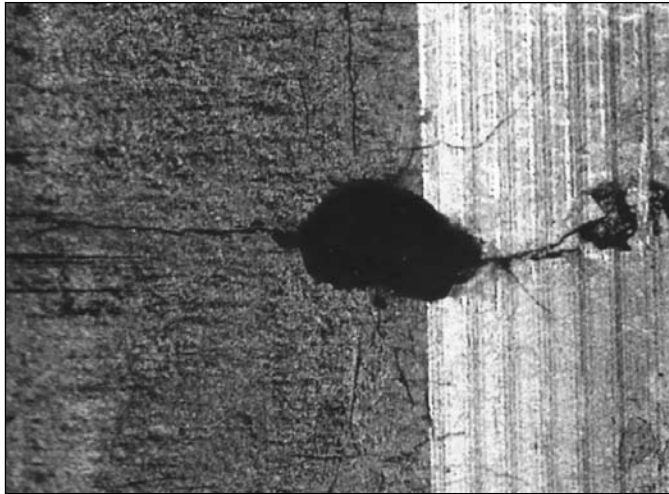


The welded top of inner container #1 was sectioned to look for evidence of corrosion within the crevice formed by the top plug and sidewall. Although large pits were found in the plug and sidewall there was no evidence of crevice corrosion. In many cases the pits that were observed were associated with the cracks as shown in Figure 9. The small cracks had multiple orientations relative to the pits. The growth patterns for these cracks indicated a complex stress state near the weld.

The welded tops of the inner container specimen exposed to the vapors of the boiling magnesium chloride solution had small cracks in both the sidewall and top after five days of exposure. The cracks were not through-wall. The container specimen interior showed only a small degree of corrosion although the surface was wetted during testing. The container specimen was sectioned by EDM so that the interior surface of the crevice could be inspected for pitting and cracking since the use of dye penetrant testing was unsuccessful. Several pie-shaped sections were cut from the container specimen. The crevice was revealed by flattening. Large



**Figure 9.** 3013 inner-container welded-top section after exposure to boiling magnesium chloride solution showing pit associated with cracking in sidewall



pits and small axial cracks were found inside the crevice and when the sample sections were flattened to open the crevice, the cracks also opened up (Figure 10). Additional cracks were found on the side of plug.

### Convenience Container

The two convenience container specimens both cracked in the boiling magnesium chloride test. One container did not leak after forty-eight hours while the other leaked to such an extent that the test had to be stopped after only 5.5 hours of exposure. Most of the cracks were in the region of the diameter change of the container specimen (Figure 11). No cracks were found on the bottom of one convenience container specimen, while the other had radial cracks. The convenience container specimens that lasted for forty-eight hours showed only minimal leaking during the post-test leak check, but leaked severely after tapping to loosen the cracks.

### 304L Teardrop Coupons

304L teardrop coupons with autogenous welds were exposed to plutonium-oxide-bearing material with 0.2 percent calcium chloride in simulated 3013 corrosion tests performed at room temperature. These specimens cracked after 166 hours of exposure.<sup>6</sup> The relationship of corrosion susceptibility of these teardrop coupons to flow formed 304L containers has not been established. As a measure of this relationship, teardrop coupons identical to those used in the small scale test were tested in boiling magnesium chloride solution. The teardrop coupons failed after approximately 1.3 hours of exposure with a full-width through-wall crack (Figure 12). The crack was near the weld but outside the HAZ. The small-sized teardrop coupon failed in approximately two hours with a through-wall crack at a similar location to the cracks in the large teardrop coupons.

**Figure 10.** 3013 inner-container welded-top section exposed to vapors of boiling magnesium chloride solution: interior container crevice between the side wall and seal plug spread open showing small cracks



**Figure 12.** 304L teardrop coupons after exposure to a boiling magnesium chloride solution



### Inner Container – Welded Top – Calcium Chloride Test

The test with the inner container welded-top specimen exposed to calcium chloride solutions at 100°C was performed for approximately eighty-four hours. Multiple cracks grew perpendicular to the weld in the sidewall, similar to those in the boiling magnesium chloride tests. The cracks were approximately 0.5-0.7 cm (0.2-0.27 in) long as measured macroscopically on the exterior sidewall. Many of these cracks were through-wall. Cracks were also found in the top plug but only two were suspected to be through-wall.

### Discussion

The boiling (155°C) magnesium chloride test is designed to indicate the susceptibility of stainless steels and related alloys to SCC and is not meant to be a quantitative test. The test was used in

**Figure 11.** Convenience container section after exposure to boiling magnesium chloride solution: container exterior with axial cracks in sidewall



this study to identify locations of high residual stresses associated with fabrication and welding of the stainless steel 3013 container. Time to failure in these solutions is inversely related to the level of residual stress.<sup>9</sup>

The 3013 outer, inner, and convenience containers all had sufficient residual stresses to crack in the boiling magnesium chloride solution, although in some tests where leaking did not occur the time to failure is not known. For the 316L outer containers, leaking did not occur during the test, but cracks were evident in the as-fabricated container specimen after forty-eight hours. The closure welded regions of the outer container specimens also developed similar cracks. The cracks observed in the as-fabricated outer container specimen, however, were not as numerous as those observed in the closure welded container specimens. Cracks observed in the laser closure welded container specimens were numerous and appeared to be more severe when compared to those observed in the GTAW closure welded specimens.

The 304L teardrop coupons had a very short time to failure (approximately 1.3 hours) and clearly provide a conservative estimate for the behavior of the 3013 containers. The stress levels in a teardrop coupon have been shown to exceed the yield stress and approach levels equivalent to the ultimate tensile strength.<sup>8</sup> By comparison a welded top of an inner container specimen failed in two hours, which suggests that the residual stresses in the weld may be lower than the stresses in the teardrop coupons. The other welded top of an inner container specimen was tested for 3.5 hours and had a more significant degree of cracking with a circumferential crack running parallel to the weld. The perpendicular and parallel cracking near the weld indicate a complex stress state in the weld region. The inner container bottom section appears to have lower stress levels than those in the seal welds since the degree of cracking was less (i.e., smaller number of through-wall cracks) and the time to cracking is greater (i.e., one container tested for forty-eight hours had no cracks in the sidewall).

The times to cracking for the convenience container specimens were approximately 5.5 hours. Fabrication stresses for the convenience container may thus approach those resulting from welding since times to failure were similar to the welded tops of the inner container specimens.

Additionally the inner container welded-top specimen cracked in the vapors of the boiling magnesium chloride solution. The cracks were small and not through-wall, but extended exposure beyond the five-day test period could have resulted in similar cracking to those inner container welded-top specimens exposed directly to the boiling magnesium chloride solution. These results show that the residual stresses in a weld are sufficient to cause cracking when chloride-containing vapors condense on the stainless steel surface.

The results from the calcium chloride test showed that cracking can occur in the 3013 containers in environments less severe than a boiling magnesium chloride solution, and as expected, the time to cracking was significantly longer. Testing was conducted with only an inner container welded-top specimen. Similar results would be expected for the other containers but only at longer times since they failed at longer times in the magnesium chloride tests. The cracking morphology was similar to that observed in the magnesium chloride tests, i.e., short perpendicular cracks to the weld. Cracking also is possible in the vapor space of such environments since cracking occurred in the 304L teardrop coupons, which was exposed to the vapor of a 40 percent calcium chloride solution. The vapor space cracking was significantly less than that observed on teardrop coupons immersed in the solution. Crack growth rates were not determined for the immersed teardrop coupons because multiple cracks initiated.

## Conclusion

The 3013 container is a nested set of three low-carbon grade 300 series stainless steel containers and is robust for packaging plutonium-bearing materials and eventual storage at various sites in the DOE Complex. Corrosion associated with impurities (specifically chlorides and fluorides) in the plutonium-bearing materials may lead to SCC of the containers. ASTM standard G-36, an aggressive testing procedure with boiling magnesium chloride solution, was used to identify the regions of the 3013 container that are most susceptible to potential degradation associated with SCC. For the 3013 outer container, significantly large residual stresses were in the bottom half of the as-fabricated container, which resulted from the base to container fabrication weld. This observation indicated that regardless of the closure weld technique, sufficient residual stresses exist to provide the stress component necessary for SCC. Cracks observed in both the lid and the body of the GTAW and the laser closure welded containers indicates that significant residual stresses are inherent in the closure welding process regardless of the closure weld method.

Testing of 3013 inner and convenience containers has shown



that residual stresses sufficient to support SCC exist at both the inner container closure weld and in sections of the containers where the container diameter changes, i.e., near the container bottom. Cracking was found to occur sooner in the inner container welded-top specimen than the container bottom specimen of either the inner or convenience container. This shorter time is indicative of higher residual stresses from welding than fabrication. The microstructure in the HAZ is likely to provide an added component for pitting corrosion and SCC.

Teardrop coupons are a conservative marker for the containers since failure in the boiling magnesium chloride test occurred in even shorter times than the welded top. Cracking from the condensed vapors of both the hot calcium chloride and boiling magnesium chloride solutions occurred, so SCC may be a plausible mechanism for the 3013 containers if a thin chloride-bearing film forms above the oxide/salt mixture. The chloride concentrations in the 3013 containers are expected to be a small fraction of those used in this testing.

The net result of these studies is that the microstructure of the austenitic stainless steel and the residual stresses present in the steel combine to create 3013 containers (convenience, inner, and outer) that are susceptible to chloride induced stress-corrosion cracking. Therefore, assurance against such cracking must be provided by environmental controls during the packaging and storage processes. The 0.5 wt percent moisture limit is the primary control designed to provide this assurance.

## Acknowledgements

The authors acknowledge the talented assistance of Elise LaBord and Karen Hicks in conducting the experimental work and Dr. Mac Louthan, Jr. for helpful discussions.

*John Mickalonis is a fellow engineer at Savannah River National Laboratory. He holds a Ph.D. in materials engineering from Lehigh University. He holds an M.S. in materials science and engineering from Rensselaer Polytechnic Institute.*

*Kerry A. Dunn is an advisory engineer at the Savannah River National Laboratory. She has an M.S. in Materials Science and Engineering and a B.S. in metallurgy from Pennsylvania State University.*

## References

1. DOE. 2004. DOE Standard: Stabilization, Packaging, and Storage of Plutonium-Bearing Materials. *DOE-STD-3013-2004*. Washington, D.C.: U.S. Department of Energy.
2. Kolman, G. D. 2001. A Review of the Potential Environmentally Assisted Failure Mechanisms of Austenitic Stainless Steel Storage Containers Housing Stabilized Radioactive Compounds, *Corrosion Science* 43, 99-125.
3. Dunn, K. A., M. R. Louthan, G. B. Rawls, R. L. Sindelar, P. E. Zapp, and J. W. McClard. 2009. Container Materials, Fabrication and Robustness, *Journal of Nuclear Materials Management*, Vol. 38, No. 2.
4. ASTM G36-94 (Reapproved 2006). *Standard Practice for Evaluating Stress-corrosion Cracking Resistance of Metals and Alloys in a Boiling Magnesium Chloride Solution*, ASTM International, West Conshohocken, Pennsylvania USA.
5. Jin, L.-Z. 1995. The Chloride Stress-corrosion Cracking Behavior of Stainless Steels under Different Test Methods, *Journal of Materials Engineering and Performance*, 4, 734-739.
6. ASTM G123-00 (Reapproved 2005). *Standard Test Method for Evaluating Stress-corrosion Cracking of Stainless Steel Alloys with Different Nickel Content in Boiling Acidified Chloride Solution*, ASTM International, West Conshohocken, Pennsylvania USA.
7. Zapp, P. E. 2009. Localized Corrosion of Austenitic Stainless Steels Exposed to Mixtures of Plutonium Oxide and Chloride Salts, *Proceedings of Corrosion 2009*, NACE International, Houston, Texas, Paper # 09409.
8. Lam, P. S. 2009. Stress-corrosion Cracking in Teardrop Specimens, *Proceedings of 2009 ASME Pressure Vessel and Piping Conference*, Prague, Czech Republic, Paper #77432.
9. Alyousif, O. M., and R. Nishimura. 2008. On the Stress-corrosion Cracking and Hydrogen Embrittlement of Sensitized Stainless Steel in Boiling Magnesium Chloride Solutions Effect of Applied Stress, *Corrosion Science* 50, 2919-2926.

# Long-term Aging and Surveillance of 9975 Package Components

Elizabeth N. Hoffman, T. Eric Skidmore, William L. Daugherty, and Kerry A. Dunn  
Savannah River National Laboratory, Aiken, South Carolina USA

## Abstract

The mission of the 9975 package, originally designed only for transportation of radioactive materials, has been broadened to include storage at the Savannah River Site. Two components of this package, namely the containment vessel O-rings and fiberboard overpack, require continued integrity assessment under the storage conditions. The performance of the components over time is being evaluated using accelerated-aging studies. Compression stress relaxation (CSR) and leak testing are being used to measure the performance of O-rings. The performance of the fiberboard is being evaluated using compression strength, thermal conductivity, specific heat capacity, and other physical properties. Models developed from the data collected provide an initial prediction of service life for the two components, and support the conclusion that normal service conditions will not degrade the performance of the package beyond specified functional requirements for the first assessment interval. Increased confidence in this conclusion is derived from field surveillance data and destructive evaluation of packages removed from storage.

## Introduction

The Savannah River Site (SRS) is storing plutonium (Pu) materials in the K-Area Materials Storage (KAMS) facility. The Pu materials are packaged according to the standard DOE-STD-3013, which requires nested, welded, stainless steel containers. Within KAMS, the welded 3013 containers are stored in U.S. Department of Transportation (DOT) Type B 9975 packages. The 9975 package consists of two nested stainless steel containment vessels (CV) closed with threaded cone seal plugs, surrounded by a lead shielding body and fiberboard overpack, all contained within a thirty-five-gallon stainless steel drum (Figure 1). The 9975 package is part of the approved storage configuration for Pu materials in KAMS. As such, it will be continuously exposed to the service environment for a period of time greater than the approved transportation service period. The studies documented in this report were undertaken to verify the integrity of the containment vessels' O-ring seals and the fiberboard overpack over time in the environment they will be exposed to in KAMS for an initial storage assessment period of ten years. It is anticipated that the packages will be used up to fifty years and that replacement of aged compo-

Figure 1. Illustration of 9975 package including fiberboard, lead shielding, and double containment vessels



nents may be necessary. The work described in this paper presents data to an initial assessment period of ten years.

Each containment vessel is sealed with O-rings (compounds V0835-75 or VM835 75, Parker Hannifin Corporation, Lexington, Kentucky USA) based on Viton® GLT/GLT S fluoroelastomer (Dupont Performance Elastomers, Wilmington, Delaware USA). Viton® fluoroelastomer O-rings are placed on the cone-seal plugs in each package: two O-rings, inner and outer, sealing the primary containment vessel (PCV) and two O-rings, inner and outer, sealing the secondary containment vessel (SCV). In transportation service, the O-rings are replaced on an annual basis and leak tested to a  $1 \times 10^{-7}$  ref cc air/sec (leaktight) criterion per ANSI N14.5. However, while in storage the O rings are not replaced and cannot be leak tested. The outer O-ring in each ves-





sel is credited for containment. The inner O-ring provides a volume for leak testing and a secondary barrier to product release. To function as a seal, the O-rings must maintain mechanical elasticity and exert a compressive force against the sealing surfaces.

The overpack used in the 9975 package is Celotex® cane or softwood fiberboard (Knight Industries, Northfield, Illinois USA) and is located between the outer Type 304L stainless steel drum and the lead shield. The fiberboard performs three main functions: i) thermal insulation to limit internal temperature during a fire; ii) criticality control (by neutron moderation and spacing); and iii) resistance to mechanical crushing of the package. Properties of importance to demonstrate acceptable performance of the material over time include dimensional stability, density, compressive strength, thermal conductivity, and specific heat capacity. Baseline and initial aging data on these properties have been previously reported.<sup>1-4</sup>

## Experimental Laboratory Testing

### Viton® GLT O-rings

#### Compression Stress Relaxation

Compression stress-relaxation (CSR) is an industry standard measure of seal performance.<sup>5,6</sup> When an elastomer is compressed, the internal cross-linked polymer structure imposes a spring like counterforce on mating surfaces to provide a seal. Over time, the sealing force is reduced due to physical and chemical relaxation processes. If the elastomer is exposed to aging conditions long enough, all of the sealing force can be lost, compromising the seal in a dynamic situation. Once the elastomer ceases to apply a counterforce, it is considered to have lost 100 percent of sealing capability.

Long-term CSR behavior of the O-rings is being measured per ASTM D6147. Parker Seals O-rings (compound V0835-75) size 2-213, with a nominal thickness of 0.353 cm (0.139"), the same thickness as O-rings used in 9975 packages, are used in the CSR jigs (Figure 2) along with metallic inserts to create a nominal inner diameter (ID) stretch of 20 percent and a nominal 18 percent compression to duplicate the sealed O-ring configuration in the 9975 package. A 0.0025-0.0050 mm (0.0001-0.0002") gap is maintained between mating surfaces in the CSR jig to maintain electrical insulation between the two platens. Electrical insulation is needed for the CSR measurement device (relaxometer) to function. The sealing force is measured periodically during aging.

Samples were thermally aged at 79, 113, 121, 149, and 177°C (175, 235, 250, 300, and 350°F). The lowest temperature, 79°C, corresponds to the maximum service temperature in KAMS; 149°C is the containment vessel design temperature limit, 121°C and 177°C were chosen to flank the CV design temperature limit with 177°C being halfway between the CV design temperature limit and the O ring manufacturer's *continuous* service temperature limit. In addition to thermal effects, the possible effects of gamma radiation on CSR behavior were investigated. O-rings were irradiated to a fifty-year dose of  $8.8 \times 10^{-3}$  Gy (0.88

Figure 2. CSR jig with custom stretch insert



Mrad) at a dose rate of  $4.4 \times 10^{-3}$  Gy/hr (0.44 Mrad/hr) prior to thermal aging. This dose was selected because it corresponds to the maximum dose the O-rings would receive during fifty years of exposure in the 9975 packages at a bounding dose rate of 2 rad/hour. For comparison purposes, a non-stretched O-ring was also aged at 121°C (250°F). K-type thermocouples were mounted onto each jig to monitor temperature during aging and CSR measurement.

#### Compression Set

Compression set is a measure of permanent change in seal dimensions as a result of compression over time. Upon 100 percent loss of sealing force, O-ring samples aged at 149°C (300°F) and 177°C (350°F) were removed from the stretch inserts and measured dimensionally. The equation used for compression set (CS) comes from ASTM D395 Method B:

$$\left( \frac{0.139 - t}{0.0395} \right) \times 100 = \%CS \quad (1)$$

where  $t$  is the average thickness of the O-ring at four locations along the circumference after the compression set tests, 0.139" is the original O-ring thickness and 0.0395" is the depth the non compressed O-ring protrudes beyond the O-ring gland. This equation takes into account that the samples were compressed within an O-ring gland of known depth and could not compress more than 0.0395" (0.1 cm). Compression set is also being determined on O-rings removed from surveillance packages.

#### Leak Testing

Full-sized PCV O-rings are tested on modified Cone-Seal Plugs with an additional weep hole to allow for leak testing of both inner and outer O-rings to a criterion of  $1 \times 10^{-7}$  std cc air/sec.





The dimensions of the O-ring gland are identical to the cone seal gland in service. O-rings are being aged at two temperatures, 93°C and 149°C (200°F and 300°F), and periodically leak tested at room temperature.

### Cane Fiberboard Overpack

#### Thermal Properties

Cane fiberboard samples were tested for thermal conductivity. The thermal conductivity instrument interrogates an area of 10 x 10 cm (4 x 4 inch) within a sample up to 30 x 30 cm (12 x 12 inch) in size, following ASTM C518. Two sample orientations are tested; the axial orientation measures the conductivity of heat perpendicular to the fiberboard layers, and the radial orientation measures the conductivity of heat parallel to the fiberboard layers. Mean testing temperatures were 25, 50, and 85°C (77, 122 and 185°F). Specific heat capacity was measured following ASTM C351 on 2.5 cm (1.0 inch) diameter by 3.8 cm (1.5 inch) long cylinders.

#### Mechanical Properties

Compression testing is performed in two orientations, with the load applied either parallel or perpendicular to the plane of the fiberboard layers. A load cell that is controlled to an 11,300 kg (25,000 lb) limit, was used. Samples were 5 cm (2 inch) cubes with no side constraint. The displacement rate applied was 4.8 cm/min (1.9 inch/min) and samples were compressed at this rate until the test was terminated.

The weight and density of samples in each environment have been tracked. Each property is normalized to its initial value.

Cane fiberboard samples were taken from several different packages, with a range of package histories. Table 1 summarizes the total duration of exposures for each aging environment. Environments which include humidity control have the shortest duration, as all samples rely on a single environmental chamber and have been aged sequentially.

### Field Surveillance Testing

#### Viton® GLT O-rings

The 9975 packages selected for surveillance were disassembled in KAMS and O-rings were removed from the cone-seal plug. Within thirty minutes of loosening the containment vessel lid, thickness is measured on four areas of the O-ring in the radial and axial directions. O-rings are then individually packaged and sent to SRNL where they are re-measured an average of 100 days after field testing. Compression set values are then calculated assuming nominal initial dimensions and following Equation 1.

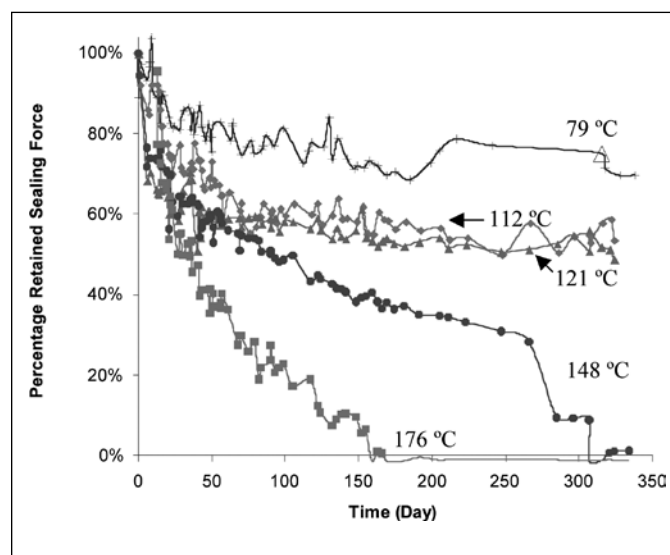
### Cane Fiberboard Overpack

The fiberboard assemblies from four packages removed from service have been destructively examined. These packages had been stored in KAMS from four months to five years. Testing included thermal and mechanical properties, following the same protocols described for aged material.

**Table 1.** Summary of fiberboard sample exposures prior to testing, for data used for statistical analysis

Temperature	Exposure in "dry" oven (weeks)	Exposure in chamber with humidity controlled to the specified value (weeks/percent RH)		
121°C (250 °F)	< 142	---	---	---
101°C (215 °F)	< 100	---	---	---
90°C (195 °F)	2	2/40	2/100	---
85°C (185 °F)	< 139	< 32/30	< 28/70	---
71°C (160 °F)	---	< 32/50	---	---
51°C (125 °F)	< 122	2/40	< 17/70	2/100
25°C (77 °F)	---	2/40	8/70	2/40

**Figure 3.** Percentage retained sealing force versus aging time; aging temperature noted in plot for each sample



## Results

### Experimental Results

#### Viton® GLT Fluoroelastomer O-ring

##### Compression Stress-Relaxation

The compression stress-relaxation behavior of Viton® GLT O-rings is shown in Figure 3. The effects vary with aging temperature. The aging temperature of 176°C (350°F) resulted in a 100 percent loss of relative retained sealing force over a period of 162 days. It is noted that this temperature is lower than the O-ring manufacturer's *continuous* service temperature limit of 204°C (400°F) based on 1,000 hours of aging and demonstrates the difficulty in using short term tests to predict long term behaviors. The O-ring exposed to an aging temperature of 148°C (300°F) resulted in a 100 percent loss of relative compression stress-relaxation force over a period of 310 days. The O-rings exposed to the lower aging temperatures have experienced less severe changes and have not yet reached complete loss of sealing force. As expected, the



O-rings exposed to the lowest aging temperature appear to have the greatest potential for the longest lifetime before failure.

No significant effect of ID stretch or irradiation has been observed. The measurable absence of irradiation effects may be due to the fact that the irradiation occurred prior to the thermal aging. This might allow some annealing or self-healing of radiation damage to occur. However, the fifty-year dose of  $8.8 \times 10^{-3}$  Gy (0.88 Mrad) is relatively low for most polymeric materials and the dose was imposed at a relatively high rate. In addition, characterization of O-rings immediately after irradiation indicates no significant damage. Dose rate effects are possible but are not expected at the low dose rates involved. However, if the lack of simultaneous irradiation and thermal exposure mitigated the irradiation damage, then the CSR-based lifetime could be shortened.

### Compression Set

The calculated CS values for the O-ring thermally aged at 148°C (300°F) for eighteen months and 177°C (350°F) for eleven and a half months were -62 percent and -70 percent, respectively. A slight difference in CS exists between the two samples with the more extreme temperature resulting in a higher CS. It is difficult to directly compare the CS values because the CS calculation assumes nominal initial dimensions. Furthermore, the time period between removing the O-ring from compression and the actual dimensional measurement varies. The 148°C O-ring was measured ten months after compression removal whereas the 177°C O-ring was measured twelve months after compression removal.

### Leak Testing

No fixtures with three-plus years of aging have failed the leak criterion.

### Cane Fiberboard Overpack

#### Physical Properties

Normalized weight and density versus time at temperature are summarized in Figures 4 and 5. Samples from multiple material source packages that have been environmentally aged show similar behavior. A continuous weight loss beyond an initial change due to moisture loss/gain is observed in samples aged at temperatures equal to or greater than 71°C (160°F). The rate of weight or density loss is greater with higher temperatures and increased humidity. No noticeable change was observed in material aged at 52°C (125°F) and below. The fluctuation in the physical properties of an overpack aged at 52°C (Figures 4 and 5) results primarily from seasonal humidity variation.

#### Mechanical Properties

Typical compression stress-strain curves for samples aged in ovens at 121°C (250°F), see Figure 6, show a noticeable drop in compression strength over time. However, no significant decrease is seen at 85°C (185°F) or lower, except in the presence of elevated humidity.

Figure 4. Normalized weight versus time at temperature for fiberboard in several temperature and relative humidity environments

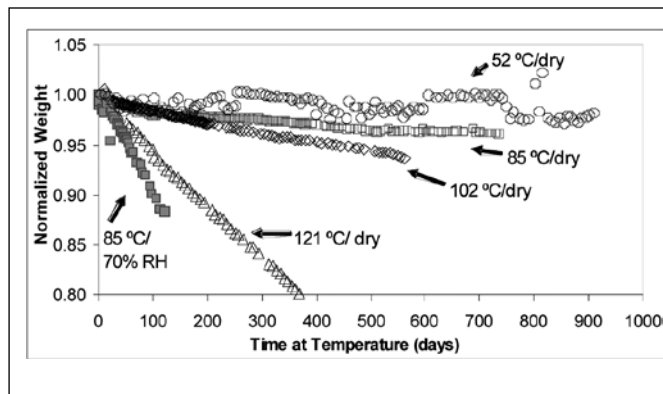
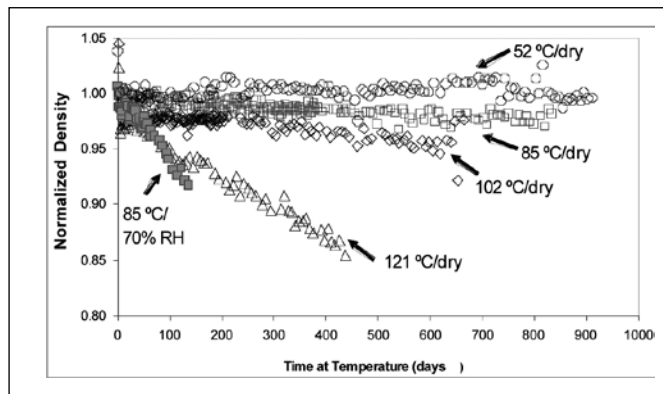


Figure 5. Normalized density versus time at temperature for fiberboard in several temperature and relative humidity environments



A range of behaviors has been observed during compression testing, making sample-to-sample comparisons difficult. The integrated area under the stress-strain curve up to a strain of 40 percent provides a relative measure of the energy absorption capability of the sample, and is a consistent metric for comparison. While the 40 percent strain level ignores part of the stress-strain curve, it provides a degree of consistency between unconstrained test samples and the partially constrained fiberboard within the package. Compressive strength varies from one package to another. However, the rate of degradation in strength is similar for all packages.

#### Thermal Conductivity

Thermal conductivity data for two aging environments are summarized in Figure 7. In Figure 7(a), samples aged at 121°C (250°F) show continued decrease in thermal conductivity over time. Figure 7(b) shows data for samples aged at 85°C (185°F), but with two humidity levels. The box symbols indicate periods when the samples were held at 70 percent relative humidity (RH), and the remainder of the time the samples were in an oven without humidity control. The relative humidity in this oven is typically 2 percent or less, depending on ambient conditions. No significant change occurs with low humidity, but a steep decrease in thermal

**Figure 6.** Engineering stress-strain compression curves for select fiber-board samples aged and tested at 121°C (250°F), (a) parallel orientation, LD2 material (b) perpendicular orientation, MSC material

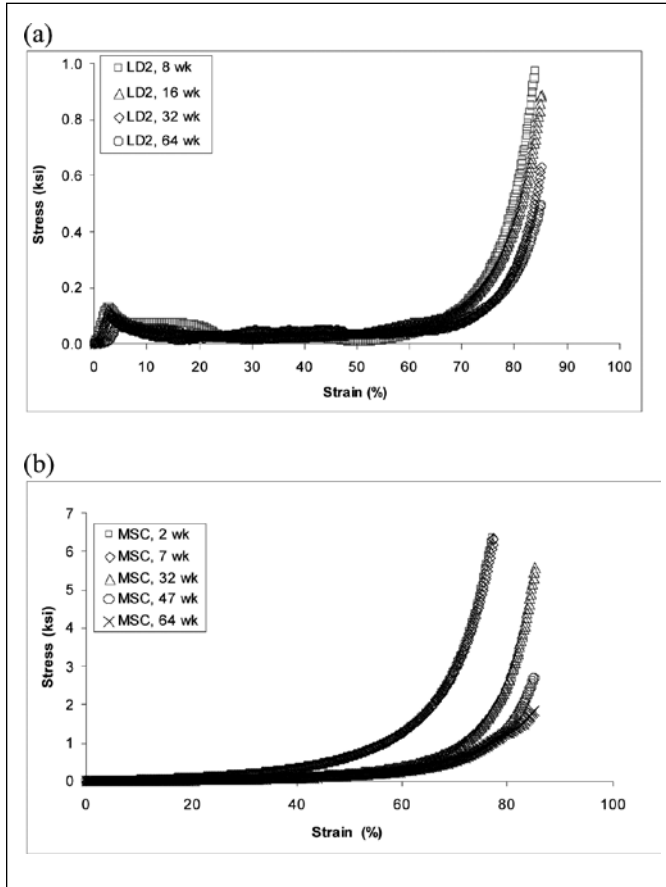
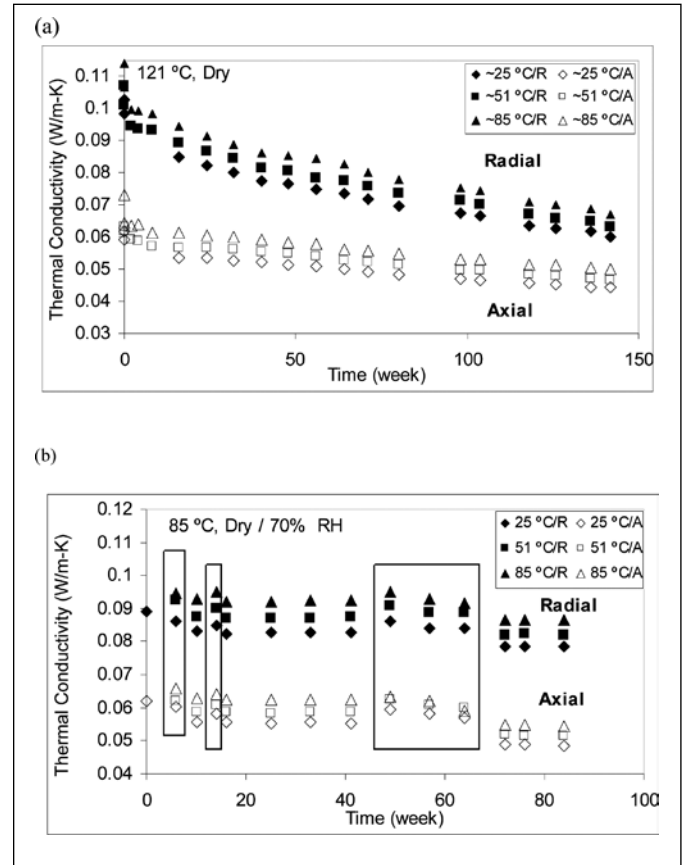


**Table 2.** Decrease in area under the stress-strain curve for material parallel and perpendicular orientation with increasing aging time period

LD2 material, parallel orientation	
Aging period (weeks)	Area under Curve to 40 percent Strain (ksi)
8	0.020
16	0.018
32	0.016
64	0.011
MSC material, perpendicular orientation	
Aging period (weeks)	Area under Curve to 40 percent Strain (ksi)
2	0.052
7	0.052
32	0.021
47	0.012
64	0.016

**Figure 7.** Thermal conductivity versus time data for two aging environments. In each plot, the test temperature is indicated by the symbol: diamonds – 25°C, squares – 51°C, triangles – 85°C. Open symbols denote axial orientation samples, closed symbols denote radial orientation samples. In plot (b) with the cycling humidity, the periods within the boxes are at 70 percent relative humidity.



conductivity is seen at 70 percent RH at this temperature. This decrease is not recovered by returning to a lower humidity.

The specific heat capacity data exhibit scatter from one trial to the next. Accordingly, the results are averaged over all samples and trials for a given aging interval and test temperature. The measured specific heat capacity decreased by about 10 percent following long-term aging at 121°C (250°F). This may be an artifact resulting from sample shrinkage, which has occurred during two-and-one-half years at this temperature. No change in specific heat capacity has been observed in materials tested in other environmental conditions.

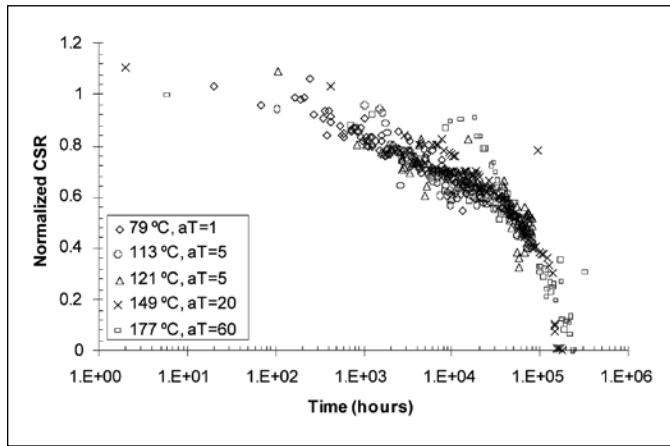
### Field Surveillance Results

#### Viton® GLT Fluoroelastomer O-rings

Approximately 480 O-rings have been evaluated from 120 field packages having up to five years of service. Dimensional measurements are taken in the field within thirty minutes of package disassembly. The average nominal CS value of O-rings from measurements performed on field packages is 26 percent after an average



**Figure 8.** Time-temperature superposition curve for V0835-75 CSR data ( $T_{ref}=76^{\circ}\text{C}$ ,  $175^{\circ}\text{F}$ )



of 1,200 days or approximately 3.3 years in service. O-rings were subsequently re-measured on average 100 days later. The later measurements showed that the average CS was found to relax to 7 percent, reverting back toward the original shape and thickness. Actual compression set values are unknown as starting O-ring dimensions and part dimensions are not documented. However, the results demonstrate that after a service exposure of ~five years at true storage conditions, the O-rings maintain elasticity and are able to relax toward original thickness.

#### *Cane Fiberboard Overpack*

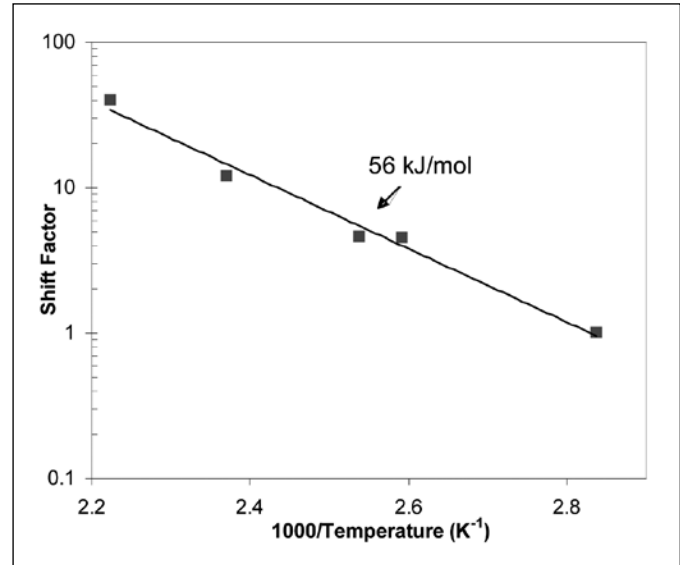
Fiberboard material from four surveillance packages has been tested following up to five years storage. Testing included thermal and mechanical properties, following the same protocols described for aged material. The fiberboard from these packages has shown a range of thermal and mechanical behavior, and that range is consistent with the range of behavior observed in laboratory samples without any exposure. While the baseline condition for these field packages is unknown, their aggregate behavior suggests that the fiberboard properties were not significantly degraded by the service history. This, in turn, supports the model predictions that indicate minimal changes in properties for nominal storage conditions.

#### **Discussion**

##### *Viton® GLT Fluoroelastomer O-ring*

Using the time-temperature superposition theory based on the William-Landel Ferry (WLF) method,<sup>7</sup> estimated times to failure can be determined for the O-rings based on the thermal aging CSR data. A master curve using  $79^{\circ}\text{C}$  ( $175^{\circ}\text{F}$ ), the lowest temperature data set, as a reference temperature,  $T_{ref}$ , was constructed from the CSR data (Figure 8). Empirically determined shift factors,  $a_T$ , were utilized to develop the master curve. The shift factors were then used to determine the activation energy,  $E_a$ , through the relationship:

**Figure 9.** Plot of  $\log a_T$  shift factors versus temperature. The activation energy derived from the linear fit is 56 kJ/mol.



$$\log a_T = E_a / (T - T_{ref}) \quad (2)$$

The calculated  $E_a$  for the degradation reaction from the fit of the shift factor at various temperatures was 56 kJ/mol, see Figure 9. From the master curve, the estimated lifetime of the O-ring is twenty to twenty-seven years at a constant seal temperature of  $79^{\circ}\text{C}$  ( $175^{\circ}\text{F}$ ), based on 100 percent loss of sealing force. This is a bounding case, assuming a constant ambient temperature of  $40^{\circ}\text{C}$  or  $104^{\circ}\text{F}$  and maximum payload of 19 W. Lower ambient temperatures and/or payloads reduce seal temperatures and increase seal lifetime. Seal temperatures also lag behind the ambient temperature by many hours or days due to the overpack thermal insulation, so the assumption of constant exposure at peak temperature is conservative. This model assumes no significant influence of radiation or ID stretch, as these effects have not yet been observed. The model also assumes that the activation energy will remain constant across the service temperature range. This is expected, though it is possible that the activation energy or degradation mechanism could change at lower temperatures. This can only be determined by continuing tests at lower temperatures or by measuring ultrasensitive parameters such as oxygen consumption rates. The activation energy of 56 kJ/mol suggests that the oxidation degradation mechanism for CSR behavior in the O-rings is impeded due to the lack of oxygen exposure with the O-ring resting in the O-ring gland. When oxygen permeation is unimpeded, activation energies associated with the oxidation reaction range from 80-120 kJ/mol.<sup>8</sup>

### Cane Fiberboard Overpack

The 9975 package does not provide an air-tight or water-tight seal for the fiberboard enclosure. However, a properly closed drum does provide a significant degree of isolation of the fiberboard from the ambient environment.<sup>4</sup> Accordingly, it is recognized that any moisture originally in the fiberboard assembly will likely remain in the package for a long time. Due to the heat generated in the 3013 containers, the fiberboard within a package will develop temperature and moisture gradients. Moisture will tend to migrate to the cooler regions of the fiberboard, and the total moisture content of the package will change very slowly.

During a postulated loss of ventilation accident in the KAMS facility, the maximum ambient temperature is 58°C (137°F), and the corresponding lead shielding body temperature is 91°C (196°F). The maximum fiberboard temperature is assumed to be similar to the Shielding Body temperature. However, the normal ambient temperature in KAMS is less than 32°C (90°F), even in the summer. The fiberboard temperature should remain below -65°C (-150°F). Therefore, testing for storage-induced changes in the fiberboard must include exposure to several temperatures.

Exposures of the fiberboard to moisture and temperature cause time dependent property changes. Such changes may occur as the sample comes to equilibrium in the 9975 package. The change in moisture content simply induced by the thermal gradients developed in the package may produce changes in the sample's properties and long term changes may occur as a result of degradation. The literature identifies that slow pyrolysis occurs at modest temperatures.<sup>9</sup> In addition to water vapor, compounds from pyrolysis are evolved at temperatures as low as 95°C (203°F). This is strongly evidenced in samples aged at 121°C (250°F). Such samples show an immediate weight loss of 8-10 percent (moisture loss), followed by an additional 15-20 percent per year weight loss. At the higher temperature and humidity levels, test samples change visually. The samples darken, and the coarse fibrous appearance changes to a finer particulate texture.

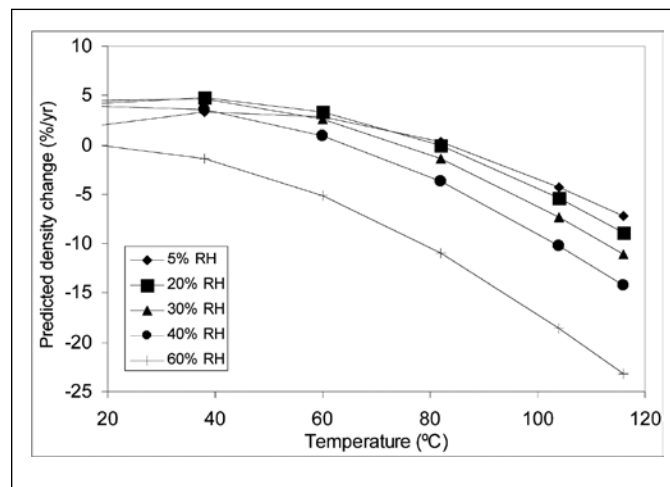
The aging models that are discussed below do not include the effect of initial moisture and given the tendency for the 9975 drum to provide a high degree of isolation, significant moisture-related changes might not occur in service unless the package was closed in a very humid atmosphere.

### Fiberboard Service Life Estimates

Data for each property have been analyzed statistically for best fit models. The model for fiberboard density and the corresponding service life predictions are described below. A similar approach is used for the other properties and provides additional service life estimates. The limiting property may vary depending on the specific service conditions.

Density data were fit to a model that predicts the rate of change as a function of temperature and humidity. The rate is the percentage change in density per year, T is the exposure tempera-

Figure 10. Predicted density change of fiberboard versus aging temperature



ture in °C, and RH is the percent relative humidity. A constant rate of change is consistent with the data shown in Figure 5.

$$\begin{aligned} \text{Rate (density)} = & 0.0004496 - 4.876E-6 * \\ & T - 2.389E-6 * RH - 5.446E-8 * (T - 76.11)^2 - \\ & 7.18E-8 * (T - 76.11) * (RH - 21.65) - \\ & 1.263E-7 (RH - 21.65)^2 * 365 * 100 \end{aligned} \quad (3)$$

Predictions from this model are shown in Figure 10 for several temperature/humidity combinations. Density is predicted to increase slightly at the lower temperature environments, while the data have shown no net change in these mild environments. This tendency of the model to predict a density change is likely a result of the minor seasonal fluctuations driven by variation in ambient humidity. While this produces no long-term change in density, some samples that were aged for shorter durations may show a net increase or decrease in density depending on when they began aging. This aspect of the model should improve with the accumulation and incorporation of additional data.

Predictions from the density model can provide a service life estimate based on density. The minimum allowable density to provide the required criticality control is 0.21 g/cc, and the minimum measured density for a fiberboard assembly is 0.242 g/cc. Therefore, the service life within a specific environment will be the time required for a 13 percent decrease in the overall density of the fiberboard assembly. Since the fiberboard will develop temperature and moisture gradients in service, potential exists for local variations in degradation rate throughout the assembly.

For an ambient temperature of 28°C, typical fiberboard temperatures in service might range from -35°C along the outer diameter surface to -58°C along the ID surface, with a maximum heat load present. The total moisture content will vary from package to package, but it can be assumed that the typical package will have no more moisture than would be absorbed from the air at



23°C and 100 percent RH. Without any redistribution of moisture, the elevated service temperatures would reduce the relative humidity in the package to ~55 percent along the outer diameter surface and ~17 percent along the inner diameter surface. For these conditions, the model predicts no decrease in density along either the inner diameter or outer diameter surface.

In reality, however, there will be moisture redistribution within the package. As the local humidity increases above 55 percent for a range of temperatures, the model predicts a decrease in density over time, with a corresponding finite service life. However, this rate would apply only to a local region along the fiberboard exterior surface. The overall average rate of density change for the full assembly will still be low, and is judged to provide a service life in excess of the initial storage period in KAMS. This judgment is supported by observation of packages removed from service after up to five years storage in KAMS. Examination of these packages has shown a range of fiberboard densities consistent with that of un-aged fiberboard, with no discernable change in the fiberboard exterior surface compared to the rest of the assembly.

## Conclusions

Two components of the 9975 package, Viton® GLT fluoroelastomer O-rings and Celotex cane fiberboard overpack, have been studied for lifetime evaluation in KAMS storage conditions. The GLT fluoroelastomer O-rings were subjected to accelerated thermal and radiation aging and evaluated for changes in compression stress-relaxation, compression set, and leakage behavior. Fiberboard was evaluated for changes in dimensions, thermal conductivity, specific heat capacity, and mechanical strength. Service life is strongly dependent on actual storage conditions. Combined surveillance and laboratory results conclude that both the Viton® GLT based fluoroelastomer O-rings and Celotex® cane fiberboard are expected to exceed the initial storage period in KAMS. Based on current data, O-rings are expected to last at least twenty years in service, but may require replacement before the end of the total storage period. Increased confidence in this conclusion is expected with the accumulation of additional data from both the laboratory testing and surveillance.

## Acknowledgements

The contributions of the following individuals to this report are greatly appreciated: Carla Loftin, Dr. Elliot Clark, Chip Few, Dominio' Strom, Connie Yung, Tony Curtis, Larry Feutral, Chris Beam, SRNL/EES Machine Shop, and the SRNL High Pressure Laboratory. Consultation with Dr. Robert Bernstein at Sandia National Laboratory and Dr. Mark Wilson at Kansas City Plant is much appreciated.

*Elizabeth N. Hoffman is a Senior Engineer A at Savannah River National Laboratory. She holds a Ph.D. in materials science and engineering and a B.S. in materials engineering from Drexel University.*

*T. Eric Skidmore is a Fellow Engineer at Savannah River National Laboratory. He holds an M.S. in bioengineering from Clemson University and a B.S. in materials science and engineering from North Carolina State University.*

*William L. Daugherty is a Fellow Engineer at Savannah River National Laboratory. He holds a Ph.D. in nuclear engineering from North Carolina State University.*

*Kerry A. Dunn is an advisory engineer at Savannah River National Laboratory. She has an M.S. in materials science and engineering and a B.S. in metallurgy from Pennsylvania State University.*

## References

1. WSRC-SA-2002-00005, *Material Storage Facilities Documented Safety Analysis*, Rev. 3.
2. Vormelker, P. R., and W. L. Daugherty. 2005. Thermal Properties of Fiberboard Overpack Materials in the 9975 Shipping Package, PVP2005-71569, *Proceedings of PVP2005: ASME Pressure Vessels & Piping Division Conference*.
3. Daugherty, W. L., and P. R. Vormelker. 2005. Mechanical Properties of Fiberboard Overpack Materials in the 9975 Shipping Package, PVP2005-71568, *Proceedings of PVP2005: ASME Pressure Vessels & Piping Division Conference*.
4. Daugherty, W. L. 2007. Properties of Fiberboard Overpack Material in the 9975 Shipping Package Following Thermal Aging, PVP2007-26114, *Proceedings of PVP2007: ASME Pressure Vessels & Piping Division Conference*.
5. Gillen, K. T., M. Celina, and R. Bernstein. 2003. Validation of Improved Methods for Predicting Long-term Elastomeric Seal Lifetimes from Compression Stress-Relaxation and Oxygen Consumption Techniques. *Polymer Degradation and Stability*, 82 1. 25-35.
6. Edmondson, A. L. 1997. Compressive Stress Relaxation, A Comparison of Methods and Fixtures, *Presented at the Service Life Prediction Symposium*, University of Akron.
7. Hiemenz, P. 1984. *Polymer Chemistry, The Basic Concepts*. New York: Marcel Dekker.
8. Gillen, K. T., M. Celina, and .M. R. Keenan. 1999. *Better Methods for Predicting Lifetimes of Seal Materials*. SAN099-0623C. Sandia National Laboratories, Albuquerque, NM USA.
9. Browne, F. L. Theories of the Combustion of Wood and Its Control a Survey of the Literature, *FPL Report #2136*, Forest Products Laboratory, USDA.

# Thermal Analysis of 3013/9975 Configuration

Narendra K. Gupta

Savannah River National Laboratory, Aiken, South Carolina USA

## Abstract

The 3013 containers are designed in accordance with the DOE-STD-3013-2004<sup>1</sup> and are qualified to store plutonium (Pu) bearing materials for fifty years. The U.S. Department of Energy (DOE) certified Model 9975 shipping package is used to transport the 3013 containers to the K Area Material Storage (KAMS) facility at the Savannah River Site (SRS) and to store the containers until the plutonium can be properly dispositioned. Detailed thermal analyses to support the storage in the KAMS facility are given in References 2, 3, and 4. The analyses in this paper serve to provide non accident condition, non bounding, specific 3013 container temperatures for use in the surveillance activities. This paper presents a methodology where critical component temperatures are estimated using numerical methods over a range of package and storage parameters. The analyses include factors, such as ambient storage temperature and the content weight, density, heat generation rate, and fill height, that may impact the thermal response of the packages. Statistical methods are used to develop algebraic equations for ease of computations to cover the factor space. All computations were performed in BTU FT-Hr-°F units.

## Introduction

### 9975 Packaging Configuration

The 9975 package is designed by analysis and testing to meet the requirements of 10 CFR Part 71<sup>2</sup> to ensure that the environment and public health are not adversely impacted when the package is used to transport radioactive materials (RAM) under normal conditions of transport (NCT) and under hypothetical accident conditions (HAC). Figure 1 shows the schematic of the 9975 package in a vertical orientation. Only the vertical orientation is analyzed in this paper since this is the orientation for both transportation and storage. The package consists of an outer thirty-five gallon stainless steel (SS) drum, a primary containment vessel (PCV) for the RAM, a secondary containment vessel (SCV) for added protection, a lead shield, and Celotex as the insulating and energy-absorbing material for the protection of containment vessels during accidental impact and fire conditions.

### 3013 Container Assembly

The 3013 container assembly consists of an outer container, an inner container, and, in most assemblies, a convenience container. The convenience container houses the RAM contents and loosely

fits inside the inner container. The inner container in turn loosely fits inside the outer container that goes inside the PCV. The outer container is a standard British Nuclear Fuels Limited (BNFL) welded design; it is made of 316L SS, one design is 254 mm tall and 125 mm in diameter.<sup>6</sup> The inner container designs are U.S. Department of Energy (DOE) site specific but are designed to fit inside the standard BNFL outer container. The analyzed inner container is also a welded design: it is made of 304L SS, is 213 mm tall and 117 mm in diameter.<sup>6</sup> Figure 2 shows a 3013 container assembly with Rocky Flats inner container and a convenience container inside a PCV.

### Surveillance Program

The 9975 package was designed as a transportation package and was not qualified for the long-term storage of materials. Therefore, a comprehensive surveillance program was set up to assess the material and thermal performance of the 9975 components to ensure that the design limits of the package are not violated under the long-term storage conditions.<sup>7</sup> In addition, since the outer and inner 3013 containers have high residual stresses and contain chlorides and moisture, the stress corrosion potential of these vessels is an important consideration in the surveillance program. The program examines the outer and inner containers, samples for signs of stress corrosion, tests O-rings for leakage rate, and tests Celotex properties at elevated temperatures to ensure that their performance is not degraded over time. The 3013 container assemblies are also examined for gas generation and pressure build up to ensure that the design limits are not violated during the long-term storage.

### Thermal Output Variables

Thermal output variables required to meet the surveillance needs are the temperatures of the O-rings, Celotex, and the 3013 container at selected locations. This paper covers the 3013 assembly component temperatures. The containers temperatures are calculated at three locations (T1, T2, and T3) on the inner container, the outer container, and the convenience container. These locations are shown in Figure 3.  $T_G$  is the average gas/content temperature.

### Design Parameters

Thermal performance of the 9975 packaging depends upon its content characteristics (i.e., density, weight, and decay heat rate) and the ambient storage conditions. Limits are placed on the





Figure 1. 9975 schematic with key components

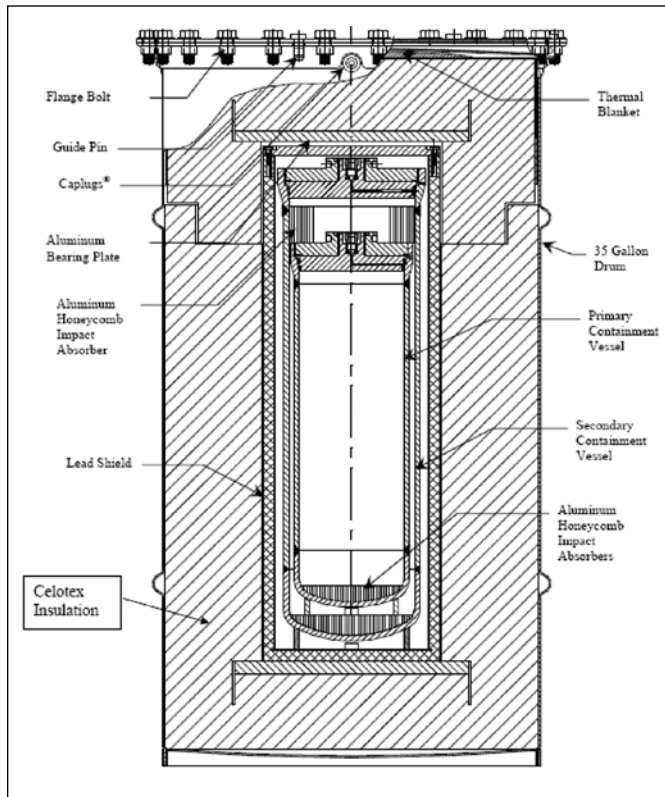


Figure 2. 3013 container in PCV

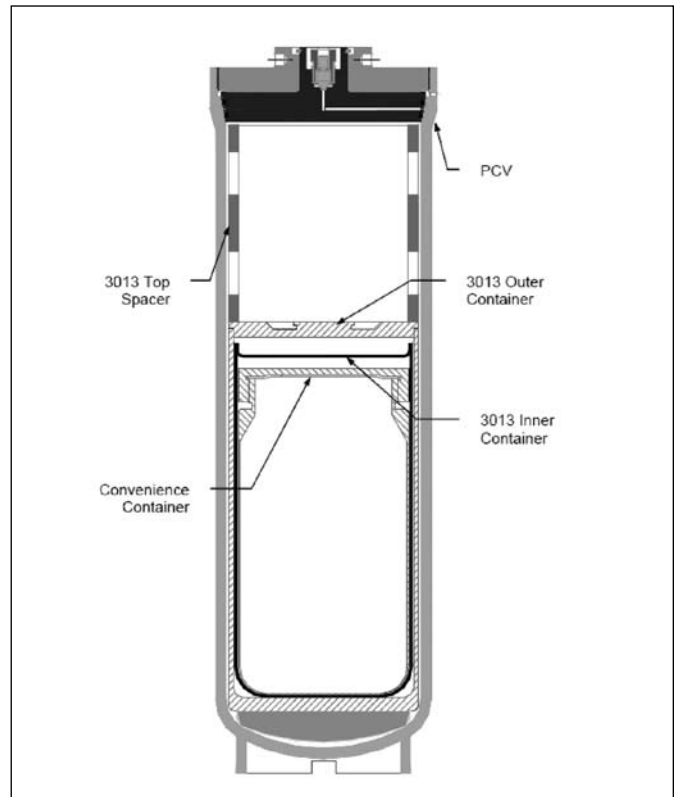
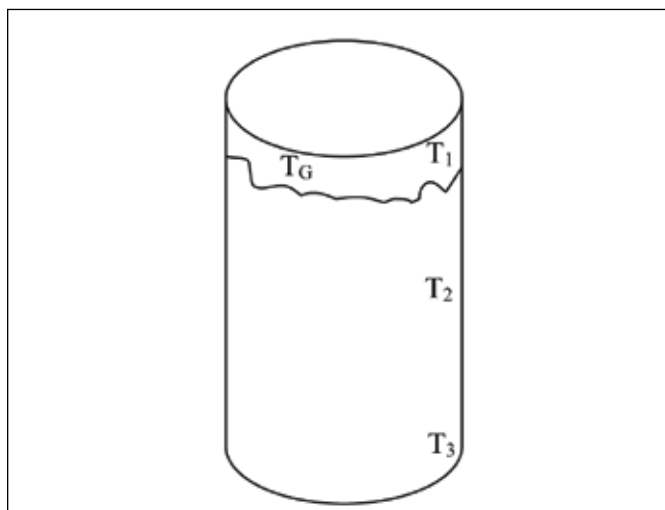


Figure 3. Output locations



maximum decay heat rate (19 watts) and the fill height (17 cm) of the radioactive material inside the convenience containers. Performance also varies to a small extent based on the composition of the fill gases since the thermal properties of the oxide contents vary with the fill gases. The fill gas assumed in this paper is a mixture of 75 percent He and 25 percent air at atmospheric con-

ditions to simulate the “no greater than 5 percent oxygen limitation” required in the 9975 package Safety Analysis Report for Packaging (SARP).<sup>5</sup> The 3013 containers are normally loaded in glove boxes with a helium environment and therefore no air is expected in the fill gases. Since the thermal conductivity of helium is higher than the conductivity of the He-Air mixture, the temperatures reported here are conservative (2°F to 3°F higher). Table 1 gives the *expected* values of parameters and the limitations for the plutonium oxide (PuO<sub>2</sub>) contents in the Rocky Flats 3013 container assembly.

PuO<sub>2</sub> fill heights and heat rates are calculated based on oxide mass and bulk density, but are never to exceed a fill height of 17.0 cm or a heat rate of 19.0 watts. Table 2 gives the resulting heat loads consistent with the fill height and the powder density.

### Mathematical Model

The computational thermal model solves the following steady state heat transfer equation in cylindrical coordinates.

$$k_1 \frac{\partial^2 T}{\partial r^2} + \frac{k_1}{r} \frac{\partial T}{\partial r} + k_2 \frac{\partial^2 T}{\partial z^2} + q''' = 0 \quad (1)$$





Where  $q'''$  is the volumetric heat generation by the fissile material per unit time,  $k_r$  and  $k_z$  are the thermal conductivities of the materials in the r and z directions, and T is the temperature. The values of  $k_r$  and  $k_z$  are the same since the materials are isotropic. For some materials thermal conductivity is a function of temperature.

Table 1. 3013 plutonium oxide variables

Variable	Low	Mid	High
Fill height (cm)	?	?	17.0
Oxide bulk density (g/cc)	1.0	3.0	5.0
Heat generation (W/kg)	3.0	6.0	12.0
Total heat load (W)	5.0	10.0	19.0
Oxide mass (g)	2000	3000	5000

a Height to be calculated to meet the constraints

### Statistical Methods

Estimating the 3013 component temperatures for parameter (density, heat load, and storage temperature) values other than used in Table 1 is best accomplished by performing regression analyses. However, regression analysis is a statistical method and certain conditions must be met for the regression equation to be a good predictor.<sup>8</sup> These conditions are:

1. The errors (residuals) have a zero mean.
2. The errors (residuals) have constant variance.
3. The errors (residuals) are uncorrelated, i.e., they are independent.
4. The errors (residuals) are normally distributed.

A general linear regression equation is of the form:

$$T = \beta_0 + \beta_1 D + \beta_2 W + \beta_3 T_a + \beta_4 D^2 + \beta_5 W^2 + \beta_6 T_a^2 + \beta_7 DW + \beta_8 DT_a + \beta_9 WT_a + \epsilon$$

Where:

T is the component temperature, (°F)

D is the content density, g/cc

W is the content decay heat, watts

$T_a$  is the ambient temperature

DW,  $DT_a$ , and  $WT_a$  are the interaction terms,

$\epsilon$  is the error term, and

$\beta_1, \beta_2,$  etc. are the regression parameters that will be calculated from the computed temperature data.

### Thermal Models

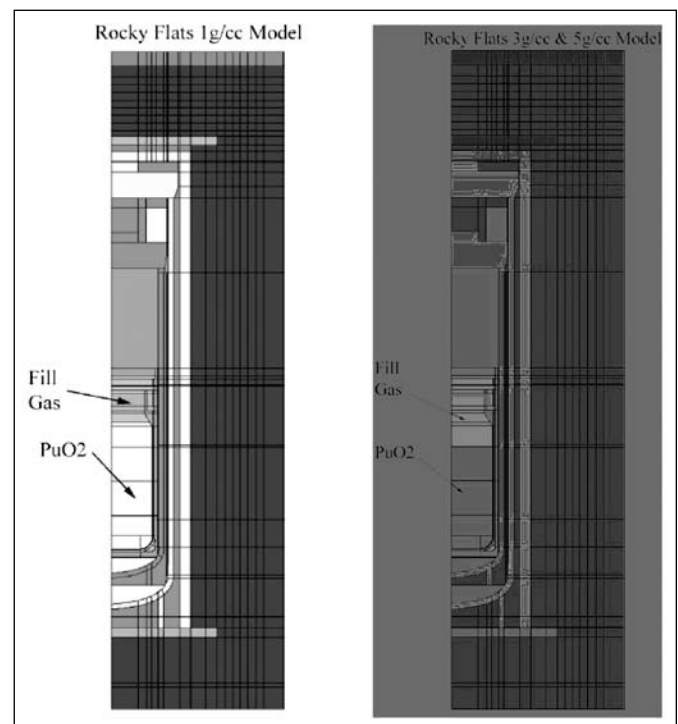
The differential equation 1 is solved numerically by a general purpose conduction-radiation computer code MSC/PATRAN/Thermal.<sup>9</sup> The data required for creating the thermal models are

the component geometries, material properties, thermal loads, and boundary conditions. The inputs and simplifying assumptions made in creating these models are given in detail in the project report in Reference 10. Since the 9975 and 3013 geometries are cylindrical, two axisymmetric models were created consistent with the fill heights shown in Table 2. These two models with materials depicted as different colors are shown in Figure 4.

Table 2. Fill height of PuO<sub>2</sub>

Density (g/cc)	Rocky Flats Configuration		
	Height (cm/inches)	Weight (kg)	Heat Load (watts)
1	17/6.693	1.592	4.78
3	13.62/5.364	3	10
5	13.62/5.364	5	19

Figure 4. Rocky Flats 9975 models



### Boundary Conditions

The boundary conditions are the ambient storage temperatures, natural convection losses, and the radiation losses from the 9975 packaging surface. The convection correlations and surface emissivities used in the models are given in Reference 10. The 9975 package is modeled in an upright configuration with the bottom assumed adiabatic and heat losses occurring only from its cylindrical and top surfaces.

### Analysis Runs



The two models shown in Figure 4 are analyzed for different values of PuO<sub>2</sub> density, heat rate, and ambient storage temperatures. Additional analyses are also performed to include low probability cases of high density contents with impurities having low heat rates and contents with low density and high heat rates. Table 3 gives the analyses that were performed to cover the entire parameter space. Inclusion of these additional analyses (Analyses 13 to 20 in Table 3) will result in more accurate response surface when regression analyses are performed.

## Results

Table 3. Model analyses

Analysis No.	Density (g/cc)	Decay Heat Rate (Watts)	Ambient Temperature (°F)
1	1	4.78	55
2	1	4.78	85
3	1	4.78	120
4	1	4.78	162
5	3	10	55
6	3	10	85
7	3	10	120
8	3	10	162
9	5	19	55
10	5	19	85
11	5	19	120
12	5	19	162
13	1	19	55
14	1	19	85
15	1	19	120
16	1	19	162
17	5	4.78	55
18	5	4.78	85
19	5	4.78	120
20	5	4.78	162

The analyses enumerated in Table 3 are run using the MSC/Thermal computer code.<sup>9</sup> Temperatures at locations T1, T2, and T3 are picked from the nodes in the models close to the locations shown in Figure 3. Gas temperature is the nodal average of the entire content volume. Regression analyses error tests are performed using the statistical software MINITAB.<sup>11</sup>

## Outer Container

### Temperatures

The temperatures at the indicated locations in the outer 3013 container are summarized in Table 4. The highest gas temperature is 281°F while the highest container temperature is 293°F.

### Regression Analyses

The regression analysis results in terms of PuO<sub>2</sub> density (D), heat rate (W), and storage temperature (T<sub>a</sub>) are given below. The statistical error independence test and normality test results for location T1 are shown in Figures 5 and 6. These figures show that the errors are independent and normally distributed. The errors for location T2, T3, gas temperature T<sub>G</sub> are also independent and are normally distributed.

The regression equations using statistical software MINITAB are:

$$\text{Temp (T1)} = -9.16 + 0.322 D + 9.038 W + 0.983 T_a - 0.146 W^2 + 0.237 DW - 0.0058 WT_a$$

$$\text{Temp (T2)} = -12.66 + 0.407 D + 10.53 W + 0.981 T_a - 0.187 W^2 + 0.321 DW - 0.006 WT_a$$

$$\text{Temp (T3)} = -13.66 + 0.372 D + 9.73 W + 0.985 T_a - 0.187 W^2 + 0.353 DW - 0.005 WT_a$$

$$\text{Temp (Gas)} = -10.7 + 0.361 D + 9.56 W + 0.983 T_a - 0.162 W^2 + 0.270 DW - 0.006 WT_a$$

## Inner Container

### Temperatures

The temperatures at the indicated locations in the inner 3013 container are summarized in Table 5. The highest gas temperature is 285°F while the highest container temperature is 295°F.

### Regression Analyses

The regression analysis results in terms of PuO<sub>2</sub> density (D), heat rate (W), and storage temperature (T<sub>a</sub>) are given below. The statistical error independence and normality test results for location T1 are shown in Figures 7 and 8. These figures show that the errors are independent and normally distributed. The errors for location T2, T3, gas temperature T<sub>G</sub> are also independent and are normally distributed.

The regression equations using statistical software MINITAB are:

$$\text{Temp (T1)} = -9.19 + 0.325 D + 9.16 W + 0.983 T_a - 0.146 W^2 + 0.237 DW - 0.006 WT_a$$

$$\text{Temp (T2)} = -12.37 + 0.360 D + 10.66 W + 0.978 T_a - 0.190 W^2 + 0.326 DW - 0.006 WT_a$$

$$\text{Temp (T3)} = -14.8 + 0.726 D + 10.33 W + 0.983 T_a - 0.186 W^2 + 0.303 DW - 0.006 WT_a$$

$$\text{Temp (Gas)} = -10.57 + 0.355 D + 9.76 W + 0.983 T_a - 0.162 W^2 + 0.270 DW - 0.006 WT_a$$



Table 4. Outer container temperatures

Density D (g/cc)	Decay Heat W (watts)	Temp. Ta (°F)	Location T1 (°F)	Location T2 (°F)	Location T3 (°F)	Gas (°F)
1	4.78	55	84.47	87.35	83.14	85.18
1	19	55	162.78	173.62	159.49	165.72
3	10	55	126.25	136.09	128.74	129.42
5	19	55	182.75	200.56	188.87	188.51
5	4.78	55	90.62	95.56	91.84	92.15
1	4.78	85	113.18	116.03	112.09	113.92
1	19	85	188.70	199.39	186.07	191.69
3	10	85	153.44	163.07	156.22	156.56
5	19	85	208.20	225.70	214.71	213.87
5	4.78	85	119.12	123.96	120.50	120.65
1	4.78	120	146.80	149.59	145.94	147.55
1	19	120	219.35	229.88	217.41	222.39
3	10	120	185.45	194.84	188.52	188.50
5	19	120	238.38	255.58	245.36	243.98
5	4.78	120	152.51	157.22	154.04	154.03
1	4.78	162	187.34	190.07	186.74	188.11
1	19	162	256.95	267.34	255.82	260.06
3	10	162	224.25	233.39	227.64	227.24
5	19	162	275.69	292.55	283.24	281.21
5	4.78	162	192.81	197.37	194.49	194.31

Figure 5. Error independence test for outer container

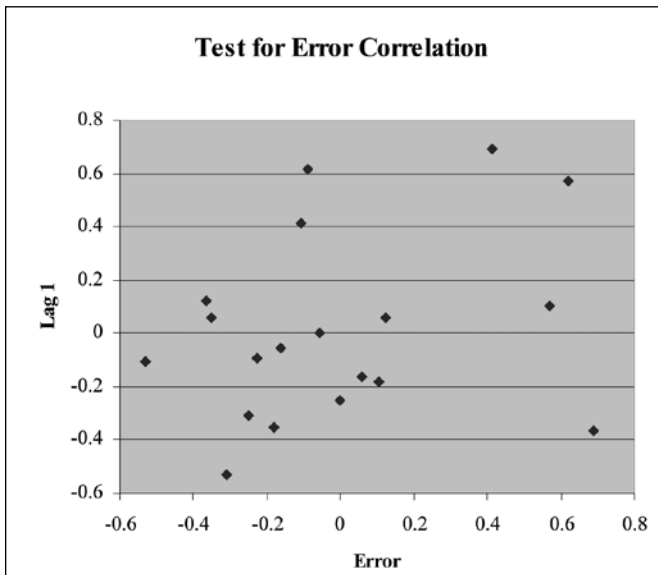
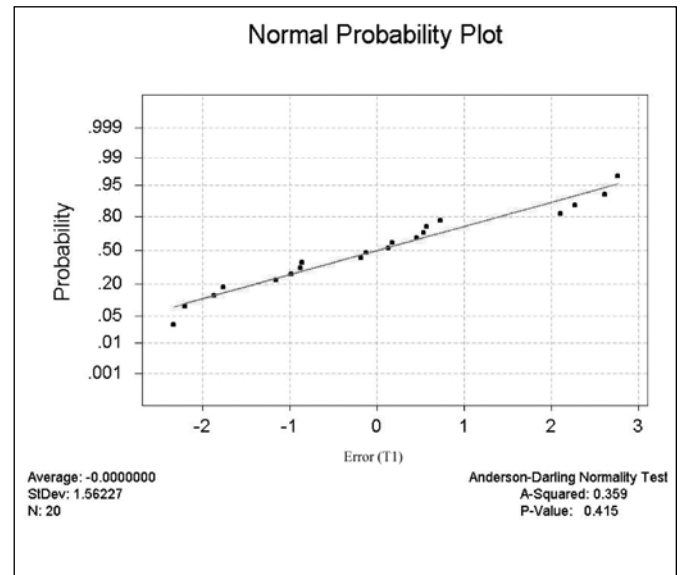


Figure 6. Error normality test for outer container





**Table 5.** Inner container temperatures

Density D (g/cc)	Decay Heat W (watts)	Temp. Ta (°F)	Location T1 (°F)	Location T2 (°F)	Location T3 (°F)	Gas (°F)
1	4.78	55	84.98	87.92	84.80	86.24
1	19	55	164.70	175.65	169.08	169.60
3	10	55	127.32	137.30	133.06	131.45
5	19	55	184.67	202.74	196.19	192.25
5	4.78	55	91.14	96.18	93.98	93.19
1	4.78	85	113.68	116.57	113.68	114.95
1	19	85	190.59	201.37	195.49	195.47
3	10	85	154.49	164.24	160.36	158.58
5	19	85	210.10	227.82	221.76	217.59
5	4.78	85	119.64	124.56	122.55	121.66
1	4.78	120	147.29	150.12	147.45	148.55
1	19	120	221.21	231.81	226.65	226.07
3	10	120	186.48	195.97	192.46	190.50
5	19	120	240.24	257.65	252.13	247.67
5	4.78	120	153.01	157.80	155.99	155.00
1	4.78	162	187.82	190.57	188.15	189.07
1	19	162	258.76	269.21	264.86	263.63
3	10	162	225.26	234.48	231.38	229.22
5	19	162	277.52	294.56	289.68	284.88
5	4.78	162	193.30	197.29	196.33	195.25

**Figure 7.** Error independence test for inner container

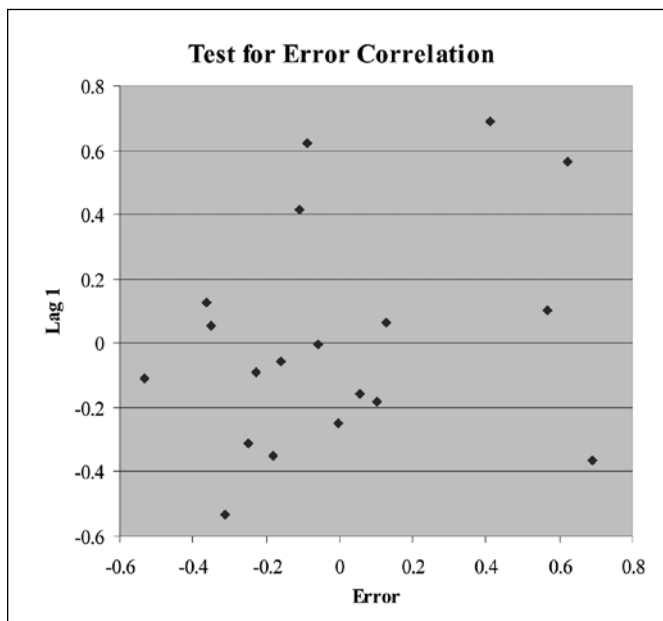


**Figure 8.** Error normality test for inner container

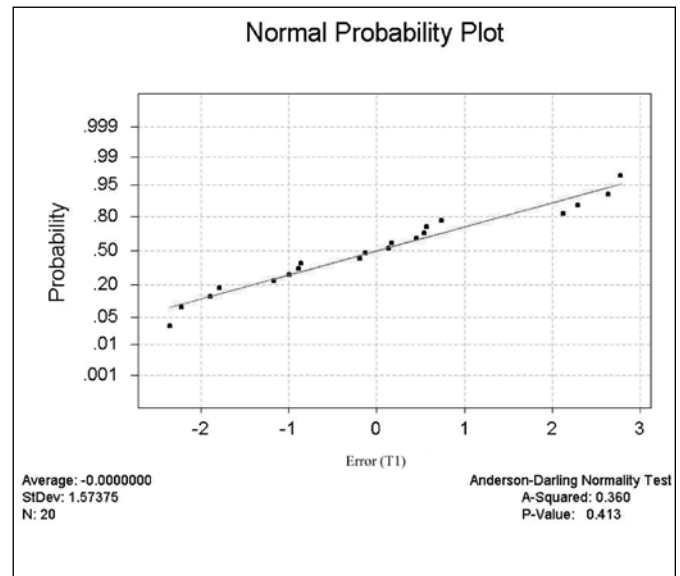




**Table 6.** Convenience container temperatures

Density D (g/cc)	Decay Heat W (watts)	Temp. Ta (°F)	Location T1 (°F)	Location T2 (°F)	Location T3 (°F)	Gas (°F)
1	4.78	55	86.91	89.17	84.05	93.73
1	19	55	171.82	180.30	162.75	199.58
3	10	55	130.50	141.64	131.33	146.48
5	19	55	190.23	210.50	193.45	212.74
5	4.78	55	92.68	98.34	93.17	98.40
1	4.78	85	115.57	117.80	112.96	122.46
1	19	85	197.56	205.94	189.21	225.53
3	10	85	157.60	168.49	158.71	173.57
5	19	85	215.53	235.47	219.14	238.10
5	4.78	85	121.14	126.67	121.77	126.87
1	4.78	120	149.12	151.31	146.77	156.09
1	19	120	228.01	236.30	220.43	256.21
3	10	120	189.51	200.11	190.91	205.47
5	19	120	245.55	265.16	249.63	268.22
5	4.78	120	154.47	159.85	155.26	160.21
1	4.78	162	189.59	191.74	187.52	196.63
1	19	162	265.39	273.61	258.69	293.86
3	10	162	228.19	238.51	229.92	244.17
5	19	162	282.69	301.92	287.32	305.48
5	4.78	162	194.71	199.92	195.65	200.45

**Figure 9.** Error independence test for convenience container

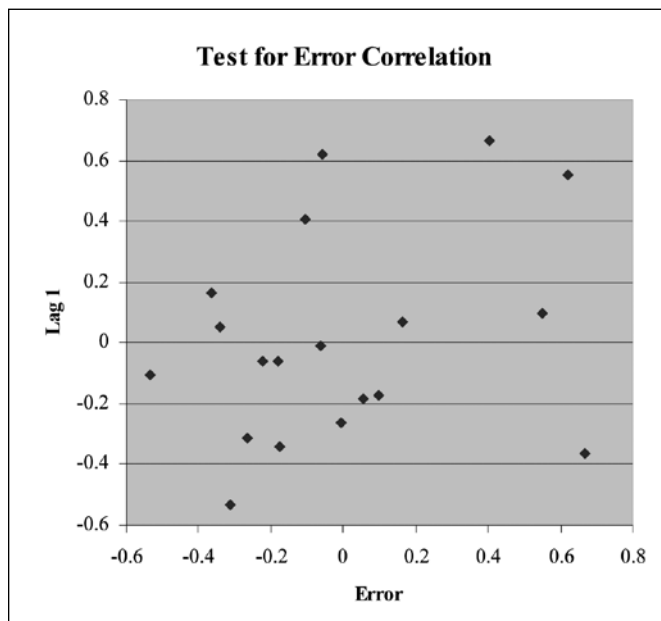
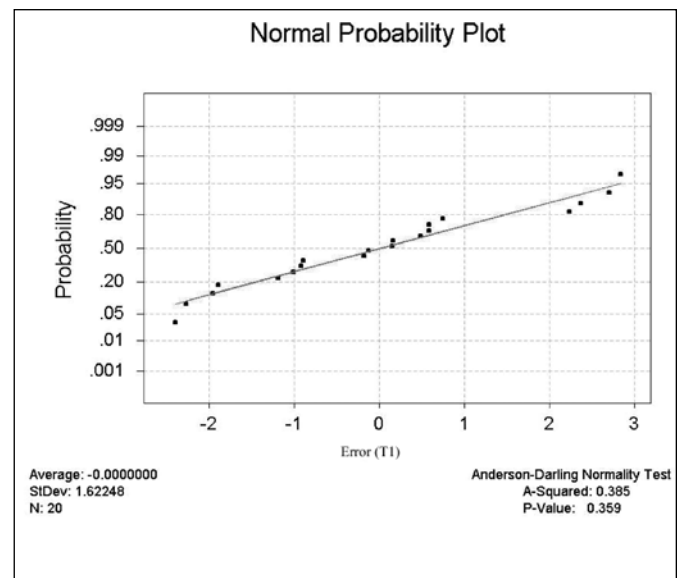


**Figure 10.** Error normality test for convenience container





## Convenience Container

### Temperatures

The temperatures at the indicated locations in the convenience 3013 container are summarized in Table 6. The highest gas temperature is 305°F while the highest container temperature is 302°F.

### Regression Analyses

The regression analysis results in terms of PuO<sub>2</sub> density (D), heat rate (W), and storage temperature (T<sub>a</sub>) are given below. The statistical error independence and normality test results for location T1 are shown in Figures 9 and 10. These figures show that the errors are independent and normally distributed. The errors for location T2, T3, gas temperature T<sub>G</sub> are also independent and are normally distributed.

The regression equations using statistical software MINITAB are:

$$\text{Temp (T1)} = - 8.51 + 0.326 D + 9.43W + 0.983 T_a - 0.141 W^2 + 0.217 DW - 0.006 WT_a$$

$$\text{Temp (T2)} = - 14.31 + 0.448 D + 11.33 W + 0.98 T_a - 0.208 W^2 + 0.361 DW - 0.006 WT_a$$

$$\text{Temp (T3)} = - 14.32 + 0.397 D + 10.1 W + 0.984 T_a - 0.196 W^2 + 0.369 DW - 0.005 WT_a$$

$$\text{Temp (Gas)} = - 13.79 + 0.386 D + 12.31 W + 0.98 T_a - 0.198 W^2 + 0.142 DW - 0.006 WT_a$$

## Conclusions

Detailed finite element analyses are performed to assess the thermal performance of the 3013/9975 container configuration. Temperatures are calculated at specific locations of the 3013 container components. Regression equations are developed for the temperatures in terms of PuO<sub>2</sub> density, heat rate, and the ambient storage temperature. The gas temperatures of a convenience container may exceed 300°F as may the temperature of the container wall, depending on the regression variables. Although these temperatures are higher than those anticipated in actual containers, it is clear that the predicted temperatures are sufficient to support corrosion-induced degradation processes.

*Narendra K. Gupta is a principal engineer at Savannah River National Laboratory. He holds an M.S. in aerospace engineering and another in mechanical engineering.*

## References

1. 2004. DOE Standard: Stabilization, Packaging, and Storage of Plutonium Bearing Materials. DOE-STD-3013-2004. 2004. Department of Energy, Washington, DC.
2. Norkus, J. K. 2004. *Steady State Thermal Analysis of KAMS for No Flow Conditions (U)*, S-CLC-K-00203, Rev. 0. Washington Safety Management Solutions, Aiken, South Carolina USA.
3. Norkus, J. K., 2005. *Thermal Analysis of Fires KAMS for No Flow Conditions (U)*, S-CLC-K-00204, Rev. 1. Washington Safety Management Solutions, Aiken, South Carolina USA.
4. Salyer, W. D. 2005. *Integrated Thermal Analysis of the 9975 and SAFKEG Shipping Packages for KAMS for Phase 6 (U)*, S-CLC-K-00194, Rev. 1. Washington Safety Management Solutions, Aiken, South Carolina USA.
5. 2007. *Model 9975 B(M)F-96, Safety Analysis Report for Packaging (U)*, WSRC-SA-2002-00008, Rev. 1. Washington Savannah River Company, Aiken, South Carolina USA.
6. Drawings:
  - Outer Can – SRS: M-PV-F-0017
  - Rocky Flats Inner Can – SRS: M-PV-F-0016
  - Rocky Flats Convenience Can – DMW: 1509-02
7. 2006. *K-area Materials Storage Facility Documented Safety Analysis, CN5A*, WSRC-SA-2002-00005, Rev. 1. Washington Savannah River Company, Aiken, South Carolina USA.
8. Montgomery, D. C., and E. A. Peck. 1992. *Introduction to Linear Regression Analysis*. 2nd Edition. New York: John Wiley & Sons.
9. MSC.PATRAN THERMAL 2003 r2. Online Manual. MSC Software Company, Santa Ana, California USA.
10. Gupta, N. K., 2007. *Thermal Models for the 3013 Containers in KAMS*, M-CLC-M-00720 Rev.1. Washington Savannah River Co., Aiken, South Carolina USA.
11. *MINITAB Statistical Software*, Release 13. 2000. State College, Pennsylvania USA: MINITAB Inc.

# Thermal Conductivity of High-purity and Impure Plutonium Oxide Materials

D. Kirk Veirs and F. Coyne Prenger

Los Alamos National Laboratory, Los Alamos, New Mexico USA

## Abstract

The thermal conductivity of self-heated materials such as those containing plutonium determines the temperature profile, relative humidity profile, and, therefore, the potential for material phases to vary within a finite volume of initially homogeneous material. The thermal conductivity of complex powdered materials is difficult to reliably estimate from composition alone and is strongly influenced by processing history and impurities. The thermal conductivity of a high purity plutonium oxide and a number of MIS represented materials consisting of plutonium oxide and salt-based impurities are determined from measured temperature gradients in 3013 containers. The influence of material heat generation, fill level, and thermal conductivity on the magnitude of thermal gradients expected within materials in 3013 containers is discussed.

## Introduction

A complete description of the thermal behavior of filled DOE STD 3013 (3013) containers requires accurate values for the thermal conductivity of the contained materials. Detailed thermal analyses of 3013 containers have been conducted to ensure that gas pressures remain within design criteria<sup>1</sup> and to ensure that containers stored for more than five years can be opened safely during surveillance.<sup>2</sup> A correlation by Deissler and Eian is used in these analyses to calculate the effective thermal conductivity of the plutonium oxide powder/fill gas combination (note: the thermal conductivity of the powder, including the gas and the solid powder, will be referred to as the effective thermal conductivity).<sup>3</sup> The Deissler-Eian correlation describes the effective thermal conductivity in terms of the porosity of the powder and the thermal conductivity of the crystalline solid material and the fill gas.

The Deissler-Eian correlation is derived assuming particle arrays consisting of solid cylinders and spheres. Plutonium oxide powder particles have a complicated geometry with considerably more surface area than a solid sphere of the same size. The measured surface to volume ratios indicate that the plutonium oxide particles have internal voids accessible to gas and are not consistent with the Deissler-Eian assumptions. We have experimentally determined the effective thermal conductivity of a high-purity plutonium oxide powder using both He and Ar as the fill gas.<sup>4</sup> The plutonium oxide powder was obtained from oxalate precipi-

tate from nitric acid anion exchange purified plutonium solution. The powder has a particle size distribution and specific surface area typical of weapons grade plutonium oxides packaged in 3013 containers. The observed effective thermal conductivity differs from the effective thermal conductivity calculated using the Deissler-Eian correlation. We developed a model that reproduces the observed effective thermal conductivity over a broad range of pressures of the Ar and He fill gases, referred to as the Bielenberg Model and described further below. In order to accurately fit the observed trends, a parameter related to the size of internal voids was necessary. The first section of this paper will describe important aspects of this model and contrast the differences in effective thermal conductivity calculated using this model with those calculated using the Deissler-Eian correlation.

Plutonium oxides with chlorine impurities are problematic materials within 3013 containers due to their demonstrated ability to cause corrosion, especially stress corrosion cracking. Temperature gradients within the contained material can cause large differences in the local relative humidity. Such differences in combination with specific material and water contents can result in conditions conducive to corrosion at the container walls in material that would not be corrosive if there were no thermal gradients. The effective thermal conductivity of impure chloride materials is thus of importance to the long-term integrity of the 3013 containers. The second section of this paper will report measurements of the effective thermal conductivity of chloride materials in 3013 containers and evaluate the ability to determine the effective thermal conductivity in stored materials using what is known about their elemental composition. The results can be used in assessing thermal gradients in the various configurations of stored 3013 containers and their effect on relative humidity gradients and ultimately the potential for corrosion within 3013 containers.

## The Bielenberg Model

A model for determining the thermal conductivity of materials with large void fractions was developed using experimental observations of temperature profiles in beds of high-purity plutonium oxide with He and Ar fill gases.<sup>4</sup> The experimental data covers fill gas pressures from 0.05 kPa to 334 kPa. The plutonium oxide bed was kept constant while the fill gas and pressure were changed. The bed geometry was a cylinder where the centerline tempera-



ture near the midpoint of the bed height was determined by the heat generation and the effective thermal conductivity of the material. The heat conduction was mainly in the radial direction at this bed height. The model had to explain a number of unusual observations:

- The centerline temperature continued to decline as the fill gas pressure increased above one atmosphere, for both He and Ar, indicating that the effective thermal conductivity continues to increase with increasing gas pressure.
- At pressures above one atmosphere, the ratio of the increase in temperature from the wall to the centerline for He and Ar fill gases (approximately 2.8) was much smaller than the ratio of the thermal conductivity of the gases alone (8.2).
- At very low pressures the increase in centerline temperature exceeded 350°C and the radial temperature profile could not be fit by considering conduction pathways only but required the inclusion of thermal radiation effects.

A thermal conductivity model was developed to predict the thermal behavior of this fine, highly porous powder because the experimental measurements could not be reasonably interpreted using existing thermal conductivity models. The following discussion is a simplified version of the more complete discussion found in Bielenberg. The thermal conductivity expression was derived using the powder schematic in Figure 1.

Heat conduction occurs through two parallel pathways in the *gas* and *solid* regions of the powder. The bed porosity ( $\epsilon_b$ ) is used to define the relative areas of the *gas* and *solid* regions in the powder and, as defined herein, is synonymous with void fraction defined later in Equation 6. The gas region is defined here as the gas-only region of the powder whereas the solid region contains two solid particles (that may or may not have a porous structure) thermally in series with an interparticle domain that contains both solid–solid and gas–solid conduction pathways. Because the conductances are additive for parallel pathways, the effective thermal conductivity ( $k_{eff}$ ) is written as

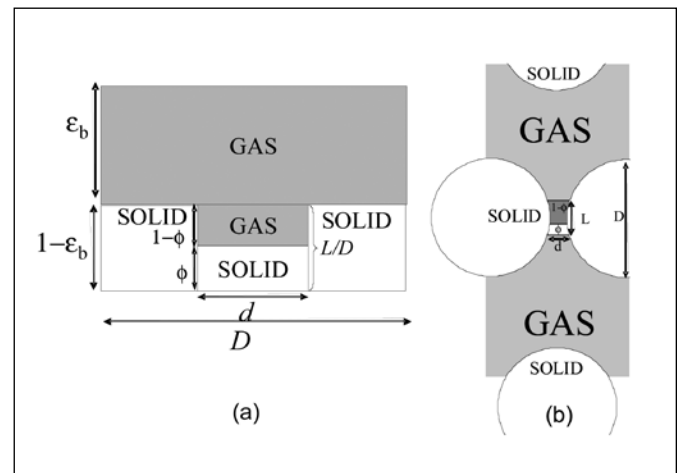
$$k_{eff} = \epsilon_b k_{g,o} + (1 - \epsilon_b)(L/D)k_s \quad (1)$$

In this expression,  $k_{eff}$  is the effective thermal conductivity of the powder,  $\epsilon_b$  is the bed porosity,  $k_{g,o}$  is the thermal conductivity of the fill gas in the outer pore region,  $k_s$  is the thermal conductivity of the solid region, and  $L/D$ , the interparticle contact fraction, defines the region where conduction occurs between the solid particles across a small gap. The thermal conductance of the solid region is a series combination of conductance through the solid particles and the interparticle region. The interparticle region contains parallel gas and solid conductance pathways. The resulting conductivity of the solid region is given as:

$$k_s = \frac{1}{\frac{\delta}{\phi k_{PuO_2} + (1-\phi)k_{g,in}} + \frac{1}{k_{PuO_2}}} \quad (2)$$

In this expression,  $k_{PuO_2}$  is the thermal conductivity of solid  $PuO_2$  crystals at theoretical density,  $k_{g,in}$  is the gas thermal conductivity in the interparticle area where the effective pore size is much smaller than the pore size in the outer “gas” region,  $\delta$  is the contact roughness (defined as the interparticle distance ( $d$ ) divided by the total cell distance ( $D$ )), and  $\phi$  defines the solid-solid contact region in the interparticle contact fraction. Combining Equation 1 and Equation 2 yields Equation 3, the effective thermal conductivity across the powder cell shown in Figure 1.

**Figure 1.** (a) Schematic for the powder thermal conductivity model. The model includes two parallel pathways through the gas and solid regions of the powder with the fractions determined by the bed porosity or void fraction ( $\epsilon_b$ ). Within the solid,  $1-\epsilon_b$  region, conduction occurs between the solids phase through a small contact length,  $L$  (nondimensionalized as the parameter  $L/D$ ). The relative areas of the solid-solid contact vs. the solid-gas-solid contact in the interparticle contact fraction ( $L/D$ ) are set by the parameter,  $\phi$ , the sphericity. The other parameter in this model,  $\delta$ , is the interparticle distance,  $d$ , divided by the total cell distance ( $D$ ). (b) Idealized schematic of particle packing and contact in the powder.



$$k_{eff} = \epsilon_b k_{g,o} + \frac{(1 - \epsilon_b)(L/D)}{\frac{\delta}{\phi k_{solid} + (1-\phi)k_{g,in}} + \frac{1}{k_{solid}}} \quad (3)$$

To calculate the thermal conductivity from this expression, the porosity is experimentally measured, the gas and solid thermal conductivities are available from the literature, and the sphericity ( $\phi$ ), contact roughness ( $\delta$ ), and interparticle contact fraction ( $L/D$ ) are fit parameters. A fit to the measured radial temperature





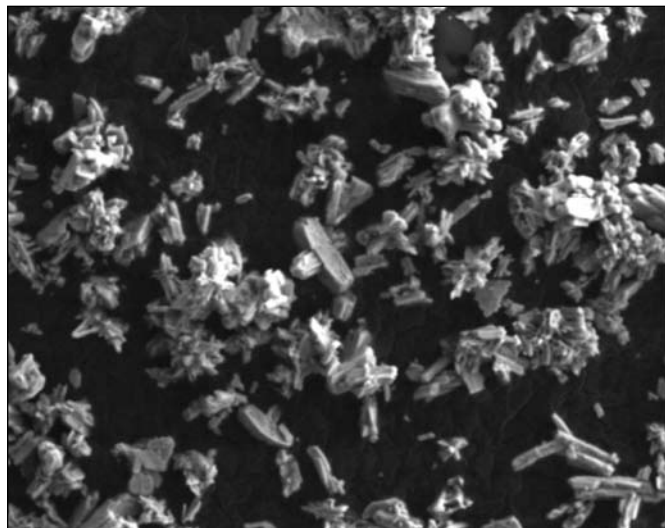
profiles at various pressures for He and Ar yielded values of the fit parameters that should be the same for oxalate precipitation derived high-purity plutonium oxide powders. The parameters are given in Table 1 as reported by Bielenberg. The parameters  $\lambda_{in}$  and  $\lambda_o$  are the pore size in the interstitial region and the outer pore region respectively.

Table 1. PuO<sub>2</sub> parameter

Parameter	Value
$\delta$	$2.86 \times 10^{-3}$
$\phi$	$1.71 \times 10^{-4}$
L/D	0.086
$\lambda_{in}$ ( $\mu\text{m}$ )	0.56
$\lambda_o$ ( $\mu\text{m}$ )	15.6

The interstitial and outer pore sizes are reasonably in agreement with images of the particles that make up the powder. A scanning electron microscopy (SEM) image of the high-purity plutonium oxide powder used by Bielenberg is given in Figure 2. The particles are best described as non-regular interpenetrating plates or columns with many internal voids. The particle's surfaces are rough, with a low probability of two particles having significant contact area.

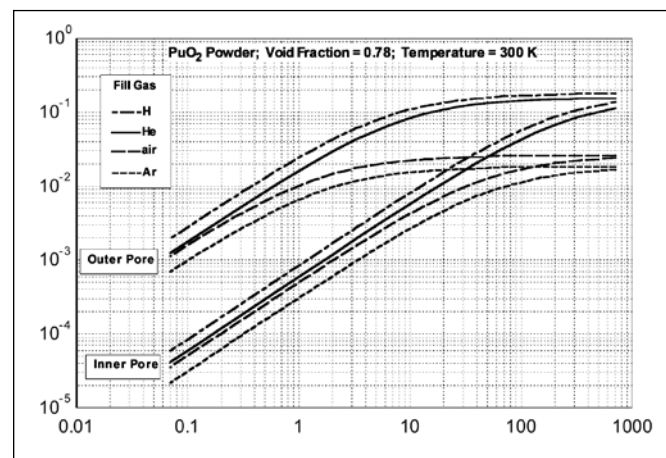
Figure 2. SEM of high-purity plutonium oxide powder. The powder was derived from oxalate precipitation of nitric acid anion exchange purified solution. The oxalate was calcined at 600°C and then 975°C for four hours. The length bar is 20  $\mu\text{m}$ .



With these parameters, the behavior of the effective thermal conductivity as a function of fill gas, fill gas pressure, and temperature can be explored. The thermal conductivity of solid PuO<sub>2</sub> at theoretical density is taken from Bielenberg. The thermal conductivity values for gases are built into the Engineering

Equation Solver (EES)<sup>5</sup> software. EES solves large sets of non-linear algebraic and differential Equations providing linear and non-linear regression, optimization, unit conversion and consistency checking, and uncertainty analyses. Built-in functions are provided for thermodynamic and transport properties of many substances, including steam, air, refrigerants, cryogenic fluids, Joint Army-Naval-Air Force (JANAF) table gases, hydrocarbons, and psychrometrics. Property data are provided using high-accuracy Equations of state models or from tabular data from National Institute of Standards and Technology (NIST), American Society of Heating, Refrigeration, and Air Conditioning Engineers (ASHRAE), and other sources. The behavior of the effective thermal conductivity with pressure is complicated by the existence of two pore sizes. At high pressures, the gas thermal conductivity is in the continuum regime where the conductivity is relatively independent of pressure. At low pressures, the gas thermal conductivity operates in the free molecular regime where it is a linear function of pressure. A transition region exists at intermediate pressures where the gas thermal conductivity is a function of both the continuum and free molecular thermal conductivities. The ratio of the mean free path to the pore size determines the location of the transition region. The thermal conductivity of the gases He, Ar, air, and H<sub>2</sub> in the outer pore region and the interstitial pore region are illustrated in Figure 3. In the outer pore region, the transition pressure regime for the light gases helium and hydrogen is between 10 and 100 kPa and for the heavier gases argon and air the transition pressure regime is between 2 kPa and 20 kPa. In contrast, in the interstitial pore region, the transition pressure regime is just starting to appear at 500 kPa for the lighter gases and the transition pressure regime is between 40 and 400 kPa for the heavier gases. It is the interstitial region with its nearly linear increase in the interstitial gas thermal conductivity at the higher pressures that is responsible for the

Figure 3. The gas thermal conductivity in the outer pore region and the interstitial pore region for fill gases He, Ar, air, and hydrogen as a function of the fill gas pressure at 300 K.

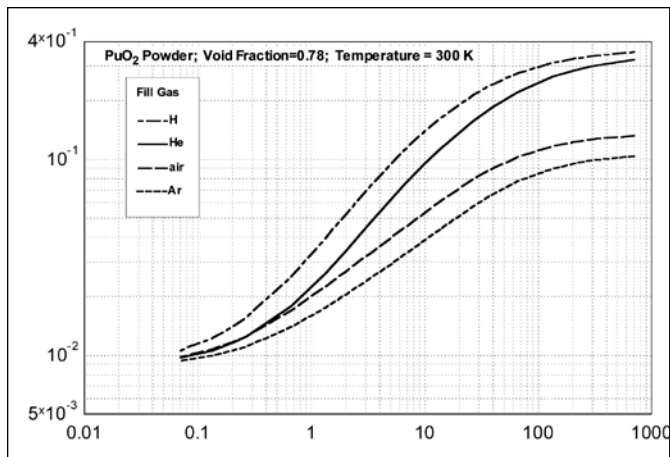




pressure dependence of the powder's effective thermal conductivity as reported by Bielenberg.

The effective thermal conductivity for this high-purity oxide for the four fill gases, as a function of pressure at a temperature of 300 K, is illustrated in Figure 4. At low pressures (below 0.1 kPa),  $k_{\text{eff}}$  is approximately  $0.013 \text{ W m}^{-1} \text{ K}^{-1}$  and is independent of the fill gas. At this very low value of the effective thermal conductivity the centerline temperature of the plutonium oxide powder can become quite high and was observed to be nearly  $350^\circ\text{C}$  above the wall temperature. If gas is reintroduced into the container, the heat stored in the bed center is rapidly conducted to the walls, resulting in a significant temperature rise, which can be problematic if unexpected. The effective thermal conductivity rapidly rises as the pressure of the fill gas approaches 100 kPa. Above 100 kPa the effective thermal conductivity begins to level off, but, for the light gases, still has a strong pressure dependence at 700 kPa. Typically, the thermal conductivity of gases is assumed to be independent of pressure at these pressures but the small pore sizes found in these powders negates this assumption. And finally, the effective thermal conductivity is strongly dependent upon the fill gas.

**Figure 4.** The effective thermal conductivity of high purity plutonium oxide powder with He, Ar, air, and hydrogen fill gases as a function of the fill gas pressure. The temperature for all curves is 300 K.

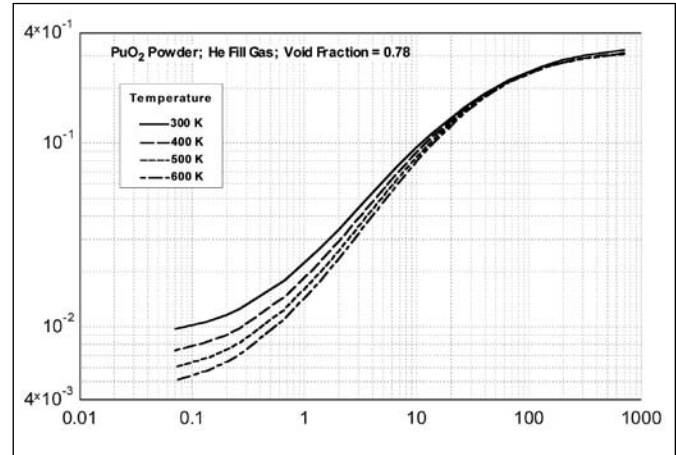


The temperature dependence of the effective thermal conductivity with He as fill gas as a function of pressure is given in Figure 5. At high pressures, the effect of temperature is minimal. At low pressures, the effective thermal conductivity decreases from 0.013 to  $0.007 \text{ W m}^{-1} \text{ K}^{-1}$ . This decrease is due to the temperature dependence of the thermal conductivity of the  $\text{PuO}_2$  solid at theoretical density, which decreases by a factor of two over this temperature range.

#### The Deissler-Eian correlation

The Deissler-Eian correlation allows the effective thermal conductivity of a packed powder bed to be calculated in terms of the gas

**Figure 5.** The effective thermal conductivity of high-purity plutonium oxide with He as fill gas calculated for temperatures from 300 K to 600 K as a function of fill gas pressure.



thermal conductivity ( $k_g$ ), the solid thermal conductivity of the particles ( $k_s$ ), and the void fraction ( $V_g$ ). Four cases are defined:

1. All gas and no solid where  $V_g = 1$  and  $k_{\text{eff}} = k_g$ .
2. Solid cylinders in a square array where  $V_g = 0.2146$  and the effective thermal conductivity is given by:

$$k_{\text{eff}} = \frac{k_g \pi}{2 \left( \frac{k_g}{k_s} - 1 \right)} - \frac{k_g \left( \frac{\pi}{2} - \sin^{-1} \left( \frac{k_g}{k_s} - 1 \right) \right)}{\left( \frac{k_g}{k_s} - 1 \right) \sqrt{2 \frac{k_g}{k_s} - \left( \frac{k_g}{k_s} \right)^2}} \quad (4)$$

3. Solid spheres in a cubical array where  $V_g = 0.4764$  and the effective thermal conductivity is given by:

$$k_{\text{eff}} = k_g \left( \frac{\pi \left( \left( \frac{k_g}{k_s} - 1 \right) - \ln \left( \frac{k_g}{k_s} \right) \right)}{2 \left( \frac{k_g}{k_s} - 1 \right)^2} + 1 - \frac{\pi}{4} \right) \quad (5)$$

4. All solid and no gas where  $V_g = 0$  and  $k_{\text{eff}} = k_s$ .

The effective thermal conductivity for a powder with a void fraction of  $V_g$  is determined by interpolating between the two cases that bound the void fraction. The method of interpolation is not stated. Knight and Steinke use a linear interpolation and Lam uses the natural logarithm of the effective thermal conductivity endpoints. For comparison purposes, we will use the method of Lam.

#### Results for Impure Oxides

The Bielenberg model reproduced the data for the high-purity oxide with 0.78 void fraction. However, material in 3013 containers is very diverse. The actinide content can vary from



88 wt percent (high-purity oxide) to 30 wt percent. The void fraction of materials from packaged 3013 containers can be calculated from the pycnometer density and bulk density measured during destructive evaluation (DE). The void fraction is given by

$$\epsilon_b = \left( 1 - \frac{\rho_b}{\rho_p} \right) \quad (6)$$

where  $\rho_b$  is the bulk density and  $\rho_p$  is the pycnometer density. The range of observed void fractions from 33 DEs is 0.57 to 0.81. The lower void fractions correspond to materials with impurities. In order to evaluate if either model is capable of predicting the effective thermal conductivity of impure 3013 materials, measurements on containers with impure materials were conducted.

The centerline temperature has been measured for two 3013 containers during destructive evaluation. After gas analysis, the convenience container lid was removed and replaced with a special lid with thermocouples. One thermocouple was aligned with the centerline of the container and a second thermocouple was located at 3.30 cm from the centerline. Both were located at a height of 6.86 cm from the can bottom. A thermocouple was also attached to the sidewall of the container at the same height. The fill gas was essentially air. The parameters for the two beds, designated R610806 (RFETS) and H003119 (Hanford), along with the high purity PuO<sub>2</sub> bed are shown in Table 2. As shown, the bulk densities and void fractions of the beds decrease with increasing impurities.

The material in the RFETS container was 77 percent actinide with 13 percent impurities and a void fraction of 0.71 with an effective thermal conductivity of 0.14 W m<sup>-1</sup> K<sup>-1</sup> calculated from the wall temperature and the centerline temperature. The material in the Hanford container was 70 percent actinide with 19 percent impurities and a void fraction of 0.68 with an effective thermal conductivity of 0.16 W m<sup>-1</sup> K<sup>-1</sup>. The thermal results for these beds are shown in Figure 6. The effective thermal conductivities of these impure 3013 materials are higher than the effective thermal conductivity of the high-purity oxide.

### Discussion

The effective thermal conductivity equation is required to determine the temperature gradients within the materials stored in 3013 containers. However, the effective thermal conductivity is strongly dependent upon the fill gas. The containers begin with mostly helium with up to 20 percent air. With time the oxygen that is associated with the air is depleted and the hydrogen increases, depending upon the amount of water present. Hydrogen has a gas thermal conductivity larger than helium. The effective thermal conductivity with any fill gas can be calculated using the models described above if the material properties are represented correctly. The measured effective thermal conductivities of the three materials studied to date are given in Table 3 along with the effective thermal conductivities calculated using the Bielenberg Model and the Deissler-Eian correlation.

In the case of the high-purity oxide PEOF1, the Bielenberg model is fit to the observed data and therefore, the values for

**Table 2.** Bed parameters for the tested impure oxide beds and for the pure oxide bed used for the Bielenberg

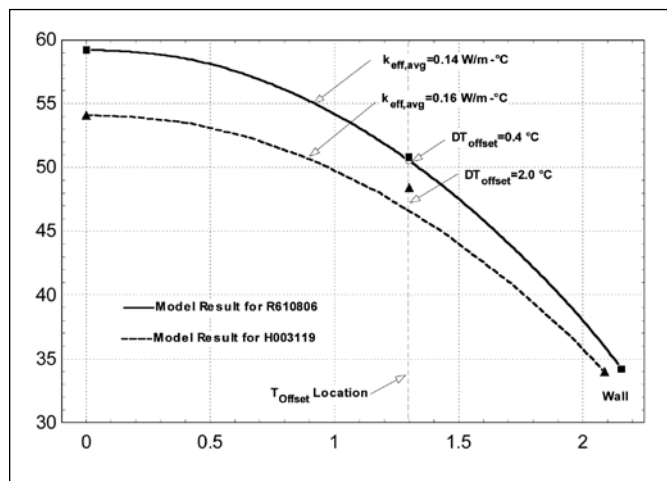
Material	Description	Mass	Volume	Power	Pycnometer Density	Bulk Density	Void Fraction	Measured Centerline Temperature
		[kg]	[cm <sup>3</sup> ]	[W/kg]	[g/cm <sup>3</sup> ]	[kg/m <sup>3</sup> ]		[°C]
PEOF1	100% PuO <sub>2</sub>	5.00	1929	2.05	11.46	2.59	0.77	--
R610806	77% Actinides 13% Impurities	4.26	1696	1.92	8.65	2.51	0.71	59.2
H003119	70% Actinides 19% Impurities	2.43	1013	2.28	7.47	2.40	0.68	54.1

**Table 3.** The effective thermal conductivity (W m<sup>-1</sup> K<sup>-1</sup>) measured and calculated using the Bielenberg model and the Deissler-Eian correlation. The temperature of the calculation is 300°K.

Material	Void	Measured keff with air as fill gas	Bielenberg Model (P=100 kPa)			Deissler-Eian Correlation		
			He	air	Ar	He	air	Ar
PEOF1	0.78	---	0.24	0.10	0.081	0.32	0.063	0.045
R610806	0.71	0.14	0.27	0.13	0.098	0.41	0.083	0.060
H003119	0.68	0.16	0.29	0.14	0.107	0.45	0.094	0.068



**Figure 6.** The temperature profile of two 3013 convenience containers modeled using the  $k_{\text{eff}}$  of 0.14 W m<sup>-1</sup> K<sup>-1</sup> for the RFETS container and 0.16 W m<sup>-1</sup> K<sup>-1</sup> for the Hanford container. The  $k_{\text{eff}}$  is determined from the wall temperature and the centerline temperature. The RFETS convenience container has a slightly larger diameter than the Hanford convenience container. The offset temperature is reasonably close to the calculated temperature profile.



He and Ar are the observed values. The Deissler-Eian correlation overestimates the effective thermal conductivity for PEOF1 with He by 33 percent and underestimates for PEOF1 with Ar by 55 percent. The measured effective thermal conductivities of the materials with the lower void fractions were estimated using both models. The effective thermal conductivities calculated using the Bielenberg model are closer to the measured values than those calculated using the Deissler-Eian correlation. When He fill gas is modeled, the Deissler-Eian correlation yields values that are 50 percent higher than the Bielenberg model which would decrease or underestimate the temperature gradient within the 3013 containers by a factor of  $\sim 1.5$ .

## Conclusions

An estimate of the effective thermal conductivity of materials within 3013 containers is needed in order to obtain realistic temperature gradients, which influence the water distribution within the material. Temperature measurements across high-purity plutonium oxides have been used to develop a model (the Bielenberg model) to calculate the effective thermal conductivity taking into account the void fraction and the nature of the fill gas. The new model is necessary because existing models do not reproduce the experimental data. Temperature measurements across impure

plutonium oxide materials with different void fractions have been used to test the Bielenberg model. The Bielenberg model performs better than the Deissler-Eian correlation previously available. The Bielenberg model provides an effective tool to estimate the effective thermal conductivity of the plutonium containing materials stored in 3013 containers and thus provides a basis to determine thermal gradients and water distribution within 3013 containers.

## Acknowledgements

Funding for this work was provided by the Surveillance and Monitoring Program, US Department of Energy Office of Environmental Management. This work was conducted at Los Alamos National Laboratory operated by Los Alamos National Security, LLC under contract DE-AC52-06NA25396.

*D. Kirk Veirs is a staff scientist at Los Alamos National Laboratory. He has a Ph.D. in physical chemistry from Pennsylvania State University and a B.S. in chemistry and environmental science from Northern Arizona University.*

*F. Coyne Prenger is a retired Registered Professional Engineer. He has a Ph.D. in mechanical engineering from Colorado State University.*

## References

1. Knight, T. D., and R. G. Steinke. 1997. *Thermal analysis of plutonium materials in British Nuclear Fuels, Ltd., containers*. Los Alamos National Laboratory LA-UR-97-1866.
2. Gupta, N. K. 2007. *Thermal Models for the 3013 Containers in KAMS*. Savannah River National Laboratory M-CLC-K-00720.
3. Deissler, R. G. and C. S. Eian. 1952. *Investigation of effective thermal conductivities of powders*. NASA NACA-RM E52C05.
4. Bielenberg, P. A., F. C. Prenger, D. K. Veirs, and G. F. Jones. 2006. Effects of Pressure on Thermal Transport in Plutonium Oxide Powder. *International Journal of Heat and Mass Transfer* 49, 3229-3239.
5. Klein, S. A. 2009. *Engineering Equation Solver*, 8.351. F-Chart Software: Madison, WI.

# Alpha-Particle-Induced Prompt Gamma-Ray Analysis of Plutonium-Bearing Materials Packaged in 3013 Containers

Joshua E. Narlesky, Lynn A. Foster, Elizabeth J. Kelly, and Roy E. Murray IV  
Los Alamos National Laboratory, Los Alamos, New Mexico USA

## Abstract

More than 5,500 containers of excess plutonium-bearing materials have been packaged for long-term storage following the requirements outlined in the DOE-STD-3013. Knowledge of the chemical impurities in the packaged materials is important because certain impurities, such as chloride salts, affect the behavior of the material in storage leading to gas generation and corrosion when sufficient moisture also is present. In most cases, the packaged materials are not well characterized, and information about the chemical impurities is limited to knowledge of the material's processing history. The alpha-particle activity from the plutonium and americium isotopes provides a method of nondestructive self-interrogation to identify certain light elements through the characteristic, prompt gamma rays that are emitted from alpha-particle-induced reactions with these elements. Gamma-ray spectra are obtained for each 3013 container using a high-resolution, coaxial high-purity germanium detector. These gamma-ray spectra are scanned from 800 to 5,000 keV for characteristic, prompt gamma rays from the detectable elements, which include lithium, beryllium, boron, nitrogen, oxygen, fluorine, sodium, magnesium, aluminum, silicon, phosphorus, chlorine, and potassium. The lower limits of detection for these elements in a plutonium-oxide matrix increase with atomic number and range from 100 or 200 ppm for the lightest elements such as lithium and beryllium, to 19,000 ppm for potassium. The peak areas from the characteristic, prompt gamma rays can be used to estimate the concentration of the light-element impurities detected in the material on a semiquantitative basis. The use of prompt gamma analysis to assess impurity concentrations avoids the expense and the risks generally associated with performing chemical analysis on radioactive materials. The analyzed containers are grouped by impurity content, which helps to identify high risk containers for surveillance and in sorting materials before packaging.

## Introduction

Beginning in 1999, excess plutonium oxide from various U.S. Department of Energy (DOE) facilities has undergone stabilization and packaging for long-term storage, according to the requirements of DOE-STD-3013, "Stabilization, Packaging, and Storage of Plutonium-Bearing Materials."<sup>1</sup> The material ranges in composition from pure plutonium oxide (or mixed plutonium-

uranium oxide) to impure, scrap material from various processes. The actinide content of the materials is well-known, but the other physical and chemical properties, such as the density, particle size, and chemical impurities, are not well-known. For much of the material, the only information concerning these properties is based on its processing history. Certain impurities, such as chloride salts, are of concern because they may increase the risk of time dependent container degradation. However, the cost and time associated with chemical analysis are too high for such analyses to be practical. Therefore, prompt gamma (PG) analysis has been used to identify some of the light-element impurities present in the plutonium oxide packaged in DOE Standard 3013 containers. The light elements detectable by PG analysis include lithium, beryllium, boron, nitrogen, oxygen, fluorine, sodium, magnesium, aluminum, silicon, phosphorus, chlorine, and potassium. The heavier elements, calcium through bismuth, are generally not detectable by this method. The qualitative results from the PG analysis are used to bin the containers by impurities present and to identify containers with chloride salt impurities that may be at greater risk for container degradation. This information is used to guide field surveillance activities. The gamma-ray peak areas for the light elements identified in the PG analysis correlate with concentration when normalized to the peak areas for the plutonium isotopes. Calibration curves have been developed between the normalized peak areas obtained from the PG analysis and the concentration of the light elements. Prompt gamma analysis therefore offers a semiquantitative, nondestructive method of chemical analysis for the plutonium oxide materials.

## Background

Prompt gamma analysis is a nondestructive, nuclear, elemental analysis technique that uses charged particle reactions to activate and interrogate a sample. In this technique, elements present in the sample matrix are identified through the characteristic gamma rays that are emitted during or following nuclear activation. Previous research has shown that alpha particles emitted from plutonium have sufficient energy to activate certain light elements in the material matrix.<sup>2,3</sup> This phenomenon was studied by McKibben in mixtures of <sup>238</sup>Pu oxide (80 atomic percent <sup>238</sup>Pu) and reagent-grade compounds containing various light elements as a method to detect light-element impurities in materials used



in heat-source production.<sup>2</sup> Martin also observed the reactions in mixtures and compounds of <sup>239</sup>Pu oxide (presumably 93 atomic percent <sup>239</sup>Pu) with the same light elements to explain the unusually high neutron-emission rates of waste materials containing plutonium.<sup>3</sup> Both researchers compiled catalogues of gamma-ray spectra showing the characteristic gamma rays associated with each light element detected. The most comprehensive catalogue of alpha-particle-induced PG rays was published by Giles and Peisach and included the observed gamma rays and sensitivities for twelve light elements from lithium to potassium and twenty-six of the heavier elements from calcium through bismuth on the periodic table.<sup>4</sup> However, gamma rays produced from alpha-particle-induced reactions on transition metal impurities in plutonium have not been observed. Giles and Peisach bombarded sheets or discs of pure metals or pellets of powdered compounds with 5 MeV <sup>4</sup>He<sup>+</sup> ions produced in a Van de Graaff accelerator, thereby eliminating the “plutonium background” in the gamma-ray spectra. Elimination of the plutonium background was necessary because many of the gamma rays produced from alpha particle-induced reactions on the transition metals are found in the region of the spectrum that is dominated by gamma rays from the decay of the plutonium and americium. This makes the detection of the transition metals difficult or impossible when they are present as impurities in plutonium oxide. The light elements that PG analysis can detect in nuclear fuels are listed in Table 1 along with the associated reactions and gamma rays used for detection.

Attempts have been made at using PG analysis as a method to quantify the light elements present in nuclear fuels.<sup>2,5,6</sup> The gamma-ray yields and lower limits of detection for alpha particle-induced reactions were measured for various mixtures of the light elements with plutonium. The gamma-ray yields have also been calculated for the light elements in various types of nuclear fuel, <sup>238</sup>Pu, <sup>239</sup>Pu, <sup>241</sup>Am, and U-Pu mixed fuels using computer models.<sup>7</sup> Thick-target yields for the light elements have also been determined by irradiation of light-element samples in alpha-particle beams.<sup>8,9,10</sup> However, the gamma-ray yields obtained in the various studies are not directly applicable to the analysis of impure plutonium-oxide materials. The results depend on the experimental conditions, which include the chemical form of the element, particle size, sample size, density, and isotopic composition of the plutonium.<sup>3,7</sup> These properties control the amount of alpha particles that react with the light elements. Because these properties are not known for the material packaged in each 3013 container, it would be impossible to accurately obtain theoretical yields for the alpha-particle-induced reactions.

Another approach was to use statistical methods to develop the trends between the gamma count rates for the alpha-particle-induced reactions and the concentration of the light elements measured in plutonium-oxide samples into a calibration. One correlation was developed by Fazzari to estimate chlorine content (as chloride salt) in scrap plutonium oxide from the electrorefining process.<sup>11</sup> The estimates of chloride concentration for the

**Table 1.** Light elements sensitive to PG analysis and corresponding reactions and gamma rays used for detection<sup>4</sup>

Element	Reaction	Gamma Ray (MeV)
Lithium	<sup>7</sup> Li( $\alpha,\alpha'\gamma$ ) <sup>7</sup> Li	0.478
Beryllium	<sup>9</sup> Be( $\alpha,n\gamma$ ) <sup>12</sup> C	4.439
Boron	<sup>10</sup> B( $\alpha,n\gamma$ ) <sup>13</sup> C	3.684
Nitrogen	<sup>14</sup> N( $\alpha,p\gamma$ ) <sup>17</sup> O	0.871
Oxygen	<sup>18</sup> O( $\alpha,n\gamma$ ) <sup>21</sup> Ne	2.438
Fluorine	<sup>19</sup> F( $\alpha,n\gamma$ ) <sup>22</sup> Na	0.891
Sodium	<sup>23</sup> Na( $\alpha,p\gamma$ ) <sup>26</sup> Mg	1.809
Magnesium	<sup>25</sup> Mg( $\alpha,n\gamma$ ) <sup>26</sup> Mg	1.779
Aluminum	<sup>27</sup> Al( $\alpha,p\gamma$ ) <sup>30</sup> Si	2.236
Silicon	<sup>28</sup> Si( $\alpha,p\gamma$ ) <sup>31</sup> P	2.234
Phosphorus	<sup>31</sup> P( $\alpha,p\gamma$ ) <sup>34</sup> S	2.127
Chlorine	<sup>35</sup> Cl( $\alpha,p\gamma$ ) <sup>38</sup> Ar	2.168
Potassium	<sup>39</sup> K( $\alpha,p\gamma$ ) <sup>42</sup> Ca	1.524

materials analyzed by this method showed good agreement with those obtained by analytical chemistry.<sup>12</sup> However, this correlation was detector specific and required that the concentration of <sup>241</sup>Am, a significant contributor to the alpha-particle activity, was the same for all materials. Because the age of the materials being packaged in 3013 containers varies considerably, the <sup>241</sup>Am concentration also varies and must be considered. Therefore, we have developed a method to estimate the concentrations of various light elements, including aluminum, beryllium, chlorine, fluorine, magnesium, potassium, and sodium that are present as impurities in plutonium oxide. In this method, the PG data are normalized to the count rates of <sup>239</sup>Pu and <sup>241</sup>Am. The normalization corrects for the amounts of <sup>239</sup>Pu and <sup>241</sup>Am, which together account for approximately 80 percent of the alpha-particle activity in the material. The normalization also provides an internal correction for the counting system efficiency and attenuation, both self-attenuation of the material and attenuation caused by shielding from the container and the detection system. Using the normalized PG data and analytical chemistry data available for 113 pure and impure plutonium-oxide samples, calibration equations have been developed. The calibration equations can be used to predict the concentration of several impurity elements found in the packaged materials, particularly those found in chloride salts that could lead to the degradation of the steel containers. The original calibration curves have since been revised with the addition of eighty-eight standards to the dataset.<sup>13,14</sup>



## Materials and Methods

Prompt gamma analysis is performed on each 3013 container packaged with plutonium-oxide mixtures that have an actinide concentration of less than 85 wt percent (pure  $^{239}\text{PuO}_2$  has an actinide concentration of approximately 87 percent). The containers are counted using a high-resolution, coaxial high-purity germanium detector as part of the nondestructive analysis (NDA) process. Originally, the containers were counted for fifteen minutes, but the count time was later extended to sixty minutes to increase detection capability. The gamma-ray spectrum files are analyzed with Prompt Gamma Analysis (PGA) Software developed at Los Alamos National Laboratory.<sup>15</sup> The analysis software reads the raw spectrum files, performs an energy calibration, locates all peaks in the spectrum, determines the area under each peak, and computes the normalized peak areas for the peaks that correspond with alpha-particle-induced reactions. The software then identifies the sensitive light elements present in the material based on the characteristic gamma rays observed in the spectrum, and provides the necessary data records.

The normalized peak areas  $N_i$  are unitless quantities and are obtained by determining the net counts  $P_i$  for a given peak and dividing by the normalization factor  $n$  and the attenuation factor  $A_i$  as shown in Equation 1. The net counts were obtained by determining the gross counts  $G_i$  and subtracting the average background. The gross counts are the sum of the counts  $c$  in the region of interest (ROI) containing the  $j$  channels corresponding to the peak.

$$N_i = \frac{P_i}{n \cdot A_i} = \frac{G_i - B_i}{n \cdot A_i} = \frac{\sum_{j \text{ channels}} c_j - B_i}{n \cdot A_i} \quad (1)$$

The normalization factor is obtained from the net counts from the  $^{239}\text{Pu}$  peak at 0.414 MeV and the  $^{241}\text{Am}$  peak at 0.662 MeV, as shown in Equation 2.

$$n = \left( \frac{n_{414 \text{ keV}} \cdot S_{\text{Pu-239}}}{A_{414 \text{ keV}} \cdot S_{\text{Pu-239}}} + \frac{n_{662 \text{ keV}} \cdot S_{\text{Am-241}}}{A_{662 \text{ keV}} \cdot S_{\text{Am-241}}} \right) 10^{-6} \text{ [counts]}, \quad (2)$$

where  $S_{\text{Pu-239}}$  and  $S_{\text{Am-241}}$  are the specific alpha activities of  $^{239}\text{Pu}$  and  $^{241}\text{Am}$  and  $s_{\text{Pu-239}}$  and  $s_{\text{Am-241}}$  are the specific gamma activities of  $^{239}\text{Pu}$  at 0.414 MeV and  $^{241}\text{Am}$  at 0.662 MeV, respectively. The attenuation factor  $A_i$  is applied to correct for the differences in thickness for the various container configurations that may be counted. For example, the material may be counted in its packaged state in the 3013 container, which is a nested configuration consisting of the outer 3013 container, the inner container, and the convenience container, or it may be counted in just the convenience container. For a given container configuration, the attenuation factor is calculated from Equation 3.

$$A_i = \exp \left[ - \left( \frac{\mu}{\rho} \right)_i \cdot \rho \cdot t \right] \quad (3)$$

where the quantity  $(\mu/\rho)$  is the mass attenuation coefficient for the steel for the energy of peak  $i$ ,  $\rho$  is the density of the steel, and  $t$  is the total wall thickness of the steel containers.

Lead absorbers are often used to shield the counting system from the low-energy gamma rays from  $^{241}\text{Am}$  to reduce the dead time. Historically, the use of absorbers has not been recorded; however, it may be determined using the ratio  $\chi$  of the  $^{239}\text{Pu}$  peak at 0.414 MeV to the  $^{239}\text{Pu}$  peak at 0.646 MeV. It has been demonstrated experimentally that values of  $\chi$  less than or equal to thirty-nine indicate that the attenuation is significant, and a correction must be applied.<sup>14</sup> This is done by determining the absorber thickness  $t$  from the  $\chi$  using Equation 4.

$$\begin{aligned} t &= 1.26 - 0.31 \cdot \ln(\chi) \quad (\chi < 39) \text{ [in]} \\ t &= 0 \quad (\chi \geq 39) \end{aligned} \quad (4)$$

Equation 3 can then be used to calculate the attenuation caused by the absorbers (if present) using the appropriate density and the mass attenuation coefficients for each peak.

The estimated concentrations for several light-elements impurities may be calculated using calibration equations. These equations were developed using the normalized peak areas obtained by PG analysis and analytical chemistry data obtained for the 113 standards.<sup>13,14</sup> The fitted equations are in the form of power functions as shown in Equation 5.

$$[C_i = k_0 \cdot N_i^{k_i} \text{ [ppm]} \text{ multiplied by some random error.} \quad (5)$$

The data were fitted using a linear regression model of the form shown in Equation 6.

$$\begin{aligned} \ln[C_i] &= k_1 \cdot \ln(N_i) + k_2 \text{ [ppm]} \\ &\text{plus random error, where } k_2 = \ln(k_0). \end{aligned} \quad (6)$$

The parameters  $k_1$  and  $k_2$  are listed in Table 2 along with the range of concentrations over which the calibration equations are valid. The parameters  $k_1$  and  $k_2$  are the slope and intercept of the calibration line. These parameters along with the  $R^2$  values for each of the calibrations are also listed in Table 2. The  $R^2$  value shows the proportion of the variance in the log chemistry data that is removed by conditioning on the log PG data. The  $p$ -values are obtained from an F-test that tests the importance of the slope or linear term. The  $p$ -values should be less than 0.05 to show there is only a 5 percent or less chance that the linear term is not important. The  $p$ -values for all of the fits are less than  $1 \times 10^{-6}$ . The uncertainties in the estimates, which are obtained from the 95 percent prediction intervals, are +/- 100 percent of the esti-



**Table 2.** Calibration parameters used to estimate concentration of light-element impurities in packaged 3013 containers with plutonium oxide<sup>14</sup>

	$k_1$	$k_2$	$R^2$	Range (ppm)
$C_{Al}$	0.878	13.36	0.60	700—40,000
$C_{Be}$	1.169	11.76	0.83	100—11,000
$C_{Cl}$	1.039	16.40	0.88	5,000—200,000
$C_F$	1.014	13.47	0.89	500—230,000
$C_{Mg}$	1.310	15.74	0.60	100—310,000
$C_K$	0.694	14.57	0.59	10,000—70,000
$C_{Na}$	1.180	12.96	0.91	40—60,000
$C_{Cl} = f(N_{Na})$	0.709	12.79	0.50	40—60,000 ppm Na

mate or larger because of the large amount of scatter in the data set. Therefore, the estimates obtained from these equations are considered semiquantitative.

### Lower Limits of Detection

Prompt gamma analysis can only provide estimates of impurity concentration when elements that have calibration equations are detected. For cases where those elements are not detected or where a calibration equation is not available, the lower limits of detection (LLD) can provide an estimate of the maximum concentration for the sensitive light elements. The LLDs for the sensitive light elements in plutonium oxide were obtained using a method described by Gedcke (see Equation 7) that uses a Gaussian distribution to model the difference between the observed counts and background counts (the difference of two Poisson distributions).<sup>16</sup> This method relies on the assumptions that the Gaussian distribution is a good approximation to the Poisson distribution and that concentration  $C$  is equal to some constant  $k$  multiplied by the integrated net peak area  $P$ . The net area of the peak is obtained by subtracting the background  $B$  from the total integrated area. The background is estimated by integrating two additional regions of width  $(\eta_B/2)$  at equal distances to the left and right of the peak. The value of  $\eta_B$  is arbitrary, but was selected so that neighboring peaks were avoided. The parameter  $\eta_p$  is the peak width, and  $L$  is the live time. The LLD is the value for which there is only a 5 percent chance of a false positive and a 5 percent chance of a false negative (based on the Gaussian distribution for the difference of the observed counts and background counts).

$$C_{LLD} = 3.29 \cdot C \sqrt{\left(1 + \frac{\eta_p}{\eta_B}\right) / \left(\frac{P}{B}\right) \cdot \left(\frac{P}{L}\right)} \cdot L \text{ [ppm]}. \quad (7)$$

**Table 3.** Results of LLD calculation for 60 and 600-minute count times

Isotope	Isotopic Abundance (percent)	LLD60 min (ppm)	LLD600 min (ppm)	Detection Rate (percent of total containers)
<sup>7</sup> Li	92.5 percent	240	Not available	0.05 percent
<sup>9</sup> Be	100.0 percent	80	20	11 percent
<sup>10</sup> B	19.9 percent	100	Not available	0.6 percent
<sup>14</sup> N	99.6 percent	Not available	Not available	Not available
<sup>18</sup> O	0.2 percent	250	90	31 percent
<sup>19</sup> F	100.0 percent	2,000	330	24 percent
<sup>23</sup> Na	100.0 percent	140	20	47 percent
<sup>25</sup> Mg	10.0 percent	60	10	58 percent
<sup>27</sup> Al	100.0 percent	1,300	330	11 percent
<sup>28</sup> Si	92.2 percent	Not available	Not available	Not available
<sup>31</sup> P	100.0 percent	8,200	3,600	3.9 percent
<sup>35</sup> Cl	75.8 percent	5,000	1,200	19 percent
<sup>39</sup> K	93.3 percent	19,000	7,000	11 percent

### Results and Discussion

The elements routinely observed with PG analysis of the packaged materials include beryllium, fluorine, sodium, magnesium, aluminum, chlorine, and potassium. Lithium, boron, and phosphorus were detected in less than 5 percent of the 3013 containers. Oxygen is detected in about one-third of the oxide containers through the  $(\alpha, \gamma)$  reaction on <sup>18</sup>O. Although plutonium oxide (PuO<sub>2</sub>) contains about 12 percent oxygen, the gamma-ray yield for the <sup>18</sup>O( $\alpha, \gamma$ ) reaction is very low because of the low abundance (0.2 percent) for <sup>18</sup>O. In addition, the 2,438 keV peak is often masked by the nearby broad peaks for magnesium and sodium when the materials have a high salt content. Therefore, prompt gamma rays from <sup>18</sup>O are usually only observed in pure plutonium oxides. Although about 28 percent of the PG spectra show a peak at 871 keV that could be attributed to nitrogen, it was assumed that this peak was produced by alpha-scattering reactions on <sup>17</sup>O, because nitrogen is not generally found in the chemical components present in these materials. Silicon is present in some of the packaged materials, which is evident from the analytical chemistry data for the standards. However, the prompt gamma rays produced by the alpha particle-induced reactions with silicon are not unique and are also produced by alpha particle-induced reactions with aluminum and other elements making detection and quantification difficult.

The LLDs for several of the light elements in <sup>239</sup>PuO<sub>2</sub> were obtained for one-hour and ten-hour count times. The LLDs for nitrogen and for silicon could not be determined. As shown in Table 3, the LLDs for the light elements tend to increase with an increasing atomic number because of the increased charge in the





nucleus of the heavier elements. Other factors affecting the LLDs include the intensity of the peaks used for detection as well as the physical and chemical form of the element. In some cases, the highest intensity peaks cannot be used because of interferences with other elements. Using less-intense peaks results in the detection of fewer gamma rays for the reactions and raises the LLD.

It is evident from the  $R^2$  values in Table 2 that the data used to develop the calibration equations have significant scatter, resulting in large uncertainties for the predicted values (greater than 100 percent of the estimated value). The large uncertainty is caused by variations in the gamma-ray production for different samples having the same concentration for a given element. The variation results from differences in the degree of contact between the light element atoms and the alpha-particle emitters in the material. The alpha-particle-interaction rate and ultimately the gamma-ray production rates are very sensitive to the degree of contact because the kinetic energy of the alpha-particles is necessary to initiate a reaction with the light elements. As the alpha particles travel through the material, they continually deposit their kinetic energy within a short distance. The range of the alpha particles in the material matrix is on the order of tens of microns depending on the density of the material. In addition, the reaction cross-section or probability of reaction decreases sharply with energy of the alpha particle and, therefore, with the distance that the alpha particles must travel before encountering a light-element atom. Therefore, light-element atoms must be within several microns of the alpha-particle emitters in order for the reaction to occur. The reaction cross-section also decreases for the heavier components (phosphorus, chlorine, and potassium), which makes having a high degree of contact especially important. For this reason, the heavier elements tend to have lower interaction rates and higher LLDs.

The chemical and physical forms of the impurities, particularly the heavier components, in the material matrix can affect the interaction rates substantially. For example, a given amount of a light element that is chemically or physically bound to the plutonium would yield more gamma rays than if it was simply mixed with the plutonium oxide. It was demonstrated that simple mixtures of 5 percent NaCl/KCl in pure  $^{239}\text{Pu}$  oxide did not even yield sufficient PG rays for detection.<sup>17</sup> The PG rays for sodium, potassium, and chlorine were observed in the  $\text{PuO}_2$ -salt mixtures only after the mixtures were heated to at least  $800^\circ\text{C}$ , which is the temperature necessary to cause the impurities to become molten. After heating, the salt was physically bound to the plutonium oxide, and the reaction gamma rays were observed. For the lighter components, however, the chemical and physical forms are less important. For example, it was also demonstrated that the fluorine in calcium fluoride can be detected in a simple mixture with pure plutonium oxide because the reaction cross-section for fluorine is about an order of magnitude higher than that of chlorine. Calcium fluoride was also added to the 5 percent NaCl/KCl- $\text{PuO}_2$  mixture, and the interaction rate for fluorine actually

**Table 4.** Prompt gamma results from a  $\text{PuO}_2$ -salt mixture prepared and calcined at various temperatures<sup>13,17</sup>

	Predicted Cl percent	Predicted F percent	Predicted Na percent
As-Received	--	6.5	0.03
Stabilized at $600^\circ\text{C}$	0.2	6.5	0.05
Stabilized at $800^\circ\text{C}$	4.2	5.2	1.72
Stabilized at $950^\circ\text{C}$	3.9	4.8	1.77
	Actual [Cl]: 5 wt percent in as-received sample	Actual [F]: 5 wt percent in as-received sample	Actual [Na]: 1.8 wt percent in as-received sample

decreased slightly after heating at  $800^\circ\text{C}$  suggesting that the chloride salt components were displacing the calcium fluoride.

Based on the results obtained from the PG analysis of the standards, we expect the PG to reliably identify and quantify the light-element impurities commonly found in the materials packaged in 3013 containers on a semiquantitative basis. The heavier components are in the form of chloride salts that melt when the material is heated. Much of the material was stabilized at  $950^\circ\text{C}$  or higher prior to packaging, which ensures that the salts became molten and good physical contact with the plutonium has been achieved. Some of the packaged material was stabilized at  $750^\circ\text{C}$ . Although this temperature is below the melting temperature of the chloride salts, the processing history of the material ensures that the material reached temperatures that exceed the melting temperatures of the chloride salts during the lifetime of the material. Because the lighter elemental impurities have higher reaction cross-sections, the physical contact with the plutonium is less important, and these elements are detected even as simple mixtures. Although detection of the impurities is reliable above the LLDs, the degree of contact of the impurities and the plutonium varies from container to container affecting the interaction rates and ultimately the uncertainty in the estimated concentrations.

Prompt gamma analysis is primarily used to provide a qualitative record of the light-element impurities present in the packaged plutonium oxides. This information is used to group the 3013 containers by impurity content and place each container into a prompt gamma group (PGG). The PGGs include materials with chloride (PGCl), materials with high concentrations of fluoride without chloride (PGFHi), materials with low concentrations of fluoride without chloride (PGFLo), materials with impurities other than chloride or fluoride (PGMisc), and materials without any impurities detected by PG (PGNoImp). This information is used to match each 3013 container to one or more representative samples in the shelf-life surveillance program that are likely to exhibit similar behavior during the fifty-year storage and to provide some information as to the chemical process that



generated the material.<sup>18</sup> The quantitative data from PG analysis is most frequently used in the binning process to select specific containers for field surveillance activities.<sup>19</sup>

Chlorine is considered the most important elemental impurity in the material. Alkaline earth chloride salts such as  $MgCl_2$  and  $CaCl_2$  are hygroscopic and have the capacity to absorb moisture from the glovebox air prior to packaging. Radiolysis of the absorbed moisture can lead to pressurization of the sealed container over time. If sufficient amounts of absorbed moisture are present in the material, the alkaline earth chloride salts may form liquid phases that increase the potential for corrosion of the stainless steel container. Currently in the binning process, any positive PG results for chlorine forces the item into the corrosive category because chloride salts and moisture are expected to be the leading causes of stress corrosion cracking and pitting. The quantitative PG results are used to estimate the amount of alkaline chloride salts that may be present in the containers.

Fluorine is known to promote pitting in austenitic stainless steels, but its involvement in gas generation is relatively unknown. The LLD for fluorine is lower than the LLD for chlorine by about a factor of three, which results in a large population of containers with small amounts of fluorine and no chlorine detected. To prevent dilution of the pressurization and corrosion bin, only items with fluorine concentrations above 0.8 wt percent were placed in the corrosive category. It is expected that these containers would have the greatest risk of the containers in the fluoride group, and that any problems associated with fluorine would be observed in these containers.

The PG results can also be used to guide engineering judgment decisions. For example, small-scale shelf-life experiments identified a material with a particular composition that simultaneously generated both hydrogen and oxygen in flammable concentrations and produced corrosion on the surfaces of the test container.<sup>20</sup> The material was 90 wt percent plutonium oxide and approximately 2 wt percent soluble salt components (magnesium, calcium, sodium, potassium, chlorine, and fluorine) with the remainder comprised of insoluble metal oxides. The PG results were used to identify materials in storage with similar compositions that may have the potential to exhibit similar behavior. However, the gas generation behavior observed in the small-scale shelf-life experiments is not considered likely because the moisture concentration of the containers identified by PG was significantly lower than the test container.

## Conclusion

Prompt gamma analysis has been used as a semiquantitative NDA technique to identify and quantify the light-element impurities in more than 3,600 containers of plutonium oxide packaged according to DOE-STD-3013. For most of the containers, PG analysis provides the only record of the impurities present in the material because analytical chemistry data were not available. The informa-

tion obtained from PG analysis has been used to place the containers into groups with similar impurities and to match the containers to representative containers in the shelf-life surveillance program. Most importantly, this information has been used to identify containers that may have a higher risk of corrosion and/or pressurization resulting from the chloride salts and the absorbed moisture so that they may be closely examined in field surveillance activities.

## Variables and Constants

$A_i$  = Attenuation factor for peak  $i$

$B_i$  = Average background under peak  $i$  [counts]

$c_j$  = Counts in channel  $j$  [counts]

$C_i$  = Concentration of the impurity element corresponding with peak  $i$  [ppm]

$G_i$  = Gross area under peak  $i$  [counts]

$k_m^i$  = Regression constants,  $m = 0, 1, 2$

$L$  = Live time [s]

$n$  = Normalization factor

$N_i$  = Normalized peak area of peak  $i$

$P_i$  = Net counts from peak  $i$  [counts]

$s_{Pu-239}^{\gamma}$  = Specific gamma activity of  $^{239}Pu$  at 413.7 keV =  $3.457 \times 10^4$  [ $g^{-1}s^{-1}$ ]

$s_{Am-241}^{\gamma}$  = Specific gamma activity of  $^{241}Am$  at 662.4 keV =  $4.624 \times 10^5$  [ $g^{-1}s^{-1}$ ]

$S_{Pu-239}^{\alpha}$  = Specific alpha activity of  $^{239}Pu$  =  $2.299 \times 10^9$  [ $g^{-1}s^{-1}$ ]

$S_{Am-241}^{\alpha}$  = Specific alpha activity of  $^{241}Am$  =  $1.245 \times 10^{11}$  [ $g^{-1}s^{-1}$ ]

$t$  = Absorber thickness [in]

$\chi$  = Ratio of counts of the 413.7 keV peak to the 662.4 keV for  $^{239}Pu$

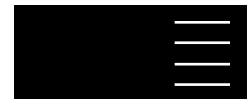
$\eta_p$  = Width of the peak

$\eta_B$  = Width of the region used for calculation of background

## Acknowledgements

Funding for this work was provided by the Surveillance and Monitoring Program, U.S. Department of Energy Office of Environmental Management. This work was conducted at Los Alamos National Laboratory operated by Los Alamos National Security, LLC under contract DE-AC52-06NA25396.

*Joshua E. Narlesky is a research and development scientist at Los Alamos National Laboratory. He received his B.S. from New Mexico Institute of Mining and Technology and his M.S. from Colorado State University, both in chemical engineering. He served as the technical lead for prompt gamma (PG) analysis for the Surveillance and Monitoring Program for the past seven years. During that time he developed the PG analysis software and performed the PG analysis of more than 3,600 containers of plutonium oxide sealed in 3013 containers for long-term storage.*



Lynn Foster received his B.S., M.E., and Ph.D. in nuclear engineering from Texas A&M University. He is a member of the Nuclear Material Management group at Los Alamos National Laboratory. He has worked in the area of non-destructive assay (NDA) of nuclear materials at the Los Alamos Plutonium Facility since 1993. Foster is responsible for certification of NDA instruments for routine accountability measurements and has also collaborated with others to investigate new NDA techniques and new applications of existing NDA technologies.

Elizabeth J. Kelly has a Ph.D. in biostatistics from the University of California at Los Angeles and a M.A. and a B.S. in mathematics from the University of Southern California. Kelly is a scientist in the Statistical Sciences Group at Los Alamos National Laboratory. The mission of the Statistical Sciences Group is to bring statistical reasoning and rigor to multi-disciplinary scientific investigations through development, application, and communication of cutting-edge statistical sciences research. Her research has focused on statistical sampling and analysis to support risk-based decision-making in many areas, particularly in the area of environmental risk. Kelly has served on numerous NSF and EPA advisory boards, including the NSF Advisory Committee for Environmental Research.

Roy E. Murray IV is currently a graduate student at the University of Delaware. He is pursuing his Ph.D. in physics with his research emphasis in organic materials for novel photovoltaics. He received his B.S. degree in physics from New Mexico Institute of Mining and Technology. He worked at Los Alamos National Laboratory as a summer student in 2008 and 2009 researching neutron and alpha-induced PG analysis.

## References

1. 2004. Stabilization, Packaging, and Storage of Plutonium-Bearing Materials, U.S. Department of Energy Standard (DOE-STD-3013-2004).
2. McKibben, M. 1968. Reaction Gammas for Analysis of Impurities in Alpha Emitters, *Nuclear Applications* 4, 260-267.
3. Martin, R. H. 1975. *Reaction Gamma-Rays in Plutonium Compounds, Mixtures, and Alloys*, Dow Chemical, USA, Rocky Flats Division Report (RFP-2382).
4. Giles, I. S., and M. Peisach. 1979. A Survey of the Analytical Significance of Prompt-Gamma Rays Induced by 5 MeV Alpha-Particles, *Journal of Radioanalytic Nuclear Chemistry*, 50, 307-360.
5. Ovechkin, V. V., V. I., Melent'ev, and V. F. Gorbunov. 1975. Instrumental Method of Determination of Nitrogen and Fluorine on the Basis of an ( $\alpha, p\gamma$ ) Reaction, *Radiokhimiya* 18, 152-160.
6. Ovechkin, V. V. 1980. Gamma Rays and Neutrons from  $^{239}\text{Pu}$  Fluorides, *Atomnaya Energiya* 48, 48-49.
7. Shumakov, A. V., Vlaskin, G. N., Kositsyn, V. F., and M. A. Naumov. 1994. Estimated Detection Limits of B, C, N, O, and F in  $\alpha$ -Emitters by Using  $\gamma$ -Radiation from ( $\alpha, x\gamma$ ) Reactions, *Radiokhimiya* 36, 57-62.
8. Heaton, R. K., H. W. Lee, B. C. Robertson, E. B. Norman, K. T. Lesko, and B. Sur. 1995.  $\alpha$ -Particle Induced High-Energy  $\gamma$ -Ray Yields from Light Elements, *Nuclear Instruments and Methods* A364, 317-327.
9. Heaton, R. K. 1994. The  $\alpha$ -Induced Thick-Target  $\gamma$ -Ray Yield from Light Elements, *Lawrence Berkeley National Laboratory Report* (LBL-36651).
10. Heaton, R. K., H. W. Lee, B. C. Robertson, E. B. Norman, K. T. Lesko, and B. Sur. 1997.  $\alpha$ -Particle Induced  $\gamma$ -Ray Transitions in Light Elements, *Physics Review C*, 56, 922-937.
11. Fazzari, D. M., S. A. Jones, and C. H. Delegard. 2003. Application of Prompt Gamma-Ray Analysis to Identify Electrorefining Salt-Bearing Plutonium Oxide at the Plutonium Finishing Plant, *Pacific Northwest National Laboratory Report* (PNNL-14409).
12. Tingey, J. M., and S. A. Jones. 2005. Chemical and Radiochemical Composition of Thermally Stabilized Plutonium Oxide from the Plutonium Finishing Plant Considered as Alternate Feedstock for the Mixed Oxide Fuel Fabrication Facility, *Pacific Northwest National Laboratory Report* (PNNL-15241).
13. Narlesky, J. E., E. J. Kelly, and L. A. Foster. 2005. A Calibration to Predict the Concentrations of Impurities in Plutonium Oxide by Prompt Gamma Analysis, *Los Alamos National Laboratory Report* (LA-14258).
14. Narlesky, J. E., E. J. Kelly, and L.A. Foster. 2009. A Calibration to Predict the Concentrations of Impurities in Plutonium Oxide by Prompt Gamma Analysis, Rev. 1, *Los Alamos National Laboratory Report* (LA-14411).
15. Narlesky, J. E. 2009. Prompt Gamma Analysis Software Version 4.7 User's Guide, *Los Alamos National Laboratory Report* (LA-UR-09-04712).
16. Gedke, D. A. 2001. How Counting Statistics Controls Detection Limits and Peak Precision, Ortec Application Note (AN59).
17. Foster, L. A., J. A. Rennie, and R.E. Mason. 2002. Characterization of Plutonium Oxides by Alpha-Induced PG-Ray Analysis, *Los Alamos National Laboratory Report* (LA-UR-02-3408).
18. Narlesky, J. E., L. G. Peppers, and G. P. Friday. 2009. Complex-Wide Representation of Material Packaged in 3013 Containers, *Los Alamos National Laboratory Report* (LA-14396).



19. Peppers, L. G., E. J. Kelly, J. McClard, G. P. Friday, T. J. Venetz, and J. Stakebake. 2009. Selection of 3013 Containers for Field Surveillance: LA-14310, Rev. 1, *Los Alamos National Laboratory Report (LA-14395)*.
20. Berg, J. M., E. Garcia, G. S. Long, M. A. Martinez, J. E. Narlesky, D. K. Veirs, C. Williams, and L. Worl. 2008. The Effect of Moisture Content on Gas Generation for 011589A Substitute Materials, *Los Alamos National Laboratory Report (LA-UR-08-2546)*.



# Salt Phases in Calcined Materials and their Hydration Properties

Stephen A. Joyce, Joshua E. Narlesky, D. Kirk Veirs, Eduardo Garcia, Obie W. Gillispie, J. Matt Jackson, Brian L. Scott, and Laura A. Worl  
Los Alamos National Laboratory, Los Alamos, New Mexico USA

## Abstract

Calcined plutonium oxide salt mixtures are packaged according to U.S. Department of Energy (DOE) Standards for long-term storage in austenitic stainless steel containers. The behavior of the salts during packaging and storage can be critical to the integrity of the package because deliquescence of the salt can provide an electrolyte that supports stress-corrosion cracking of the stainless steel. Pure alkaline earth chlorides such as  $\text{MgCl}_2$  and  $\text{CaCl}_2$  are known to form crystalline hydrates and to deliquesce at low relative humidities. When the alkaline earth chlorides are calcined with other salts such as  $\text{KCl}$  and  $\text{NaCl}$ , new salt phases such as  $\text{KCaCl}_3$  and  $\text{KMgCl}_3$  can form. Little is known about the hydration and deliquescent properties of these multicomponent salts. The interactions of water vapor with the pure phase salts and calcined mixtures were studied using X-ray diffraction, a moisture sorption analyzer, and environmental scanning electron microscopy. Pure phase double and triple salts such as  $\text{KCaCl}_3$ ,  $\text{K}_2\text{MgCl}_4$ , and  $\text{K}_3\text{NaMgCl}_6$  were synthesized. For calcined  $\text{MgCl}_2/\text{NaCl}/\text{KCl}$  mixtures, a variety of phases including  $\text{K}_3\text{NaMgCl}_6$  are formed. The anhydrous salt  $\text{K}_3\text{NaMgCl}_6$  decomposes to  $\text{KMgCl}_3 \cdot 6\text{H}_2\text{O}$  (carnallite) and the respective alkali halides upon exposure to water vapor. Carnallite then controls the mutual deliquescence relative humidity at  $\sim 57$  percent relative humidity (RH). For calcined  $\text{CaCl}_2/\text{KCl}/\text{NaCl}$  mixtures,  $\text{KCaCl}_3$  (chlorocalcite) is formed. Chlorocalcite does not form crystalline hydrates before it deliquesces at  $\sim 16$  percent RH.

## Introduction

Materials packaged for storage under the U.S. Department of Energy 3013 Standard are allowed to have up to 70 percent impurities by weight.<sup>1</sup> Common impurities are residual processing salts, which can include the alkali chlorides,  $\text{NaCl}$  and  $\text{KCl}$ , and the alkaline earth chlorides,  $\text{MgCl}_2$  and  $\text{CaCl}_2$ . Generally, these processing salts contain minor amounts of the alkaline earth chlorides in a balance of the alkali chlorides. The 3013 Standard limits the amount of moisture to 0.5 wt percent or less. Moisture adsorption by plutonium oxide materials containing salts is a complex process with known mechanisms of water uptake including surface adsorption of approximately a monolayer, formation of hydrated salts, and deliquescence. Deliquescence is the transformation of a salt from a solid phase to an aqueous solution by the

sorption of vapor phase water. The deliquescent relative humidity (DRH) of a salt is the lowest humidity at which a solution forms. In equilibrium, the DRH is also the humidity above the saturated solution. For a single salt such as  $\text{NaCl}$ , the DRH is a function only of the temperature. For multicomponent salts, the DRH is also a function of composition. For humidities above the DRH, the solution becomes more dilute as the humidity is increased. Pure alkaline earth chlorides such as  $\text{MgCl}_2$  and  $\text{CaCl}_2$  are known to form crystalline hydrates and to deliquesce at low relative humidities (RH). The affinity of the alkaline earth salts for water can lead to significant water uptake at low humidities, which in turn may lead to container pressurization and  $\text{H}_2$  gas production, due to the radiolysis of the water, and corrosion of the stainless steel by high ionic strength solutions.<sup>2</sup> The 3013 Standard requires the stabilization of materials by calcining at high temperatures prior to packaging. For mixtures of alkaline earth and alkali chlorides, this heat treatment can lead to the formation of multicomponent salts such as  $\text{KCaCl}_3$  and  $\text{KMgCl}_3$ .

The thermodynamics of the interaction of water with the single salts are generally well understood.  $\text{NaCl}$  and  $\text{KCl}$  deliquesce at 75 percent and 84 percent RH respectively at room temperature.<sup>3</sup> In the saturated solutions, there are  $\sim 9$  waters per salt molecule for  $\text{NaCl}$  and  $\sim 11$  for  $\text{KCl}$  at  $25^\circ\text{C}$ .<sup>4</sup> Neither forms hydrates above  $0^\circ\text{C}$ .  $\text{MgCl}_2$  can form a number of crystalline hydrates. Between 0 and  $120^\circ\text{C}$ , the most fully hydrated form is the hexahydrate,  $\text{MgCl}_2 \cdot 6\text{H}_2\text{O}$ .<sup>5</sup> At room temperature,  $\text{MgCl}_2 \cdot 6\text{H}_2\text{O}$  forms at  $\sim 2$  percent RH and deliquesces at 33 percent<sup>3</sup> with  $\sim 9$  waters per salt molecule in the saturated solution.<sup>4</sup>  $\text{CaCl}_2$  is more complicated. The most fully hydrated forms of  $\text{CaCl}_2$  are the hexahydrate,  $\text{CaCl}_2 \cdot 6\text{H}_2\text{O}$ , up to  $-29^\circ\text{C}$ , the tetrahydrate,  $\text{CaCl}_2 \cdot 4\text{H}_2\text{O}$ , from 29 to  $45^\circ\text{C}$ , and the dihydrate,  $\text{CaCl}_2 \cdot 2\text{H}_2\text{O}$ , from 45 to  $-175^\circ\text{C}$ .<sup>6</sup> In addition, at least two metastable forms of  $\text{CaCl}_2 \cdot 4\text{H}_2\text{O}$  have been identified. At room temperature,  $\text{CaCl}_2 \cdot 6\text{H}_2\text{O}$  forms at  $\sim 21$  percent RH and the relative humidity above a saturated solution is 29 percent. There are on average only 6.1 waters per salt molecule at  $25^\circ\text{C}$  in the saturated solution.<sup>4</sup>

Candidates for the multicomponent salts that could form on calcining mixtures of alkaline earth and alkali chlorides can be established by examining the available binary and ternary phase diagrams. Based on the binary phase diagrams,<sup>7</sup> the double salts  $\text{KMgCl}_3$ ,<sup>8</sup>  $\text{K}_2\text{MgCl}_4$ ,<sup>9</sup> and  $\text{KCaCl}_3$  are stable at room tempera-



ture. Both NaCl and MgCl<sub>2</sub> are immiscible in CaCl<sub>2</sub> and do not form double salts. Based on the ternary phase diagrams, a potentially important triple salt is K<sub>3</sub>NaMgCl<sub>6</sub>.<sup>10</sup> This triple salt melts incongruently (i.e. decomposes into a liquid and another solid) at 470°C, so its formation may depend on how quickly a melt is cooled.

Information on the moisture uptake of these multicomponent salts is limited. We have not found any information in the literature on any hydrates of K<sub>2</sub>MgCl<sub>4</sub>, K<sub>3</sub>NaMgCl<sub>6</sub>, or KCaCl<sub>3</sub>. KCaCl<sub>3</sub> is a rare mineral referred to in the geochemical literature as either chlorocalcite or baumlerite and is often described as deliquescent without further detail. The only reported hydrate of these multicomponent salts is KMgCl<sub>3</sub>·6H<sub>2</sub>O, also known as carnallite. The interactions of water with carnallite have been extensively modeled due to its importance in geological systems such as the Dead Sea and in the industrial production of potash.<sup>11,12</sup> The DRH can be obtained from the solubility data computed by the thermodynamic models in.<sup>11,12</sup> The thermodynamic models have been extended to higher temperatures.<sup>13</sup> A mutual deliquescence relative humidity ternary plot for the NaCl, KCl, and MgCl<sub>2</sub> system at a temperature of 90°C has been calculated using Pitzer's thermodynamic model.<sup>14</sup> The mutual deliquescence relative humidity (MDRH) is the relative humidity at which a multicomponent salt mixture such as carnallite deliquesces. According to the model, the MDRH for carnallite is 59 percent at 25°C<sup>11</sup> and 48 percent at 90°C.<sup>14</sup>

Given the number of compounds that can potentially form when a salt mixture is calcined at high temperatures and that the interactions of water with these salts are not known, we have studied the formation and hydration properties of several calcined alkaline earth/alkali chloride mixtures. A number of single phase multicomponent salts were synthesized. Three mixtures spanning a range of compositions were prepared as well: a K/Na/Mg mixture, a K/Na/Ca mixture and a K/Na/Mg/Ca mixture. The anhydrous salts were characterized using X-ray diffraction (XRD) to determine what species were produced on calcining. The hydrate formation and deliquescence of the pure phases and mixtures were examined using XRD, an environmentally-controlled microbalance for determining hydrate formation and deliquescence, and a scanning electron microscope (SEM) equipped with an energy dispersive X-ray spectrometer to measure deliquescence and sample elemental compositions.

## Materials and Methods

The salt compounds and salt mixtures were prepared from anhydrous CaCl<sub>2</sub>, anhydrous MgCl<sub>2</sub>, and reagent grades of KCl and NaCl. As MgCl<sub>2</sub> and CaCl<sub>2</sub> are very hygroscopic and can hydrolyze when heated above 200°C in air, most of the salt compounds and mixtures were prepared in dry inert atmosphere gloveboxes. The necessary ingredients were weighed, combined, and ground into fine powders. The powders were poured into a porcelain cru-

cible and placed in a furnace set between 800°C and 850°C. The mixtures were held at temperature for fifteen to sixty minutes. After cooling to room temperature, the salts were removed from the crucible, ground with a mortar and pestle, and placed in glass vials. The initial experiments on the K/Mg/Na salts indicated that the glass vials were not effective in preventing moisture uptake over extended periods outside the glovebox. Therefore, the glass vials with the Ca-containing salts were placed in leak-tight stainless steel containers. In general, the Ca-containing samples were exposed to ambient air for less than a minute.

Moisture absorption tests were conducted on each of the prepared compounds and mixtures with the Symmetric Gravimetric Analyzer 100 (SGA-100) from VTI Corporation. The instrument, located outside of the glovebox, controls the temperature and relative humidity of the atmosphere surrounding a sample and measures the weight change of the sample as a function of time. The instrument controls the relative humidity in the sample chamber by mixing a stream of dry and wet nitrogen gas and flowing the gas mixture over the sample. A water bath is used to control the temperature of the sample chamber. The weight of the sample is measured by a microbalance; readings are given to ± 0.1 µg. Salt samples (typically 5 to 20 mg) were weighed out in the inert glovebox and placed into the quartz sample holder. The sample holder was sealed in a vial, removed from the glovebox, and taken to the gravimetric analyzer. The sample holder was removed from the vial and placed in the sample chamber, which is backfilled with dry nitrogen. The salt sample was exposed to the ambient atmosphere for approximately 5 to 10 seconds while it was transferred. The relative humidities at which the salt samples absorb moisture to form the hydrates are determined by raising the relative humidity in steps of 1 percent RH at constant temperature. The instrument controls the relative humidity for a specified time and waits for a weight change to occur prior to proceeding to the next step. If a weight change occurs, the instrument waits until the rate of change approaches zero and the sample is at equilibrium before raising the relative humidity to the next step. The DRH is determined as the relative humidity at which liquid droplets are first observed in the salt sample.

The XRD experiments were performed on a diffractometer with copper radiation and a solid state Peltier detector. The Ca-containing samples were mounted in an airtight environmental chamber in an argon atmosphere glovebox. The environmental chamber is equipped with a beryllium window to minimize the attenuation of X-rays. The environmental chamber atmosphere was controlled using sodium hydroxide solutions, and moisture levels were confirmed with a relative humidity gauge fastened to the environmental chamber. For the other samples, the X-ray diffraction experiments were conducted in room air. For some samples, either KCl or LaB<sub>6</sub> were added as internal standards to calibrate for the displacement error of the sample. All measurements were performed at ambient temperatures.

Samples of the salts were also examined in an environmental

SEM. This instrument has the ability to acquire images with an overpressure of gas, in this case water vapor. The sample temperature was controlled using a Peltier stage (0-35°C) and the sample exposed to controlled pressures of thoroughly degassed water. The procedure is to image while increasing the water vapor pressure at 0.1 Torr increments through the deliquescent relative humidity. The error in the relative humidity measurements is approximately +/- 0.5 percent RH based on calibrations using well studied salts such as NaCl and KCl. Operationally, deliquescence is determined to have occurred when the salt particles begin to change morphology and lose their sharp features due to the formation of a liquid phase. Elemental mapping by Energy Dispersive X-Ray Spectroscopy (EDS) was obtained for the elements Mg, K, Na, and Cl. Elemental maps indicate that most of the starting samples are chemically homogeneous. Exceptions are noted below.

## Results and Discussion

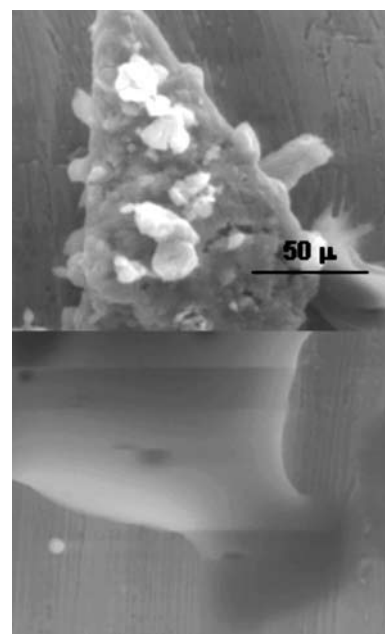
### Single Salts (KCl, NaCl, MgCl<sub>2</sub>, and CaCl<sub>2</sub>)

The interactions of water with the alkali chlorides, NaCl and KCl, have been well studied due to their importance in modeling the thermodynamics of electrolyte solutions.<sup>11-13</sup> and in the formation of atmospheric aerosols.<sup>15</sup> Deliquescence relative humidities for these salts have been determined from measurements of the relative humidity above saturated aqueous solutions and also from the formation of solution through the exposure of the solid to water vapor. Both methods are thermodynamically equivalent. Similar measurements have also been made for MgCl<sub>2</sub> including the deliquescence of the solid through vapor phase absorption of water. The humidities above CaCl<sub>2</sub> solutions have been studied extensively due to the use of such solutions as thermodynamic standards for isopiestic measurements.<sup>16</sup> The relative humidity above a saturated solution of CaCl<sub>2</sub> at room temperature is 29 percent RH.<sup>3</sup> There appears, however, to be no literature on the direct measurements of the deliquescence of CaCl<sub>2</sub> solids by water vapor. For this reason, we have examined the hydration properties of the alkaline earth chlorides. Moisture absorption tests were conducted on both MgCl<sub>2</sub> and CaCl<sub>2</sub> at 25 and 70°C to measure the relative humidity at which the various hydrates form and to determine the conditions under which these compounds form a liquid in the presence of water vapor. MgCl<sub>2</sub> forms the crystalline hydrate, MgCl<sub>2</sub>·6H<sub>2</sub>O, at ~2 percent RH (25°C) and 7 percent RH (70°C). MgCl<sub>2</sub>·6H<sub>2</sub>O deliquesces at 33 percent RH (25°C) and 27 percent RH (70°C). These results are consistent with literature values and provide a measure of the accuracy of the microbalance apparatus (~1 percent RH). The results for MgCl<sub>2</sub> and all the other pure salt phases studied are presented in Table 1.

At 25°C, as determined using the microbalance, CaCl<sub>2</sub> converts to CaCl<sub>2</sub>·2H<sub>2</sub>O at 2 percent RH. CaCl<sub>2</sub>·2H<sub>2</sub>O converts to CaCl<sub>2</sub>·4H<sub>2</sub>O at 13 percent RH. At 20 percent RH, a solution forms. This result was confirmed with the environmental SEM.

Micrographs of a CaCl<sub>2</sub> particle at 8 percent RH and 20 percent RH are shown in Figure 1. While slowly changing the humidity from 8 to 19 percent RH, the well-defined crystals were largely unchanged. Upon changing to 20 percent RH, the particle abruptly converted into a larger, rounded, and less-resolved droplet, indicating deliquescence. These experiments were repeated several times in both the microbalance and the SEM with consistent results. A reagent grade sample of the CaCl<sub>2</sub>·6H<sub>2</sub>O was examined in the microbalance and deliquesced at 30 percent RH as expected. From the available thermodynamic data, the transition from CaCl<sub>2</sub>·4H<sub>2</sub>O to CaCl<sub>2</sub>·6H<sub>2</sub>O should occur at ~21 percent RH at 25°C.<sup>17</sup> The present results suggest that conversion of the tetrahydrate to the hexahydrate or to a saturated solution occur at similar humidities and that formation of the solution by the absorption of water vapor is kinetically favored. At 70°C, CaCl<sub>2</sub>·2H<sub>2</sub>O is the most fully hydrated species which hydrated at 2 percent RH and deliquesced at 17 percent RH.

Figure 1. SEM images of a CaCl<sub>2</sub> particle just below the DRH (top) and just above the DRH (bottom)



### Multicomponent Salts

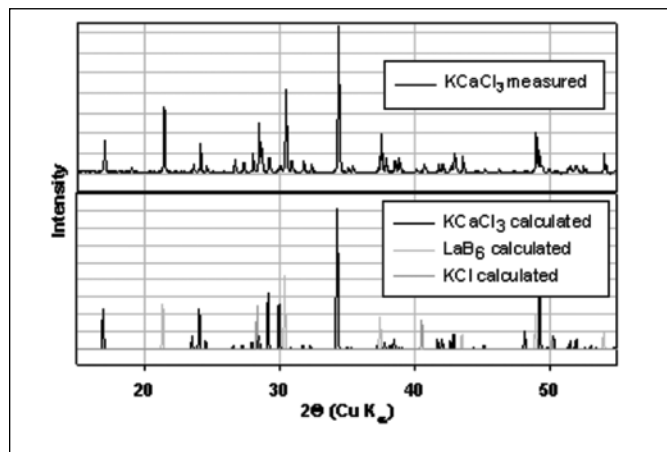
#### i. KCaCl<sub>3</sub>

A KCaCl<sub>3</sub> sample was prepared by combining CaCl<sub>2</sub> with a 10 percent molar excess of KCl. The salts were ground together, heated to 800°C for fifteen minutes, and allowed to cool in the furnace. The excess KCl was added to achieve complete conversion of the CaCl<sub>2</sub> to KCaCl<sub>3</sub>, thereby avoiding any interference from potentially unreacted CaCl<sub>2</sub> in the moisture absorption experiments.

An XRD pattern was obtained for the salt sample under anhydrous conditions. The pattern showed KCl and an unknown phase believed to be from KCaCl<sub>3</sub>. Neither anhydrous CaCl<sub>2</sub> nor any of



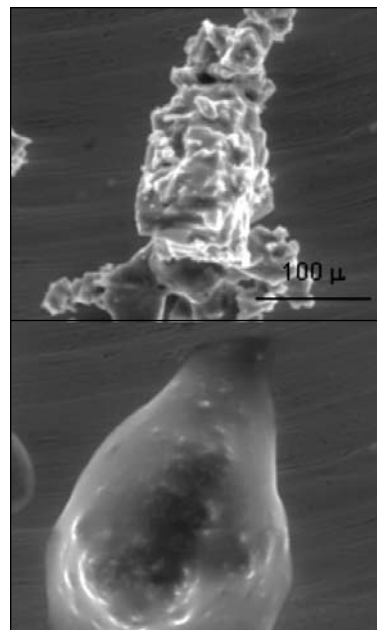
**Figure 2.** X-ray diffraction data for  $\text{KCaCl}_3$ . The experimental data is shown in the top graph and the calculated XRD pattern is shown in the bottom graph.  $\text{LaB}_6$  was added as an internal standard.



its hydrated forms were observed in the pattern, indicating the complete conversion of the  $\text{CaCl}_2$ . Based on a literature search,  $\text{KCaCl}_3$  was found to have an orthorhombic distorted perovskite structure, but the parameters necessary for calculating its pattern were not available.<sup>18</sup> Therefore, a theoretical pattern for  $\text{KCaCl}_3$  was obtained by adjusting the 020, 200, and 002 peaks in the pattern from the structurally related  $\text{KMnCl}_3$  compound and determining the d-spacings. The space group is  $\text{Pnma}$  with the resulting lattice parameters of 7.54 Å (a), 10.44 Å (b) and 7.26 Å (c) and the calculated pattern for the  $\text{KCaCl}_3$  sample is in good agreement with the observed data. The calculated and measured XRD patterns for anhydrous  $\text{KCaCl}_3$  are shown in Figure 2.

Moisture absorption tests were conducted on  $\text{KCaCl}_3$  at 25°C and 70°C. The results indicate that  $\text{KCaCl}_3$  does not form crystalline hydrates at either temperature. At room temperature,  $\text{KCaCl}_3$  is anhydrous from 0 to 15 percent RH. At 16 percent RH,  $\text{KCaCl}_3$  deliquesced. The MDRH for  $\text{KCaCl}_3$  at 70°C is 21 percent. SEM images of a  $\text{KCaCl}_3$  particle at 12 and 17 percent RH are shown in Figure 3. The well defined particle began to liquefy at 17 percent RH consistent with the moisture absorption measurements. Note that the droplet was not uniform. In particular, bright structures were observed within the droplet. These features persisted at higher relative humidity. Spot X-ray fluorescence measurements were performed on both the dry salt and the deliquesced material. The analysis of the starting material indicates that it is chemically homogeneous at the resolution of the X-ray spectrometer (~10μ). For the droplet, on the other hand, the bright features contain mainly K and Cl whereas the liquid is Ca-rich. This indicates that  $\text{KCaCl}_3$  dissolves incongruently. Many multicomponent materials exhibit incongruent dissolution where the elemental ratios in the solution are not the same as those of the compound. For  $\text{KCaCl}_3$ , the  $\text{CaCl}_2$  component dissolves preferentially resulting in an aqueous solution of  $\text{Ca}^{2+}$ ,  $\text{K}^+$  and  $\text{Cl}^-$  enriched in  $\text{Ca}^{2+}$  and  $\text{KCl}$  as the solid portion.

**Figure 3.** SEM images of a  $\text{KCaCl}_3$  particle just below the DRH (top) and just above the DRH (bottom). Note the bright features in the deliquesced particle which are  $\text{KCl}$  crystals.



## ii. $\text{KMgCl}_3$

Unlike all the other materials,  $\text{KMgCl}_3$  was prepared outside a glovebox from reagents kept in an enclosure dried with Drierite™. Equimolar amounts of  $\text{KCl}$  and anhydrous  $\text{MgCl}_2$  were mixed, heated to 825°C for one hour and allowed to cool. After the synthesis, a small weight loss was observed.  $\text{MgCl}_2$  is known to hydrolyze to  $\text{MgO}$  at high temperatures in the presence of adventitious water.<sup>5</sup> A sample of the salt was dissolved in water and the chloride concentration measured to be less than the starting materials. An estimated 10 percent conversion of the  $\text{MgCl}_2$  to  $\text{MgO}$  was consistent with both the overall weight loss and the decrease in the  $\text{Cl}^-$  concentration. X-ray fluorescence (XRF) measurements, in conjunction with the SEM studies, were performed. While the majority of the sample particles exhibited the expected stoichiometry for  $\text{KMgCl}_3$ , occasional, structurally-distinct particles did show high oxygen content, further confirming that some small amount of hydrolysis occurred during sample preparation.

Moisture sorption experiments showed that  $\text{KMgCl}_3$  forms a hexahydrate at 2 percent RH at both 25°C and 70°C. The deliquescence of a  $\text{KMgCl}_3 \cdot 6\text{H}_2\text{O}$  particle is shown in Figure 4. Onset of deliquescence occurs at ~57 percent RH. Note that the dissolution was not uniform, similar to  $\text{KCaCl}_3$ .  $\text{KMgCl}_3 \cdot 6\text{H}_2\text{O}$  is known to dissolve incongruently. X-ray fluorescence measurements confirmed that the bright features are K-rich and the solution is Mg-rich. On closer examination, it was observed that many of the brighter features are cube shaped.  $\text{KMgCl}_3 \cdot 6\text{H}_2\text{O}$  adopts a pseudo-hexagonal crystal habit;  $\text{KCl}$  adopts a cubic habit.



**Figure 4.** SEM images of carnallite,  $\text{KMgCl}_3 \cdot 6\text{H}_2\text{O}$ . (top) particle at 17 percent RH, (bottom) same particle beginning to deliquesce at 57 percent RH

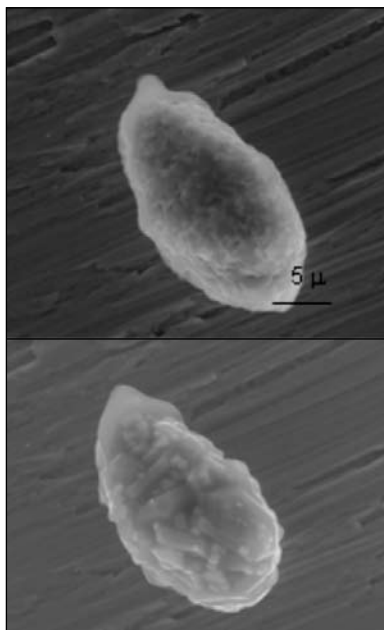
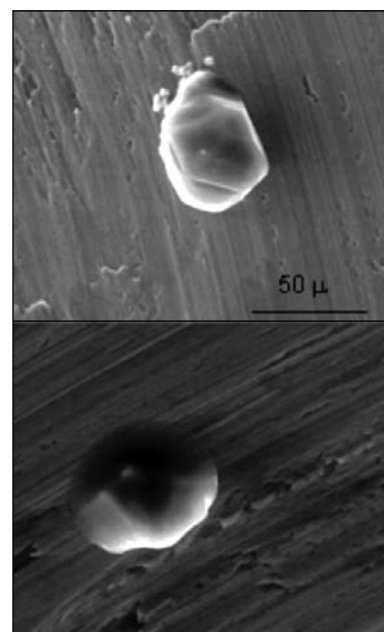


**Figure 5.** SEM images of two carnallite,  $\text{KMgCl}_3 \cdot 6\text{H}_2\text{O}$ , particles after recrystallization. The top particle exhibits the pseudo-hexagonal habit of carnallite. The bottom particle is completely phase separated into KCl (central cube) and  $\text{MgCl}_2$ .



it. We conclude that the deliquesced structures are KCl crystals in a Mg-K solution. Upon increasing the water vapor pressure, these cubes persisted to ~85 percent RH, consistent with the deliquescence relative humidity of KCl.

In thermodynamic equilibrium, when the relative humidity is lowered to just below the DRH,  $\text{KMgCl}_3 \cdot 6\text{H}_2\text{O}$  will begin to precipitate leaving the solution deficient in KCl. The remaining solution will then dissolve the solid KCl until all of the material precipitates as  $\text{KMgCl}_3 \cdot 6\text{H}_2\text{O}$ . This was not observed experimentally. Upon lowering the relative humidity over particles that had been exposed to a ~60 percent RH, the particles did not solidify or effloresce at relative humidities just below the MDRH as would be expected thermodynamically. Instead, the efflorescence relative humidity, while variable from particle to particle, generally did not occur until relative humidities below ~52 percent. An example is shown in Figure 5. Between these humidities, the droplet is a metastable, supersaturated salt solution. Such metastability upon dehydration is commonly observed in aerosol particles.<sup>15</sup> Upon solidification, two general structures were observed, often from the same original particle: pseudo-hexagonal structures, consistent with  $\text{KMgCl}_3 \cdot 6\text{H}_2\text{O}$ , and cubes, consistent with KCl. Elemental analysis from XRF supports this assignment. The extent to which carnallite or KCl and  $\text{MgCl}_2$  was formed varied from particle to particle. Some appear to be exclusively carnallite, while others appear to be completely phase separated into KCl and  $\text{MgCl}_2$ .

### iii. $\text{K}_2\text{MgCl}_4$ and $\text{K}_3\text{NaMgCl}_6$

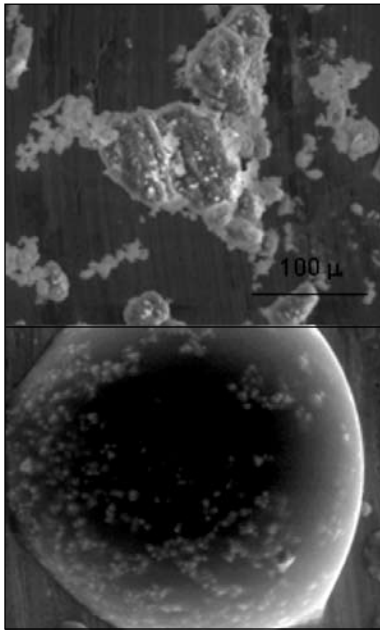
The  $\text{K}_2\text{MgCl}_4$  and  $\text{K}_3\text{NaMgCl}_6$  behaved similarly when exposed to water. Both salts were produced by calcining stoichiometric amounts of the starting single salts at 825°C for 1 hour and then cooling to room temperature.

The two samples were examined in the SEM. Both samples had been stored in only the glass vials and were outside the glove-box for up to several weeks before being studied in the microscope. Due to vapor leakage into the vials, these samples were exposed to an undetermined humidity. Based on the particle morphologies, the samples had not deliquesced, indicating that humidities obtained in the vials were not excessive. XRF measurements of the  $\text{K}_2\text{MgCl}_4$  sample showed that it was chemically homogeneous with the expected 2:1 stoichiometry of K:Mg and there were no significant impurities. Initial deliquescence occurred at ~57 percent RH and was incomplete, see Figure 6. Elemental analysis of the hydrated particle indicated that the solid components are K-rich and the droplet is Mg rich with respect to the starting material. Upon lowering the relative humidity, phase separation occurred, with regions containing mixed K/Mg and other regions containing exclusively K or Mg. Based on the XRF, no regions with a 2:1 K:Mg stoichiometry were retained after dehydration indicating that  $\text{K}_2\text{MgCl}_4$  formation from solution is unstable with respect to carnallite and the simple K and Mg salts. Similarly,  $\text{K}_3\text{NaMgCl}_6$  deliquesced at 57 percent RH and phase separated at lower relative humidity to KCl, NaCl, and carnallite.

XRD was performed on the as-made salts. For these studies,



**Figure 6.** SEM images of  $K_2MgCl_4$ . Material appeared homogeneous with respect to elemental distribution. Measured elemental fractions by ESD are K 35 percent, Mg 18 percent, Cl 47 percent (w/o O). (top) Dry particle, (bottom) 60 percent RH, deliquesced



the environmental chamber was not available and the analyses were performed in the laboratory under ambient conditions. The XRD patterns for as-made  $K_2MgCl_4$  and  $K_3NaMgCl_6$  samples are shown in Figures 7 and 8 along with the calculated patterns for the pure components.  $K_2MgCl_4$  and  $K_3NaMgCl_6$  are the major phases in the respective samples. There were no minor phases seen for the  $K_2MgCl_4$ . The  $K_3NaMgCl_6$  did have some minor, as yet unidentified phases. The unknown diffraction peaks could be from other unidentified ternary salt phases. However, elemental images of this sample did show a few particles that were highly enriched in magnesium and also contained significant quantities of Al and Si. The aluminum and silicon could have come from attack of the porcelain crucible. These samples were then examined again after exposure to room air for several days. The XRD of the  $K_2MgCl_4$  sample after eight days is shown in Figure 9. After eight days, all of the  $K_2MgCl_4$  lines were nearly gone and the new set of lines indexed to  $KMgCl_3 \cdot 6H_2O$  grew in. A similar set of experiments for the  $K_3NaMgCl_6$  were conducted. The  $K_3NaMgCl_6$  phase decreases, and the  $KMgCl_3 \cdot 6H_2O$ , KCl and NaCl phases grow in. The kinetics of the conversion of  $K_3NaMgCl_6$  are slower than  $K_2MgCl_4$ . Some  $K_3NaMgCl_6$  was still observed after six days, while the  $K_2MgCl_4$  was essentially gone after only three days.

The XRD and SEM results indicate that when these more complex salts are exposed to humid air, they decompose into their respective alkali halides and  $KMgCl_3 \cdot 6H_2O$ . Thus these salts begin deliquescing at the same relative humidity, the MDRH of carnallite (57 percent RH at 25°C). This suggests that the hydrates of  $K_2MgCl_4$  and  $K_3NaMgCl_6$  are thermodynamically unstable

**Figure 7.** X-ray diffraction data for a mixture of KCl and  $K_2MgCl_4$ . KCl was added as an internal standard. The experimental data is shown in the top graph and the calculated XRD pattern is shown in the bottom graph. The intensities have been scaled to emphasize the magnesium component of the mixture.

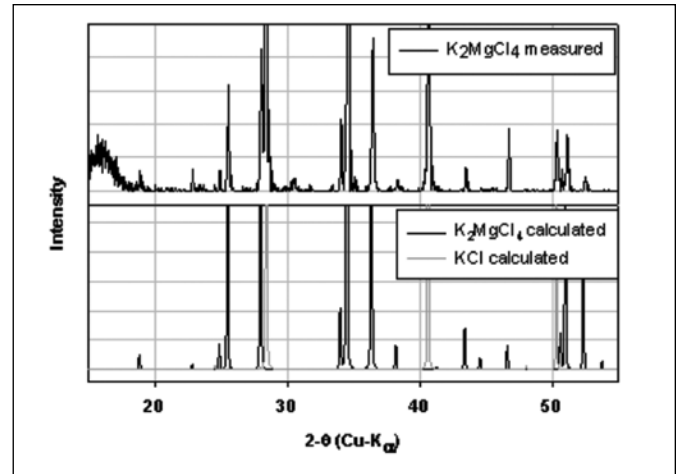
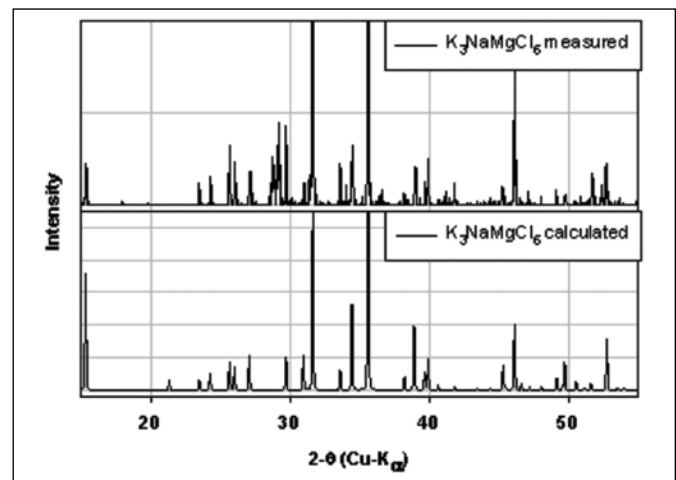


**Figure 8.** X-ray diffraction data for  $K_3NaMgCl_6$ . The experimental data is shown in the top graph and the calculated XRD pattern is shown in the bottom graph. The intensities of the graphs are scaled to emphasize the minor peaks.



with respect to carnallite in humid atmospheres. It is interesting to note that while carnallite is a naturally occurring mineral found in the evaporites from brines and seawater, to the best of our knowledge, the hydrates of more complex K:Mg chloride salts have not been reported, lending further support to their instability in humid environments.

### Salt Mixtures

The residual processing salts that have been stabilized and packaged to the 3013 standard are not simple single phase salts, but rather mixtures of several phases. As such, several salt mixtures were prepared. The first salt mixture was prepared to simulate the residues



**Figure 9.** The XRD pattern of the  $K_2MgCl_4$  material after eight days in room air. The experimental data is shown in the top graph and the calculated XRD pattern is shown in the bottom graph. The pattern is well matched to a mixture of KCl and  $KMgCl_3 \cdot 6H_2O$ . The peak just below  $35^\circ$  ( $34.6^\circ$ ) in the experimental XRD data is assigned to residual  $K_2MgCl_4$ .

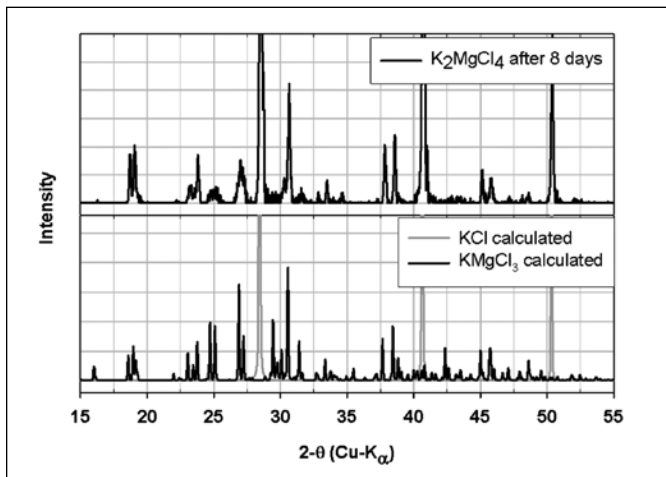
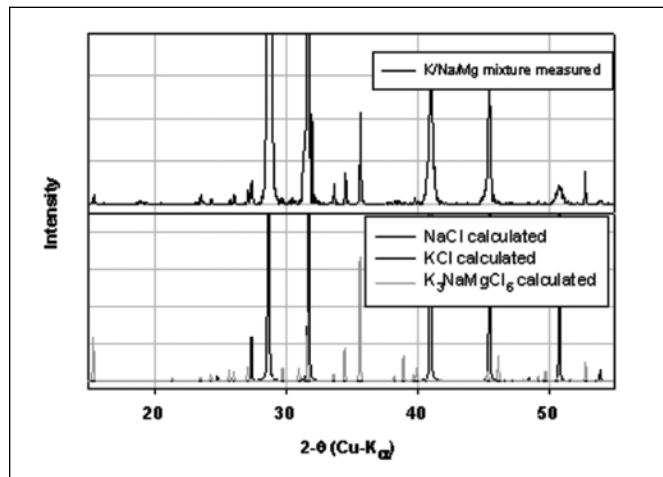


**Figure 10.** X-ray diffraction data for the K/Na/Mg salt mixture. Top graph is of the experimental data; the intensity scale is adjusted to emphasize the minor magnesium component of the salt. The bottom graph shows calculated XRD patterns of the pure components scaled so that the intensities of the principal peaks match the intensities seen in the experimental data.

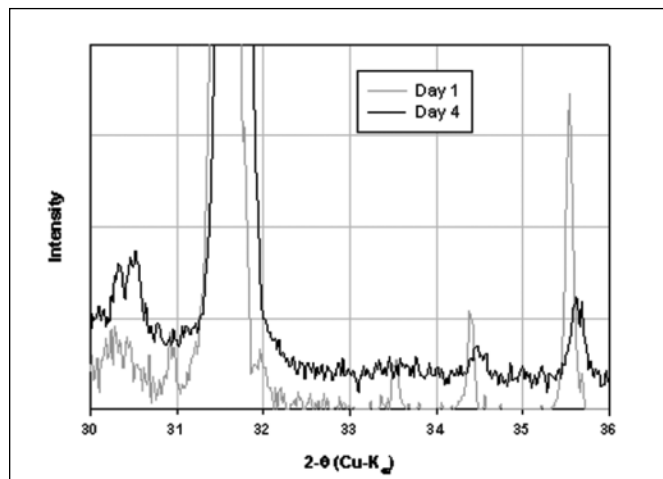


of the Pu electrorefining process at Rocky Flats and was synthesized from equimolar KCl/NaCl with 7 mole percent  $MgCl_2$ . A second salt mixture was prepared to investigate the behavior of  $CaCl_2$  in salt mixtures and was synthesized from equal weights of NaCl and KCl with 10 wt percent of added  $CaCl_2$ . The final salt mixture was prepared to investigate the behavior of the chloride salt component in a specific plutonium oxide obtained from the Rocky Flats Plant prior to closure. This material, known as 011589A, was generated prior to 1990 at Rocky Flats in Building 707 and was associated with plutonium foundry processing. The gas pressure within a test unit loaded with 011589A material at 0.5 wt percent moisture reached a maximum pressure of 225 kPa (32.6 psia) at approximately one year, at which time it contained a mixture of 46 percent  $H_2$  and 14 percent  $O_2$  with the remaining gases being nonflammable. Reports have shown that the  $O_2$  accumulation in certain test units was related to the concentration of  $MgCl_2$  and  $CaCl_2$  in the salt component and the amount of absorbed moisture.<sup>2</sup> The chloride salt component from the 011589A material was reproduced by combining the single chloride salts based upon the metal weight ratios of Mg:Ca:Na:K measured in the 011589A material.

#### i. K/Na/Mixture

Equimolar NaCl-KCl was prepared by grinding the salts together, heating to  $850^\circ C$  for one hour, and cooling to room temperature in the furnace. This salt mixture was ground to powder and 7 mole percent anhydrous  $MgCl_2$  was added. This mixture was then heated at  $850^\circ C$  for one hour. Elemental mapping in the SEM indicated multiple phases present in this salt, in contrast to the stoichiometric salts discussed above. In general, the mapping showed that in locations where potassium concentrations were high, the

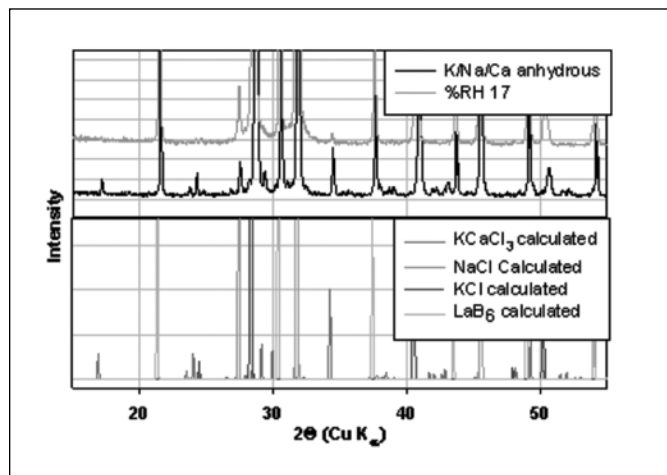
**Figure 11.** X-ray diffraction data for the K/Na/Mg salt mixture before and after exposure to room air. The scale has been expanded to highlight the minor features. The three XRD peaks for the as-made sample at  $33.5^\circ$ ,  $34.3^\circ$ , and  $35.6^\circ$  are from  $K_3NaMgCl_6$ . The peak at  $30.4^\circ$  in the exposed sample is from  $KMgCl_3 \cdot 6H_2O$ .



sodium concentrations were low and vice versa. The magnesium was generally associated with potassium. The XRD pattern, see Figure 10, shows that major phases were NaCl and KCl. All the rest of the minor phase lines, except for a small as yet unidentified peak at approximately  $18^\circ$ , can be indexed on the basis of the calculated diffraction pattern for  $K_3NaMgCl_6$ . The KCl and NaCl diffraction peaks are shifted slightly, indicating the formation of solid solutions. Based on the phase diagram for KCl/NaCl solid solutions should not exist at room temperature. The XRD results are consistent with a phase separation that quenched at  $-300^\circ C$



**Figure 12.** X-ray diffraction data for the K/Na/Ca salt mixture. The experimental data are shown in the top graph and the calculated XRD patterns are shown in the bottom graph.  $\text{LaB}_6$  was added as an internal standard.

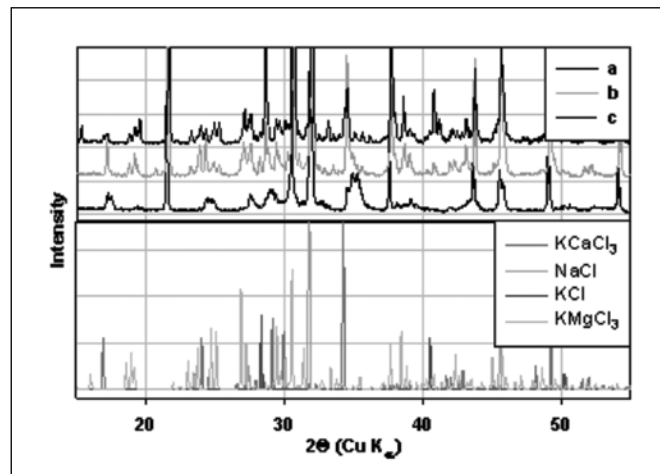


during cool down, presumably due to very slow diffusion below this temperature. An expanded view of a region highlighting the diffraction features from the  $\text{K}_3\text{NaMgCl}_6$  phase are shown in Figure 11. The three XRD peaks for the as-made sample were at  $33.5^\circ$ ,  $34.3^\circ$ , and  $35.6^\circ$  and are indicative of  $\text{K}_3\text{NaMgCl}_6$ . After exposure to room air for three days, these features decreased and a new feature at  $30.4^\circ$  indicative of  $\text{KMgCl}_3 \cdot 6\text{H}_2\text{O}$  appeared. This change in the XRD peaks indicates that water vapor absorbed during the exposure decomposed the  $\text{K}_3\text{NaMgCl}_6$  into carnallite and the alkali chlorides. The deliquescence of this mixture begins at 57 percent RH, also consistent with the presence of carnallite.

## ii. K/Na/Ca Mixture

Equal amounts of NaCl and KCl with 10 wt percent of added  $\text{CaCl}_2$  were ground together, heated to  $825^\circ\text{C}$  for fifteen minutes, and allowed to cool in the furnace. Moisture absorption tests were performed at  $25^\circ\text{C}$  and  $70^\circ\text{C}$ . The salt did not absorb any moisture prior to deliquescence at either temperature. Deliquescence occurred at 16 percent RH at  $25^\circ\text{C}$  and 21 percent RH at  $70^\circ\text{C}$ . The SEM confirmed the initial deliquescence of this mixture at 16 percent RH at  $25^\circ\text{C}$ . XRD patterns were obtained for this salt mixture using the environmental chamber at anhydrous conditions, 10 percent RH, and at 17 percent RH at room temperature. The XRD results, shown in Figure 12, indicate the presence of multiple phases that include  $\text{KCaCl}_3$ , KCl, and NaCl under anhydrous conditions and at 10 percent RH. At 17 percent RH, only the KCl and NaCl peaks were observed, indicating that the  $\text{KCaCl}_3$  phase has deliquesced. The  $\text{KCaCl}_3$  phase controls the interactions of water with this mixture at low relative humidity. The results also indicate a complete conversion of  $\text{CaCl}_2$  to  $\text{KCaCl}_3$  in this calcined mixture and that the presence of the sodium chloride

**Figure 13.** X-ray diffraction data for the K/Na/Mg/Ca salt mixture. The experimental data are shown in the top graph. The labels a, b and c refer to anhydrous, 10 percent RH and 17 percent RH respectively. The calculated XRD patterns in the bottom graph.  $\text{LaB}_6$  was added as an internal standard, refer to figure 12 for a calculated  $\text{LaB}_6$  XRD pattern.



does not affect the low humidity moisture absorption behavior.

## iii. K/Na/Mg/Ca Mixtures

This mixture was prepared by combining KCl, NaCl,  $\text{MgCl}_2$ , and  $\text{CaCl}_2$  in the same proportions of the metal cations measured for the Rocky Flats material 011589A. The mole fractions for the starting materials are: 0.28 (KCl), 0.38 (NaCl), 0.13 ( $\text{MgCl}_2$ ), and 0.21 ( $\text{CaCl}_2$ ). The salts were ground together, heated to  $825^\circ\text{C}$  for 15 minutes, and allowed to cool in the furnace. Moisture absorption tests indicate that this salt begins to absorb moisture between 1 and 2 percent RH at both  $25^\circ\text{C}$  and  $70^\circ\text{C}$ . Liquid formation occurs at 16 percent RH at  $25^\circ\text{C}$  and 18 percent at  $70^\circ\text{C}$ . XRD patterns were obtained for this salt mixture under anhydrous conditions, at 10 percent RH, and at 17 percent RH, see Figure 13. The diffraction patterns for this salt mixture are more difficult to interpret than those of the other salt mixtures. The anhydrous pattern contains numerous broad peaks. The sharp features are associated with either NaCl or the  $\text{LaB}_6$  internal standard. Broad diffraction features are typically ascribed to either small crystallites or significant lattice strain.<sup>19</sup> The peak broadening mechanism in this system is not known. The broad peaks are, however, consistent with the pattern for  $\text{KCaCl}_3$ . In the anhydrous sample, there are no clear features associated with any Mg-containing salts. The anhydrous pattern shows no evidence of KCl,  $\text{K}_3\text{NaMgCl}_6$  or  $\text{KMgCl}_3 \cdot 6\text{H}_2\text{O}$ . At this point we can only speculate that they may be present but that these phases are amorphous or their diffraction peaks are too broad to observe. At 10 percent RH, all the peaks become sharper and there are many new features, indicating a number of phases. There are clear peaks

which are indicative of  $\text{KMgCl}_3 \cdot 6\text{H}_2\text{O}$  and  $\text{KCl}$ . As the relative humidity increases to 17 percent, the  $\text{KCaCl}_3$  peaks decrease and the  $\text{KCl}$  peaks increase. The above results show that this mixture is quite complicated and contains a number of different salt phases. It is likely that  $\text{KMgCl}_3 \cdot 6\text{H}_2\text{O}$  is the species formed between 1 and 2 percent RH. At room temperature,  $\text{KCaCl}_3$  controls the formation of solutions at low relative humidities. Unlike the Mg-free salt discussed in the previous section, at  $70^\circ\text{C}$ , this salt mixture deliquesces at relative humidity that is lower than that for pure  $\text{KCaCl}_3$ . We currently do not understand this temperature effect. Nonetheless, the inclusion of Ca in the salt mixtures results in deliquescence at very low relative humidities.

### Summary and Conclusions

The results for the crystalline hydrate formation and deliquescence for all of the single phase salts studied are presented in Table 1. For pure  $\text{CaCl}_2$  at  $25^\circ\text{C}$ , exposure of the solid salt to water vapor resulted in the deliquescence of  $\text{CaCl}_2 \cdot 4\text{H}_2\text{O}$  at 20 percent RH, contrary to initial expectations that  $\text{CaCl}_2 \cdot 6\text{H}_2\text{O}$  would deliquesce at 29 percent RH. The interactions of water vapor with  $\text{KCaCl}_3$  have been examined for the first time. No crystalline hydrates are formed and  $\text{KCaCl}_3$  deliquesces at 16 percent RH at  $25^\circ\text{C}$ . The interactions of water with  $\text{K}_2\text{MgCl}_4$  and  $\text{K}_3\text{NaMgCl}_6$  have been studied and these salts decompose to  $\text{KMgCl}_3 \cdot 6\text{H}_2\text{O}$  and  $\text{KCl}$  (and  $\text{NaCl}$ ) at low relative humidities. The deliquescence and efflorescence of  $\text{KMgCl}_3 \cdot 6\text{H}_2\text{O}$  was examined. Metastable, supersaturated solutions can form on drying. Phase separation into either carnallite or  $\text{KCl/MgCl}_2$  mixtures can occur when solid phases crystallize out of these supersaturated phases. For the salt mixtures containing Mg,  $\text{KMgCl}_3 \cdot 6\text{H}_2\text{O}$  can form, leading to water uptake at low relative humidities. In the absence of Ca, the formation of aqueous solutions is controlled by the deliquescence of  $\text{KMgCl}_3 \cdot 6\text{H}_2\text{O}$  which is 57 percent RH at  $25^\circ\text{C}$ . For the Ca-containing mixtures under most of the conditions studied, the formation of aqueous solutions is controlled by the deliquescence of  $\text{KCaCl}_3$  which is 16 percent RH at  $25^\circ\text{C}$ . For the K/Na/Mg/Ca salt mixture at  $70^\circ\text{C}$ , deliquescence occurs at a lower than expected humidity through a currently unknown mechanism. These observations demonstrate that calcined Ca-containing plutonium oxide salt mixtures may deliquesce at very low relative humidities to provide a chloride containing electrolyte on an austenitic stainless steel surface in a 3013 container. Such an electrolyte can potentially support corrosion induced degradation within the container system.

### References

- DOE-STD-3013-2000, Stabilization, packaging, and storage of plutonium-bearing materials, U.S. Department of Energy, Washington, DC USA.
- Lillard, R. S., D. G. Kolman, M. A. Hill, M. B. Prime, D. K. Veirs, L. A. Worl, and P. Zapp. 2009. Assessment of Corro-


Table 1.

	Percent RH at $25^\circ\text{C}$	Percent RH at $70^\circ\text{C}$
$\text{MgCl}_2 \cdot 6\text{H}_2\text{O}$ hydrate formation	2	7
$\text{CaCl}_2 \cdot 2\text{H}_2\text{O}$ hydrate formation	2	2
$\text{CaCl}_2 \cdot 4\text{H}_2\text{O}$ hydrate formation	4	NA <sup>a</sup>
$\text{KMgCl}_3 \cdot 6\text{H}_2\text{O}$ hydrate formation	2	2
$\text{KCaCl}_3$ hydrate formation	Not Observed	Not Observed
$\text{MgCl}_2 \cdot 6\text{H}_2\text{O}$ deliquescence	33	27
$\text{CaCl}_2 \cdot 2\text{H}_2\text{O}$ deliquescence	-	17
$\text{CaCl}_2 \cdot 4\text{H}_2\text{O}$ deliquescence	20	NA
$\text{KCaCl}_3$ deliquescence	16	21
$\text{KMgCl}_3 \cdot 6\text{H}_2\text{O}$ deliquescence	57	<
$\text{K}_2\text{MgCl}_4$	Decomposes at low RH <sup>b</sup>	Not Examined
$\text{K}_3\text{NaMgCl}_6$	Decomposes at low RH	Not Examined

- NA: not applicable as this phase is thermodynamically unstable with respect to lower hydrates.
- Salt decomposes to  $\text{KMgCl}_3 \cdot 6\text{H}_2\text{O}$  and the respective alkali halides at a low, but undetermined, humidity.
- The DRH of  $\text{KMgCl}_3 \cdot 6\text{H}_2\text{O}$  at  $90^\circ\text{C}$  has been calculated at 48 percent RH 14.

sion-Based Failure in Stainless Steel Containers Used for the Long-term Storage of Plutonium-Based Salts, *Corrosion* 65, 175-188.

- Greenspan, L. 1977. Humidity Fixed-Points of Binary Saturated Aqueous-Solutions. *Journal of Research of the National Bureau of Standards* 81A, 89-96.
- Linke, W. F., and A. Seidell, editors. 1958. *Solubilities: Inorganic and Metal-organic Compounds*, American Chemical Society.
- Kipouros, G. J., and D. R. Sadoway. 2001. A Thermochemical Analysis of the Production of Anhydrous  $\text{MgCl}_2$ . *Journal of Light Metals* 1, 111-117.
- Conde, M. R., 2004. Properties of Aqueous Solutions of Lithium and Calcium Chlorides: Formulations for Use in Air Conditioning Equipment Design. *International Journal Thermal Science* 43, 367-382.
- See <http://www.crct.polymtl.ca/fact/documentation/> for a large Web-based compilation of salt phase diagrams.
- Brynstad, J., H. L. Yakel, and G. P. Smith. 1966. Temperature dependence of the absorption spectrum of nickel(II)-doped  $\text{KMgCl}_3$  and the crystal structure of  $\text{KMgCl}_3$ . *Journal of Chemical Physics* 45, 4652-4664.
- Gibbons, C.S., V. C. Reinsborough, and W. A. Whitla. 1975. Crystal Structures of  $\text{K}_2\text{MgCl}_4$  and  $\text{Cs}_2\text{MgCl}_4$ . *Canadian Journal of Chemistry* 53, 114-118.

- 
10. Fink, H. and H. J. Seifert. 1984. Quaternary Compounds in the System KCl/NaCl/MgCl<sub>2</sub>? *Thermochim. Acta* 72, 195-200.
  11. Marcus, Y. and N. Soffer. 1988. Solubilities and Vapor-Pressures in the Quinary System NaCl-KCl-MgCl<sub>2</sub>-CaCl<sub>2</sub>-H<sub>2</sub>O .1. Predictions and Measurements at 25°C, *Journal of the Chemical Society, Faraday Transactions articles 1*, 84, 3575-3585.
  12. Lerman, A. 1967. Model of the Chemical Evolution of a Chloride Lake—The Dead Sea. *Geochim. Cosmochim. Acta* 31, 2309-2330.
  13. Pabalan, R. T. and K. S. Pitzer. 1987. Thermodynamics of Concentrated Electrolyte Mixtures and the Prediction of Mineral Solubilities to High-Temperatures for Mixtures in the System Na-K-Mg-Cl-SO<sub>4</sub>-OH-H<sub>2</sub>O. *Geochim. Cosmochim. Acta* 51, 2429-2443.
  14. Pabalan, R.T., L. Yang, and L. Browning. 2002. Deliquescence Behavior of Multicomponent Salts: Effects on the Drip Shield and Waste Package Chemical Environment of the Proposed Nuclear Waste Repository at Yucca Mountain, Nevada. *Materials Research Society Symposia Proceedings* 713, JJ1.4.1-JJ1.4.8.
  15. Tang, I. N. and H. R. Munkelwitz. 1993. Composition and Temperature Dependence of the Deliquescence Properties of Hygroscopic Aerosols. *Atmospheric Environment* 27A, 467-473.
  16. Rard, J. A. and S. L. Clegg, 1997. Critical Evaluation of the Thermodynamic Properties of Aqueous Calcium Chloride. *Journal of Chemical and Engineering Data* 42, 819-849.
  17. Pitzer, K. S. and C. S. Oakes. 1994. Thermodynamics of Calcium-Chloride in Concentrated Aqueous-Solutions and in Crystals. *Journal of Chemical and Engineering Data* 39, 553-559.
  18. Seifert, H.J., H. Fink, G. Thiel, and J. Uebach. 1985. Thermodynamic and Structural Investigations on Compounds of the Systems KCl/CaCl<sub>2</sub>, KCl/CdCl<sub>2</sub>, KCl/CoCl<sub>2</sub>, KCl/NiCl<sub>2</sub>. *Zeitschrift für anorganische und allgemeine Chemie*. 520, 151-159.
  19. Popa, N.C. 1998. The (hkl) Dependence of Diffraction-Line Broadening Caused by Strain and Size for all Laue Groups in Rietveld Refinement. *Journal of Applied Crystallography* 31, 176-180.

## Acknowledgements

Funding for this work was provided by the Surveillance and Monitoring Program, U.S. Department of Energy Office of Environmental Management. This work was conducted at Los Alamos National Laboratory operated by Los Alamos National Security, LLC under contract DE-AC52-06NA25396.

*Stephen A. Joyce is a research and development scientist in the chemistry division at Los Alamos National Laboratory. He has a Ph.D. in physical chemistry from the Massachusetts Institute of Technology.*

*Joshua E. Narlesky is a research and development scientist at Los Alamos National Laboratory. He has an M.S. in chemical engineering from Colorado State University and a B.S. in chemical engineering from the New Mexico Institute of Mining and Technology.*

*D. Kirk Veirs is a staff scientist at Los Alamos National Laboratory. He has a Ph.D. in physical chemistry from Pennsylvania State University and a B.S. in chemistry and environmental science from Northern Arizona University.*

*Eduardo Garcia is an R&D manager in the chemistry division at Los Alamos National Laboratory. He has a Ph.D. in inorganic chemistry from the Iowa State University.*

*Obie W. Gillispie is an R&D engineer at Los Alamos National Laboratory. He has a B.S. in chemical engineering from the University of New Mexico.*

*J. Matt Jackson is a graduate research assistant at Los Alamos National Laboratory. He has a B.S. in mechanical engineering from the New Mexico State University.*

*Brian L. Scott is a technical staff member at Los Alamos National Laboratory.*

*Laura A. Worl is a technical staff member in the nuclear material technology division at Los Alamos National Laboratory. She has a Ph.D. in chemistry from the University of North Carolina.*



# Sampling Approach to Validate the Safe Storage of Plutonium-Bearing Materials

Elizabeth J. Kelly, Larry G. Peppers, Laura A. Worl, and James McClard  
Los Alamos National Laboratory, Los Alamos, New Mexico USA

James McClard  
Savannah River Site, Aiken, South Carolina USA

## Abstract

The 3013 surveillance sampling approach combines statistical and judgmental sampling to provide a powerful, cost-effective method for ensuring the safe storage of 3013 containers. To select the statistical sample, the population of containers is organized into three bins based on a container's contents and estimated potential for degradation. Using pressure and corrosion as the potential degradation mechanisms, the three bins are Pressure and Corrosion, Pressure Only, and Innocuous. The requirement of 99.9 percent probability of observing at least one of the worst 5 percent (in terms of potential degradation) is used to guide the statistical sampling process for the Pressure and Corrosion and Pressure Only bins. The statistical sample for the Innocuous bin is based on evaluating the assumption that these containers will show no degradation; therefore, these containers will have almost no variability in the surveillance results. The judgmental sampling uses engineering judgment and results of the shelf-life studies to augment the statistical sample with additional containers that are judged to have the greatest potential for degradation.

## Introduction

The U.S. nuclear weapons program has generated large quantities of excess plutonium. This material must be safely stored pending final disposition. Requirements for packaging and storing plutonium-bearing materials have been addressed in the Department of Energy (DOE) Standard, "Stabilization, Packaging, and Storage of Plutonium-Bearing Materials," DOE-STD-3013,<sup>1</sup> and are being implemented throughout the DOE complex. In order to ensure the safe long-term storage of plutonium in 3013 containers, the 3013 standard directed that a surveillance plan be developed and used for monitoring the condition of the containers during storage. DOE has implemented an Integrated Surveillance Program (ISP),<sup>2</sup> which is designed to integrate individual sites into a corporate, cost-effective surveillance effort. The ISP consists of two programs: the shelf-life program to closely monitor the behavior of selected materials under laboratory conditions and the field surveillance program to destructively and nondestructively evaluate the condition of production 3013 containers and materials during storage.

The field surveillance program includes evaluation of containers from statistically based and judgmentally based samples of containers. To select the statistical sample, the population of containers has been organized into three bins based on a container's contents and assumed potential for experiencing selected degradation mechanisms. Potential degradation mechanisms include corrosion due to chemical attack on the container walls and welds and pressurization due to gas generation from radiolysis of moisture and thermo-chemical reactions. The three bins have been designated: Pressure and Corrosion (pressurization and corrosion mechanisms possible), Pressure Only (pressurization only, corrosion unlikely) and Innocuous (pressurization and corrosion unlikely).

The criterion of a 99.9 percent probability of observing at least one of the worst 5 percent of the containers (worst in terms of pressurization and corrosion) is used to determine the number of containers in the statistical sample for the Pressure and Corrosion and the Pressure Only bins. Using this criterion, 128 containers are needed for the sample from the Pressure and Corrosion bin and 130 are needed for the sample from the Pressure Only bin.

A different criterion is used for the Innocuous bin. In this bin the goal is to check the assumption of little variability between containers and no observations of degradation or significant pressurization. The initial Innocuous bin sample includes ten containers.

The number of containers in the bin sample from each packaging site [e.g., Hanford Site, Lawrence Livermore National Laboratory (LLNL), Los Alamos National Laboratory (LANL), Rocky Flats Environmental Technology Site (RFETS) and Savannah River Site (SRS)] is determined by multiplying the proportion of items in a bin from that site by the total sample size for that bin.

The statistical sample is augmented with judgmental sampling to provide a powerful, cost-effective tool for assuring the safe storage of the 3013 containers. The selection of a judgmental sample is based on engineering judgment, results of the shelf-life studies, comparison of the statistical sample to the population, packaging and stabilization data and field surveillance. The judgmental sample targets items deemed to have the greatest potential for degradation.



## Background

Field surveillance began in Fiscal Year (FY) 2005 and the first documents describing the field sampling program were released at that time.<sup>3,4,5</sup> The field surveillance program has been evaluated annually and modifications have been made based on new information.<sup>6,7</sup> The new information consisted of new prompt gamma data and revised prompt gamma calibration information<sup>8</sup>, updated site packaging information, and improved moisture measurement evaluations. Modifications included changes to bin assignments that resulted in changes to the statistical sample.

The Pressure and Corrosion sample containers (128) are to have non-destructive evaluations (NDE) and destructive evaluations (DE); some NDE began in FY 2005 and DE began in 2007. These evaluations are scheduled to be completed by 2016. The Pressure Only bin requires 130 containers for the statistical sample. These containers require NDE only, because significant pressure increases can be measured by NDE techniques. These NDE evaluations began in FY 2005 and were completed in FY 2009. Since a requirement for evaluating pressurization is that the container be three years old, the 2009 completion date means that only containers produced by 2006 could be included in the Pressurization Only bin at this time. Therefore, LANL and some LLNL containers packaged after 2006 are not included in the statistical sampling. Sampling of these containers will be addressed when packaging is complete at these sites. In addition to the NDE, beginning in FY 2007 two Pressure Only containers have DE performed each year (for a minimum of three years), to validate the assumption that there is no corrosion occurring in these containers.

## Binning of Containers

Binning consists of a three-tiered review of all 3013 containers with the primary objective of placing each container into one of the three bins for the purpose of surveillance.

**Tier 1**—Decision Tree (Figure 1): containers that have already been packaged are assigned to the appropriate surveillance bin based on information in their data packages.

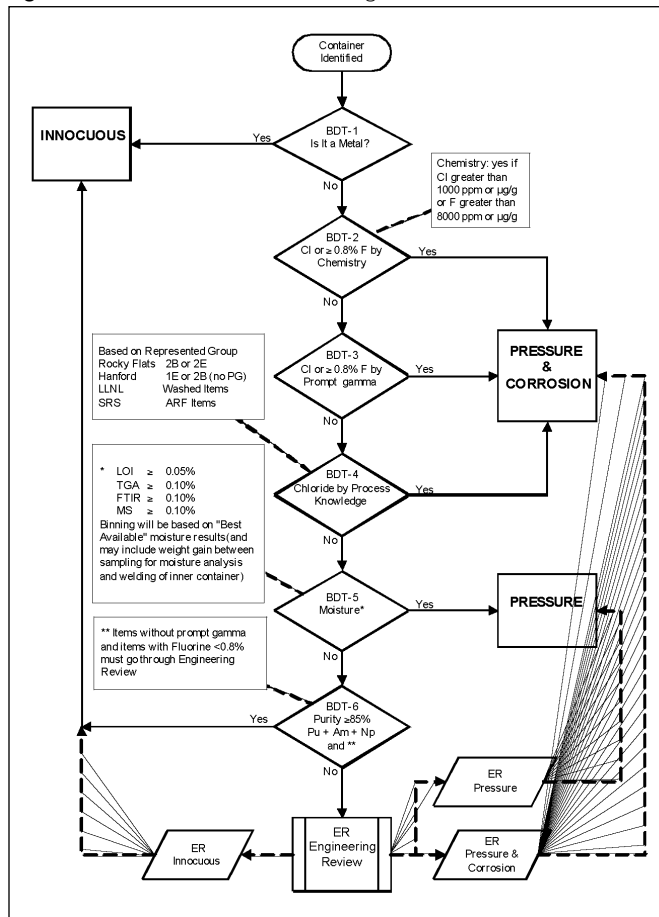
**Tier 2**—Engineering Review: containers that have already been packaged but have failed the initial decision tree screening and required an engineering review before they were assigned to an appropriate bin.

**Tier 3**—Items not yet packaged from LLNL and LANL: assigning these items to a bin requires engineering review and process knowledge. It is recognized that actual packaging numbers and bin assignments are likely to differ from current projections.

## Binning Decision Tree

The first step of the binning process is the application of the binning decision tree to the ISP database. Figure 1 shows a composite binning decision tree for all sites, however, site-specific trees

Figure 1. Generic decision tree for binning 3013 items for field surveillance



have been developed. The decision trees were developed by the Materials Identification and Surveillance (MIS) Working Group and have evolved over time.<sup>3,4,5,6,7</sup>

The initial binning decision assigns containers with Pu metal and associated metal impurities to the Innocuous bin, as illustrated by the decision tree (Figure 1). The second binning operation identifies containers with a potential for corrosion. The primary constituent for causing corrosion is chloride salts or possibly fluoride containing materials. Using information from the database, containers identified as containing either chloride (greater than 1,000 ppm) or fluoride (greater than 8,000 ppm) are placed in the Pressure and Corrosion bin. Identification of chloride or fluoride can be accomplished by chemical analysis, prompt gamma analysis, or process knowledge of the material.

The third criterion, used for the binning of pure oxide material that showed no evidence for containing corrosive materials, is the final moisture content of the oxide. For the purpose of this evaluation, *pure* plutonium oxide was defined as material where the sum of the Pu + Np + Am is greater than 85 wt percent. This means that the total impurities, other than oxygen, are less than 3 wt percent. Uranium is not included in this instance because of the high uncertainties associated with uranium measurements.



The DOE-STD-3013<sup>1</sup> sets the moisture limit for oxide materials at 0.5 wt percent. However, the actual acceptance limit for moisture content was less than 0.5 wt percent and varied from site to site depending on the uncertainty associated with the site-specific moisture analysis.

To accommodate the different measurement techniques used by each site, a conservative moisture limit was established for binning of the pure oxide materials. Containers with a loss on ignition (LOI) result greater than 0.05 wt percent were assigned to the Pressure Only bin. When moisture was measured by thermal gravimetric analysis (TGA), Fourier-transform infrared spectrometer (FTIR), or mass spectroscopy (MS) analysis, a moisture limit of greater than or equal to 0.10 wt percent was established for placing the container in the Pressure bin. Containers with pure oxide with moisture content below these limits are placed in the Innocuous bin unless fluoride is detected and/or there is no prompt gamma data.

If a container successfully passes the screening test for Pressure and Corrosion as well as for Pressure Only, and had less than 85 wt percent (Pu + Am + Np), it must have an engineering review (ER).

### Engineering Review (ER)

All existing containers selected for ER are prescreened as described above using the logic diagram shown in Figure 1. Uranium is excluded from the prescreening process because its large measurement uncertainty might skew the binning results. However, the presence of uranium is considered during the ER. The criteria for binning ER containers are listed below.

- **Criterion 1:** Containers with greater than 85 wt percent Pu + Am + Np + U (total actinide) are placed in the Innocuous bin. These containers were reviewed on an individual basis to ensure that the material came from a historically pure stream, so that the uranium measurement uncertainty cannot cause an impure material to be binned as innocuous.
- **Criterion 2:** Containers with total actinide content between 80 wt percent and 85 wt percent are reviewed on an individual basis. Those containers from a process that historically produced pure material with a moisture content of less than 0.05 wt percent are placed in the Innocuous bin unless there is a suspected problem with the moisture analysis identified through a nonconformance report (NCR) or other documented production comment. Containers not meeting the moisture criteria are placed in the Pressure Only bin.
- **Criterion 3:** Containers with a total actinide content of less than 80 wt percent are placed in the Pressure Only bin. (Exceptions are oxide containers evaluated under Criterion 4.)
- **Criterion 4:** Oxide containers produced by magnesium hydroxide precipitation from pure plutonium nitrate solutions represent a special class of items where the major impurity is magnesium oxide and prompt gamma indicates no other significant impurities. These are placed in either the Innocuous

bin or the Pressure Only bin. Details of how this decision is made can be found in reference 7.

- **Criterion 5:** If hydrogen chloride (HCl) is detected in the FTIR or MS analysis, then containers are placed in the Pressure and Corrosion bin.

Binning results for all 3013 containers (as of 2009) are summarized in Table 1. The results from an evaluation of containers yet to be packaged are also included in this table to provide a picture of the distribution of the total 3013 containers expected to be in storage.

### Sampling Approach

The requirement of 99.9 percent probability of observing at least one of the worst 5 percent (denoted as 99.9 percent/5 percent) is used to guide the statistical sampling process for the Pressure and Corrosion and Pressure Only bins. The hypergeometric distribution is used to determine the number of containers,  $n$ , that need to be evaluated to meet this requirement. The hypergeometric distribution describes an Urn Model with  $M$  red and  $K$  black balls. It is a discrete probability distribution that describes the probability of drawing  $m$  red balls and  $n-m$  black balls in a sequence of  $n$  draws from a finite population without replacement.<sup>9,10</sup> In this application, containers from the worst 5 percent are considered the  $M$  red balls and the hypergeometric distribution is used to determine the required sample size ( $n$ ) so that there is a 99.9 percent probability of seeing at least one ( $m=1$ ) red ball (e.g., at least one of the worst 5 percent) in a sample of  $n$  containers from a bin.

Using this criterion does not necessarily mean that containers have significant degradation. It simply means that (in theory) at the end of fifty years, all containers could be evaluated and ranked for their degree of degradation (higher rank, higher degradation). This ranking could take place even if there was very little, if any, degradation, and even if the containers varied little in terms of degradation. The 5 percent with the highest scores would be the *worst* 5 percent. It is not necessary to actually rank the containers to implement this statistical approach.

The main attribute of this approach is that it requires no assumptions about which containers or groups of containers are the *worst*. The random sampling alone provides the specified degree of confidence (e.g., 99.9 percent) that at least one of the containers from the worst 5 percent will be observed. It should be noted that an important assumption of this approach is that a container has a valid assessment of its ultimate (fifty years) degradation when it is examined.

The statistical calculations for the sample sizes (using the hypergeometric distribution<sup>9,10</sup>) are generally independent of population size when the population has more than 500 items (all bins meet this criterion). However, the number of items in the worst 5 percent clearly depends on the population size.



**Table 1.** Binning of ALL DOE 3013-Type Containers as of 2009

Site	Innocuous	Pressure	Pressure and Corrosion	Total
Rocky Flats Packaged	808	718	362	1888
Hanford Packaged	925	778	551	2257
LLNL Packaged as of 2006 Total Planned	9 117	9 9	56 159	74 285
SRS Packaged	744	103	71	918
LANL* Packaged as of 2006 Total Planned	0 25	0 83	0 160	0 268
<b>Total</b>	<b>2622</b>	<b>1691</b>	<b>1303</b>	<b>5616</b>

The statistical sample for the Innocuous bin is based on the assumption that these containers will show no degradation; therefore, there will be almost no variability in the pressurization evaluations. A random sample of ten containers from this bin is evaluated to test the assumptions of negligible variability in the pressurization measurement and no degradation.

The statistical samples for the Pressure and Corrosion bin and Pressure Only bin give a very high level of confidence (99.9 percent) that a potential problem affecting at least 5 percent of the population will be detected. These samples also provide data for predicting the pressurization and corrosion tendencies for the entire population. However, the question remains, what if there are just a few “problematic containers” that are very different from the rest of the containers in the population? To address this issue, the statistical samples are augmented with judgmental sampling. The judgmental sampling uses engineering judgment, results of the shelf-life studies, results of the statistical sampling, and other sources of information to target containers that could have the greatest potential for degradation. The combined approach of statistical and judgmental sampling is a powerful, cost-effective tool for ensuring the safe storage of the 3013 containers.

### Statistical Sample (2009)

Based on the number of containers in the Pressure and Corrosion and Pressure Only bins given in Table 1, sample sizes of 128 containers for the Pressure and Corrosion bin and 130 containers for the Pressure bin meet the 99.9 percent/5 percent criterion. The statistical software, *S-Plus*,<sup>10</sup> was used to determine sample sizes and generate the random samples.

The Pressure and Innocuous random NDE sampling cam-

**Table 2.** Distribution of sample sizes in the pressure and corrosion and pressure bins across sites (as of 2009)

	Pressure and Corrosion	Pressure
Hanford	54	63
LLNL	16	1
Rocky Falls	35	58
SRS	7	8
LANL	16	0
<b>TOTAL</b>	<b>128</b>	<b>130</b>

paigns began in 2005 and will be completed in 2009.<sup>6,7</sup> Containers must be at least three years old at the time of evaluation to ensure that pressurization will have occurred, if it is going to occur. Therefore, the 130 containers in the Pressure random sample and the 10 containers in the Innocuous random sample must have been packaged as of June 2006.

The random sample is allocated proportionally to each packaging site. For example, for Hanford, the number of containers in the Pressure and Corrosion bin sample is

$$\frac{551 \text{ (Hanford containers)}}{1303 \text{ (total containers in bin)}} \times 128 \text{ (bin sample size)} = 54 \text{ (Hanford containers in the sample)}.$$

For the Pressure bin the sample allocation to sites depends on the number of containers packaged in 2006, for LLNL

$$\frac{9 \text{ (LLNL 2006 containers)}}{1608 \text{ (total 2006 containers in bin)}} \times 130 \text{ (bin sample size)} = 1 \text{ (LLNL container in the sample)}.$$

Table 2 gives the distribution of sample sizes across the various sites for the Pressure and Corrosion and Pressure Only bins (as of 2009).

### Bin Change Impacts to the Statistical Sample

A key component of the surveillance sampling approach is the regular review of container bin assignments. Bin assignments can change based on new information, such as prompt gamma measurements, shelf-life study results, revised packaging information and field evaluations. The revised bin assignments can lead to revised field surveillance sampling plans. While the field surveillance approach remains fixed, the actual field sampling plans can change as needed over time. All revisions are documented in detail.<sup>6,7</sup>

There have been two major rebinning efforts.<sup>6,7</sup> These rebinnings did not change the total bin sample sizes, since the bins are large. However, the rebinnings did affect the site proportions in the bins and therefore the site-specific sample sizes. In addition, one of the rebinning efforts<sup>6</sup> resulted in a significant number of items moving from the Pressure and Corrosion bin to the Pressure Only bin. Since none of the Pressure and Corrosion bin items had been evaluated at the time of the rebinning, the statistical sample for the Pressure and Corrosion bin was simply redrawn.



However, for the Pressure Only bin many items in the sample had been evaluated. Therefore, the Pressure Only bin sample was adjusted in the following way. The total sample size ( $n$ ) was proportionately allocated between items previously in the bin and the new items, resulting in  $n_1$  sample items from the new items and  $n_2$  items from the previous items ( $n = n_1 + n_2$ ). The  $n_1$  sample was randomly selected from the new items and the  $n_2$  sample was randomly selected from the previous  $n$  sample items.

To address changes in site-specific sample sizes the following approach was taken.

1. Site-Specific Sample Size Decreases:
  - a. Pressure bin. Items from the sample have been deselected randomly. If these items have already been evaluated, it results in additional items in the sample.
  - b. Pressure and Corrosion bin, since very few items have been evaluated so far and since the cost of the DE is very high, items are deselected randomly from those items not yet evaluated.

2. Site-Specific Sample Size Increases:

For both the Pressure and Corrosion and Pressure Only bins, additional items are chosen randomly from the remaining population of items not in the sample. For the Pressure Only bin when new items entered the population, care was taken to proportionately allocate between old and new items for each site (as discussed above).

When LANL and LLNL finish packaging a decision will be made as to the need for additional Pressure Only bin sampling. A possible approach will be to determine the 99.9 percent/5 percent sample sizes for each site based on all Pressure Only bin items (e.g., those packaged by 2006 and those packaged after 2006). A proportional number of items from LANL and LLNL will be in this 99.9 percent/5 percent sample. This number of items will be randomly selected from the LANL and LLNL Pressure Only bin items. The number of items in the final sample from the other sites will decrease accordingly (since there will be around 130 items total). Therefore, for the other sites the current Pressure Only bin random sample will be more than adequate to meet the 99.9/5 percent requirement.

### **Innocuous Bin Sample**

The material in the Innocuous bin containers is either plutonium metal or relatively pure plutonium oxide with low water content. It is not credible for plutonium metal packaged per the 3013 standard to generate pressure except for the relatively low pressure of helium generated from alpha decay.<sup>11</sup> In addition, failure of the container from corrosion or metal-to-metal interaction between the plutonium metal and the storage container is not credible.<sup>12</sup> For these reasons, the MIS Working Group concluded that metals present no risk of pressurization or corrosion, and that the surveillance sample for the innocuous bin is focused on oxide containers only. This assumption will be further evaluated

at LANL when a metal item packaged at RFETS in a 3013 container is opened for programmatic use.

The ten containers that make up the initial Innocuous bin random sample were selected randomly from the oxide population of innocuous items packaged by 2006. The decision to do additional Innocuous bin sampling for LANL and LLNL will be based on surveillance results.

### **Judgmental Sample**

The statistical sample is augmented with judgmental sampling to provide a powerful, cost-effective tool for ensuring the safe storage of the 3013 containers. The judgmental sampling uses engineering judgment, results of the shelf-life studies, comparison of the statistical sample to the population, packaging, and stabilization data and field surveillance results to identify additional containers for surveillance. The judgmental sample targets containers with the greatest potential for degradation and data gaps, if any, in the statistical sample.

The process for selecting containers for the judgmental sample includes a detailed comparison of the 3013 population to the existing containers in the statistical sample to determine if there are any important properties of the population that were not represented adequately in the sample. No significant gaps in sample coverage have been identified in the sample versus the total population.<sup>5</sup>

Containers for the judgmental sample are also selected based on a specification of those properties considered to be most important in terms of potential container pressurization and/or corrosion based on the expert judgment of the MIS Working Group and others. The properties that have been identified include high water content, chloride concentration in the container, HCl generation during moisture measurement, detection of high levels of SO<sub>2</sub> or CO<sub>2</sub> during moisture measurement, weight gain between sampling and packaging, and containers with the maximum estimated pressure generation (based on an algorithm documented in Reference 13).

In addition, items are selected based on the results of the ongoing small-scale test program at LANL, which identified three categories of containers for judgmental sampling:

1. items showing significant pitting corrosion with relatively high hydrogen generation,<sup>14</sup>
2. items with the highest total gas generation of all MIS small-scale test samples,<sup>15</sup> and
3. items generating both hydrogen and oxygen gas, which has reached flammable levels in the small-scale test reactor.<sup>16,17</sup>

Finally, testing work being performed by the MIS program has indicated that there is a potential for stress corrosion cracking (SCC) under certain conditions. Containers were selected in FY2009 to evaluate SCC.



## Conclusions

The Pressure Only bin statistical sample (as of 2009) consists of 130 containers, which have all had NDE. None of these have shown significant pressure increases.<sup>18</sup> The statistical sampling is now complete for the Pressure Only bin. Based on the sampling specification, this means that there is a 99.9 percent probability that if there is any significant pressurization in the Pressure Only bin containers, it is in less than 5 percent of this population. Stronger statements as to the limits of pressurization for the Pressure Only bin can be made by analyzing the NDE radiography pressurization measurements (see Reference 18). Any additional evaluations of items from this bin will be chosen based on expert judgment to look at the effects of extended storage.

Six containers from the Pressure Only bin had DE to evaluate the assumption that corrosion was not a concern for these containers. These containers were chosen based on engineering review and none of the containers showed corrosion.

In addition to the 130 randomly selected containers, there are 16 additional Pressure Only bin containers that have had NDE. These additional NDE's targeted containers of interest and none of these targeted containers have shown significant pressure increases. Another 73 containers from the Pressure and Corrosion bin (some random, some targeted) have also had NDE's and none of these containers have shown significant pressure increases. Including these additional containers in the calculations with the assumption that the targeting is effective, the probability is very high (approximately 99 percent) that if significant pressurization exists, it is in less than 3 percent of the population.

The ten containers from the Innocuous Bin have been evaluated. None of these have shown significant pressurization or any degradation. However, because of radiography measurement differences between sites, variability evaluation is problematic. A detailed discussion of these data is provided in reference 18.

The Pressure and Corrosion bin statistical sample (as of 2009) consists of 128 containers, of which 37 have had DE. None of these containers have shown significant corrosion effects. There have been 43 DE's to date (37 from the Pressure and Corrosion bin and six from the Pressure Only bin). The results of these evaluations suggest that the binning process has successfully segregated the 3013 containers<sup>19</sup>. For example, evidence of very shallow pitting on the inner surfaces of some convenience containers from the Pressure and Corrosion bin has been associated with chloride rich particles on the container surfaces. None of the six containers having DE from the Pressure Only bin show any signs of corrosion. These results indicate that the binning has correctly focused sampling to determine the risk of corrosion-induced degradation. Continued destructive evaluations of containers from the Pressure and Corrosion bin will provide additional data to quantify the risk of corrosion induced degradation in the storage inventory.

*Elizabeth J. Kelly is a scientist at Los Alamos National Laboratory. She has a Ph.D. in biostatistics from the University of California at Los Angeles. She has an M.A. and a B.S. in mathematics from the University of Southern California.*

*Larry G. Peppers is an R&D engineer at Los Alamos National Laboratory. He has a B.S. in chemical and petroleum refining engineering from the Colorado School of Mines.*

*Laura A. Worl is a technical staff member in the nuclear material technology division at Los Alamos National Laboratory. She has a Ph.D. in chemistry from the University of North Carolina.*

*James W. McClard is a fellow technical advisor at Savannah River Nuclear Solutions. He has a B.S. in chemical engineering from Clemson University.*

## References

1. DOE. 2004. DOE Standard: Stabilization, Packaging, and Storage of Plutonium-Bearing Materials. *DOE-STD-3013-2004*. Washington, D.C.: U.S. Department of Energy.
2. LANL. 2001. Integrated Surveillance Program in Support of Long-Term Storage of Plutonium-Bearing Materials. *Los Alamos National Laboratory LA-UR-00-3246*, Rev. 1.
3. Peppers, L., E. Kelly, J. McClard, J. Stakebake, and T. Venetz. 2005. Binning of 3013 Containers for Field Surveillance. *Los Alamos National Laboratory LA-14184*.
4. E. Kelly, J. McClard, L. Peppers, J. Stakebake, and T. Venetz. 2005. 3013 Surveillance Sampling—The Statistical Sample. *Los Alamos National Laboratory LA-14185*.
5. Peppers, L., E. Kelly, K. Veirs, and J. Berg. 2005. 3013 Container Statistical and Judgmental Samples Selected for Non Destructive Evaluation (NDE) in FY 2005. *Los Alamos National Laboratory LA-UR-05-2193*.
6. L. Peppers, E. Kelly, J. McClard, G. Friday, T. Venetz, and J. Stakebake. 2007. Selection of 3013 Containers for Field Surveillance. *Los Alamos National Laboratory LA-14310*, Rev. 0.
7. L. Peppers, E. Kelly, J. McClard, G. Friday, T. Venetz, and J. Stakebake. 2009. Selection of 3013 Containers for Field Surveillance: LA-14310 Rev. 1. *Los Alamos National Laboratory LA-14395*.
8. Narlesky, J. E., L. A. Foster, E. J. Kelly, R. E. Murray IV. 2010. Characterization of Plutonium-Bearing Materials Packaged in 3013 Containers by Alpha-Particle-Induced Prompt Gamma-Ray Analysis. *JNMM*, 2010 Winter Issue.
9. Hoel, P., Port, S. and Stone, C. 1971. *Introduction to Probability Theory*. Boston, MA. Houghton-Mifflin.



10. Insightful Corporation. 2001. *S-PLUS 6 for Windows*. Seattle, Washington: Insightful Corporation Copyright © 1987–2001.
11. Spearing, D. R. and W. J. Crooks. 2003. Gas Generation Mechanisms In Pu Metal Bearing DOE-3013 Containers. *Los Alamos National Laboratory document LA-UR-03-1214*.
12. Williamson, M. A. 1999. Plutonium Storage: Phase Equilibria Issues. *Los Alamos National Laboratory document LA-UR-99-136*.
13. Friday, G. P, L. G. Peppers, and D. K. Veirs. 2008. A Method for Estimating Gas Pressure in 3013 Containers Using an ISP Database Query. *Savannah River National Laboratory report WSRC-STI-2008-00214*. Washington Savannah River Company.
14. Durrwachter, K. J., K. A. Dunn, and J. W. McClard. 2005. 3013/9975 Surveillance Program Annual Summary Report (FY05). *Savannah River Site report WSRC-TR-2005-00422*. Westinghouse Savannah River Company.
15. Narlesky, J., E., J. M. Berg, and D. K. Veirs. 2006. Identification of 3013 Containers Represented by MIS Sample C06032A. *Los Alamos National Laboratory document LA-UR-06-6460*.
16. Berg, J. M., D. K. Veirs, and L. A. Worl. 2006. Maximum pressure for structural response calculation of 3013 containers. *Los Alamos National Laboratory document LA-UR-06-4051*.
17. Friday, G. P. and L. G. Peppers. 2006. Investigation of MIS Item 011589A and 3013 Containers Having Similar Characteristics. *Savannah River National Laboratory Report WSRC-TR-2006-00236*. Washington Savannah River Company.
18. Yerger, L., L. E. Traver, J. W. McClard, T. J. Venetz, and D. Riley. 2010. Nondestructive Examination of Plutonium-Bearing Materials Packages, *JNMM, to be published in Spring 2010*.
19. Nelson, D. Z., G. T. Chandler, K. A. Dunn, T. M. Stefek, and 2010. Stainless Steel Interactions with Salt Containing Plutonium Oxides. *JNMM, to be published in Spring 2010*.

# Mark Your Calendar

INMM 51<sup>ST</sup> ANNUAL MEETING

July 11–15, 2010

Baltimore Marriott Waterfront Hotel | Baltimore, MD USA

[www.inmm.org](http://www.inmm.org)

## Author Submission Guidelines

The Journal of Nuclear Materials Management is the official journal of the Institute of Nuclear Materials Management. It is a peer-reviewed, multidisciplinary journal that publishes articles on new developments, innovations, and trends in safeguards and management of nuclear materials. Specific areas of interest include international safeguards, materials control and accountability, nonproliferation and arms control, packaging and transportation, physical protection, and waste management. JNMM also publishes book reviews, letters to the editor, and editorials.

**Submission of Manuscripts:** JNMM reviews papers for publication with the understanding that the work was not previously published and is not being reviewed for publication elsewhere. Papers may be of any length. All papers must include an abstract.

The Journal of Nuclear Materials Management is an English-language publication. We encourage all authors to have their papers reviewed by editors or professional translators for proper English usage prior to submission.

Papers should be submitted as Word or ASCII text files only. Graphic elements must be sent in TIFF, JPEG or GIF formats as separate electronic files and must be readable in black and white.

Submissions may be made via e-mail to Managing Editor Patricia Sullivan at [psullivan@inmm.org](mailto:psullivan@inmm.org). Submissions may also be made via regular mail. Include one hardcopy and a CD with all files. These submissions should be directed to:

Patricia Sullivan  
Managing Editor  
Journal of Nuclear Materials Management  
111 Deer Lake Road, Suite 100  
Deerfield, IL 60015 USA

Papers are acknowledged upon receipt and are submitted promptly for review

and evaluation. Generally, the author(s) is notified within ninety days of submission of the original paper whether the paper is accepted, rejected, or subject to revision.

**Format:** All papers must include:

- Author(s)' complete name, telephone and fax numbers, and e-mail address
- Name and address of the organization where the work was performed
- Abstract
- Camera-ready tables, figures, and photographs in TIFF, JPEG, or GIF formats. Black and white only.
- Numbered references in the following format:  
1. Jones, F.T. and L. K. Chang. 1980. Article Title. Journal 47(No. 2): 112–118. 2. Jones, F.T. 1976. Title of Book, New York: McMillan Publishing.
- Author(s) biography

**Peer Review:** Each paper is reviewed by at least one associate editor and by two or more reviewers. Papers are evaluated according to their relevance and significance to nuclear materials safeguards, degree to which they advance knowledge, quality of presentation, soundness of methodology, and appropriateness of conclusions.

**Author Review:** Accepted manuscripts become the permanent property of INMM and may not be published elsewhere without permission from the managing editor. Authors are responsible for all statements made in their work.

**Reprints:** Reprints may be ordered at the request and expense of the author. Contact Patricia Sullivan at [psullivan@inmm.org](mailto:psullivan@inmm.org) or +1-847-480-9573 to request a reprint.

# INMM Membership Application

All information should be printed or typewritten.

# MEMBERSHIP

Name \_\_\_\_\_ Date \_\_\_\_\_

Employer \_\_\_\_\_ Title \_\_\_\_\_

### Address

Address \_\_\_\_\_

City \_\_\_\_\_ State/Province \_\_\_\_\_ Country \_\_\_\_\_ Zip \_\_\_\_\_

Telephone \_\_\_\_\_ Fax \_\_\_\_\_ E-mail \_\_\_\_\_

If you would like your INMM mail sent to an alternative address, please indicate preferred mailing address:

Address \_\_\_\_\_

City \_\_\_\_\_ State/Province \_\_\_\_\_ Country \_\_\_\_\_ Zip \_\_\_\_\_

### Occupation

- Commercial Utility                       Government Contractor                       Nuclear Material Processing
- Equipment Manufacturer                       Government or International Agency                       Research or Consulting
- Other (describe): \_\_\_\_\_

Field(s)/Subject(s) of expertise \_\_\_\_\_

Total number of years work experience in nuclear materials management field(s) \_\_\_\_\_

### Education (If you are applying for a student membership, indicate the year that you anticipate receiving your degree)

College/University	Major/Degree	Year Degree Obtained/Expected
--------------------	--------------	-------------------------------

1. \_\_\_\_\_

2. \_\_\_\_\_

3. \_\_\_\_\_

If you are applying for a student membership, provide contact information for a faculty advisor to verify your full-time status:

Name \_\_\_\_\_ Telephone \_\_\_\_\_ E-mail \_\_\_\_\_

### Membership Type Desired

- |                                  |      |  |             |   |       |
|----------------------------------|------|--|-------------|---|-------|
| <input type="checkbox"/> Student | \$20 |  | Sustaining: | <input type="checkbox"/> 0 – 19 employees     | \$250 |
| <input type="checkbox"/> Regular | \$50 |  |             | <input type="checkbox"/> 20 – 49 employees    | \$500 |
|                                  |      |  |             | <input type="checkbox"/> 50 or more employees | \$750 |

From the categories listed below, please indicate your top 3 areas of interest within INMM (1 being the greatest interest):

- |   |   |
|---|---|
| <input type="checkbox"/> International Safeguards             | <input type="checkbox"/> Packaging & Transportation |
| <input type="checkbox"/> Materials Control and Accountability | <input type="checkbox"/> Physical Protection        |
| <input type="checkbox"/> Nonproliferation & Arms Control      | <input type="checkbox"/> Waste Management           |

### Membership in Other Scientific and Technical Societies (Attach additional sheet if necessary)

Society Names and Membership Grades \_\_\_\_\_

Signature \_\_\_\_\_

PAID BY:       Check       MasterCard       VISA       American Express       Diners Club

Card No. \_\_\_\_\_ Exp. Date \_\_\_\_\_

Complete the application (keep a copy for your records) and mail or fax it with membership dues to:

INSTITUTE OF NUCLEAR MATERIALS MANAGEMENT  
 111 Deer Lake Road, Suite 100 • Deerfield, Illinois 60015 USA  
 +1-847-480-9573, Fax: +1-847-480-9282  
 E-mail: inmm@inmm.org • Website: www.inmm.org





---

## February 9–12, 2010

A Multidisciplinary Workshop to  
Train the Next Generation  
Safeguards Advocate

University of Missouri  
Columbia, Missouri USA

*Hosted by:* The INMM University of  
Missouri Student Chapter in partner-  
ship with the INMM Central Region  
Chapter and the Central Region  
Chapter of INMM

*E-mail:* jscole@mail.mizzou.edu

---

## February 24–26, 2010

International Workshop for Users  
of Proliferation Assessment Tools  
Workshop I: Users in Regulatory Roles

Texas A&M University,  
College Station, TX USA

*Sponsors/Organizers:*

INMM Standing Committee on  
Proliferation Assessments and Method-  
ologies, Texas A&M University INMM  
Student Chapter, and the INMM  
Southwest Chapter

*Web site:* <http://www.inmm.org>

---

---

## March 21–24, 2010

INREC'10  
1st International Nuclear &  
Renewable Energy Conference

Jordan University of Science and  
Technology

Amman, Jordan

*Web site:* <http://inrec10.inrec-conf.org/>

---

## April 11–16, 2010

Northwest International Conference  
on Global Nuclear Security:

The Decade Ahead

Portland, OR USA

*Sponsors:* Pacific Northwest Chapter of  
INMM and Eastern Washington  
Section of ANS

*Contact:* Carrie Mathews  
Pacific Northwest National Laboratory  
+1-509-375-6783

*E-mail:* [carrie.mathews@pnl.gov](mailto:carrie.mathews@pnl.gov)  
*Web site:* [http://pnwcgs.pnl.gov/PNIC/  
PNIC.stm](http://pnwcgs.pnl.gov/PNIC/PNIC.stm)

---

## June 6–11, 2010

INMM & WINS International Work-  
shop on Containment & Surveillance:  
Concepts for the 21st Century

Oak Ridge National Laboratory  
Oak Ridge, Tennessee USA

*Contact:* Peggy York, [yorkpj@ornl.gov](mailto:yorkpj@ornl.gov)  
*Sponsored by:* The NNSA Office of Non-  
proliferation Research & Development

---

---

## July 11–15, 2010

51st INMM Annual Meeting  
Marriott Waterfront Baltimore Hotel  
Baltimore, MD USA

*Sponsor:* Institute of Nuclear Materials  
Management

*Contact:* INMM

+1-847-480-9573

Fax: +1-847-480-9282

*E-mail:* [inmm@inmm.org](mailto:inmm@inmm.org)

*Web Site:* <http://www.inmm.org/meetings>

---

## October 3–8, 2010

PATRAM 2010

16th International Symposium on  
the Packaging and Transport of  
Radioactive Materials

IMO Headquarters  
London, UK

*Hosted by:* Department for Transport of  
the United Kingdom, in cooperation  
with the International Atomic Energy  
Agency, the International Maritime  
Organization and the World Nuclear  
Transport Institute

*E-mail:* [admin@patram2010.org](mailto:admin@patram2010.org)

*Web site:* <http://www.patram2010.org>

---





TM

# SRNL

SAVANNAH RIVER NATIONAL LABORATORY

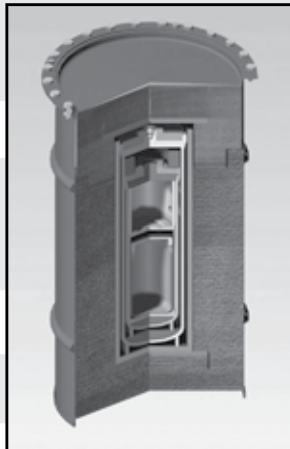
## We Put Science To Work<sup>TM</sup>

...creating applied solutions  
in Security, Energy and  
Environmental Management

Nuclear materials management initiatives at the U.S. Department of Energy's Savannah River National Laboratory are focused on homeland and global security and legacy materials disposition.

SRNL provides applied science and technology critical to:

- Nuclear Materials Package Development
  - Nuclear Materials Transportation, Storage and Disposition
  - Safeguards and Monitoring Technologies



09T01494

Visit us on the web at <http://srnl.doe.gov>

# The NEW ORTEC Micro-trans-SPEC: tailored to your application.

The Lightweight and Compact Solution  
for Heavyweight Spectroscopic Problems

- All-in-one ultra-light HPGe Spectrometer: No LN<sub>2</sub> required.
- High Sensitivity — 50 mm Ø x 30 mm HPGe detector.
- Tough — Enclosure, Display, and all connections sealed against moisture and dust. Water spray resistant.
- Amazingly light: 15 lb (6.8 kg).
- Digitally Stable electronics.
- High Visibility display.
- Removable data storage on SD card.
- Multiple choice of power sources.



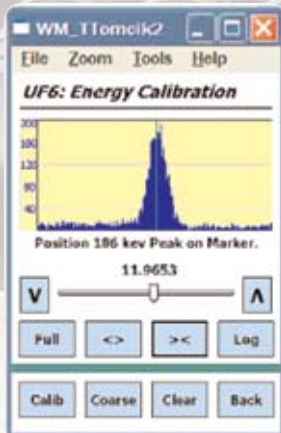
**Smart MCA Software** — Onboard ROI-based Nuclide ID and activity calculation.

**And NOW: available with Custom Software Applications**

Application Example: Simpler UF6 Cylinder assays.

Enrichment Meter Application, Built IN.

No need for an associated computer.



Nuclide	keV	Bq	±%
Be-7	477.8	0.00E+000	0.0
K-40	1462.6	1.06E+002	3.6
Ru-103	30.9	0.00E+000	0.0

The ORTEC Micro-trans-SPEC is a great NDA platform for HPGe applications. It is light, rugged, reliable, compact, and available now. Contact us with your application needs and we will work with you on implementation.

801 South Illinois Ave., Oak Ridge, TN 37831-0895 U.S.A. • (865) 482-4411 • Fax (865) 483-0396 • [ortec.info@ametek.com](mailto:ortec.info@ametek.com)  
For International Office Locations, Visit Our Website

**ORTEC**®

[www.ortec-online.com](http://www.ortec-online.com)

**AMETEK**®  
ADVANCED MEASUREMENT TECHNOLOGY